Science
AAAS

Supplementary Materials for

Genomic predisposition is associated with the direction of sex chromosome evolution

Yang Zhou *et al*.

Corresponding authors: Peng Shi, ship@mail.kiz.ac.cn; Guojie Zhang, guojiezhang@zju.edu.cn

Science **393**, eaec3449 (2026)
DOI: 10.1126/science.aec3449

The PDF file includes:

Other Supplementary Material for this manuscript includes the following:

Materials and Methods

Sample collection and library preparation

Gecko samples were collected from various locations across the USA, Australia, Honduras, Trinidad & Tobago, Puerto Rico and China, with all collections conducted under the respective permits for each region (**Table S1**). Samples were processed under protocol AR279 and AR288 approved by Marquette University Institutional Animal Care and Use Committee, and S20210312-009 approved by the Laboratory Animal Care and Use Committee of Nantong University.

High molecular weight DNA was extracted from somatic tissues by QIAGEN® Genomic DNA extraction kit (Cat#13323, QIAGEN) according to the standard operating procedure provided by the manufacturer. The extracted DNA was detected by NanoDrop™ One UV-Vis spectrophotometer (Thermo Fisher Scientific, USA) for DNA purity (OD260/280 ranging from 1.8 to 2.0 and OD 260/230 is between 2.0-2.2), then Qubit® 3.0 Fluorometer (Invitrogen, USA) was used to quantify DNA accurately. When the sample was qualified, the genomic DNA was sheared by g-TUBEs (Covaris, USA) according to the expected size of the fragments for the library. The fragmented DNA of target size was enriched and purified by MegBeads. Next, the fragmented DNA was repaired for the damage and then end-repaired. The stem-loop adaptor was linked on both ends of each DNA fragment, and the link-failed fragments were removed by exonuclease. Then the target fragments were screened by the BluePippin (Sage Science, USA) and purified to construct the library. Finally, Agilent 2100 Bioanalyzer (Agilent technologies, USA) was used to detect the size of Library fragments. After the library was constructed, DNA templates and enzyme complexes of a certain concentration and volume were transferred to the ZMWs of Sequel II system (Pacific Biosciences, USA) for real-time single-molecule sequencing.

The same DNA samples were also used for library preparation and loaded on BGISEQ500 or DNBSEQ-T1 for short reads sequencing. Tissues of the homogametic sex were used to extract DNA with the cetyltrimethylammonium bromide (CTAB) method. DNA quality and quantity were evaluated using pulsed field gel electrophoresis and Qubit® 3.0 Fluorometer. Libraries were then prepared and sequenced with BGISEQ500 or DNBSEQ-T1, following the manufacturer's protocol. We also prepared 10X (except *Phelsuma laticauda* for stlFR) libraries with the DNA and sequenced with BGISEQ500, following the protocol available at https://www.protocols.io/view/bgiseq-500-10x-library-construction-rm7vzne5rvx1/v1. For Hi-C library preparation, nuclei isolated from frozen tissues were processed as described in Rao et al. (*89*) using a combination of MboI and MseI restriction enzymes for chromatin digestion. The libraries were sequenced on lllumina instruments.

RNA extraction was performed on collected brain, eye, tail and gonads. We added TRIzol lysis buffer to samples and extracted RNA by thorough mixing with 300 μL of chloroform:isoamyl alcohol (24:1) and centrifugation (12,000 g for 8 min at 4 °C). The supernatant was transferred to a 1.5-mL centrifuge tube, gently mixed with 2/3 volume of isopropyl alcohol, and placed at -20 °C for over two hours to precipitate RNA. Finally, the precipitation was washed with 0.9 mL of 75% ethanol, air dried, and dissolved with 20 to 200 μL of DEPC-H2O or RNase-free water to obtain purified RNA. Libraries were prepared and sequenced with BGISEQ500 or DNBSEQ-T1,

following the manufacturer's protocol. Detailed information about sample collection and sequencing statistics can be found in **Tables S1 & S2**.

Genome assembling, curation and sex-linked sequences identification

We generated multiple draft assemblies to maximize contiguity and accuracy, as different assemblers show variable performance depending on read type and genome complexity. PacBio CLR long reads were independently assembled using several established long-read assemblers—FALCON (v0.5) (*90*), wtdbg2 (v2.3) (*91*), NextDenovo (v2.2-beta.0) (*92*), and Canu (v2.1.1) (*93*). These assemblers employ different algorithmic approaches: FALCON uses hierarchical assembly with error correction, wtdbg2 utilizes a fuzzy Bruijn graph approach, NextDenovo employs a string graph-based method optimized for noisy long reads, and Canu combines overlap-layout-consensus with sophisticated error correction. For each species, we compared assemblies using standard quality metrics including contig N50, total assembly, and genome completeness, selecting the most contiguous and complete draft assembly as the foundation for subsequent scaffolding and polishing steps. This comparative approach ensures optimal assembly quality tailored to each species' specific genomic characteristics. PacBio HiFi reads, when available, were assembled separately using HiCanu (v2.1.1) (*94*).

CLR-based contigs were polished using Arrow to correct residual sequencing errors. We then performed a first round of scaffolding using linked-read data generated by either 10X Genomics Chromium or single-tube long fragment reads (stlFR). stlFR is a linked-read technology tags short reads originating from the same long DNA fragment with a unique barcode, enabling long-range linkage information similar to 10X Chromium but using a streamlined single-tube library construction protocol (*21*). Linked-read scaffolding was performed using Scaff10X (v4.0).

Following linked-read scaffolding, assemblies were further polished using whole-genome BGISEQ data from the same individual with a freebayes–bcftools pipeline described in Rhie et al. (*95*). A second round of scaffolding was then carried out using Hi-C data. Hi-C reads were aligned to the draft assembly and deduplicated using Juicer (v1.6) (*96*), and the resulting contact maps were used to anchor, order, and orient scaffolds with 3D-DNA (v201008) (*97*). Hi-C scaffolds were visually inspected and manually curated using Juicebox Assembly Tools (*98, 99*).

In some cases, candidate sex-chromosome scaffolds were curated separately from autosomes. Candidate sex-linked scaffolds were initially identified based on sequencing coverage from both sexes and were subsequently evaluated using Hi-C interaction strength with the inferred sex chromosome versus autosomes (see below).

We first identified the X/Y (or Z/W) sequence and examined if there was X/Y (or Z/W) chimeric error in the assembly. Sex-linked sequences were identified with a similar method as described in Yang et al. (*100*). Briefly, we mapped male and female short reads to the assembly with BWA MEM (v0.7.17) (*101*), calculated normalized female-vs-male depth ratio for each scaffold under 50 Kb window with samtools (v1.11) (*102*) and bedtools (v2.29.2) (*103*), and visualized with ggplot2 (v3.3.6) (*104*) for manual examination. To reduce false positives arising from coverage variation or assembly artifacts, we further validated candidate sex-linked scaffolds using Hi-C interaction data, following Yang et al. (*100*). Hi-C reads were aligned to the assembly, and

contact matrices were generated using Juicer and hicConvertFormat from the HiCExplorer package (v3.7.2) (*105*). Hi-C matrices at 100-kb resolution were used for downstream analyses. For each candidate sex-linked scaffold, we quantified its Hi-C interaction strength with the inferred sex chromosome (defined as the largest confirmed sex-linked scaffold) and with each autosome. Hi-C interaction strength was calculated following Zhang et al. (*106*), using the formula:

$$\frac{\#\text{chr1 and chr2 Interactions}}{\left(\left(\frac{chr1trans}{totaltrans}\right)\left(\frac{chr2trans}{totaltans - chr1trans}\right) + \left(\frac{chr2trans}{totaltrans}\right)\left(\frac{chr1trans}{totaltans - chr2trans}\right)\right) * \left(\frac{totaltrans}{2}\right)}$$

where #chr1trans (chr2trans) is the number of interactions between chr1 (chr2) and others, #totaltrans is the total number of interchromosomal interactions, #chr1 and chr2 interactions is the number of interactions between chr1 and chr2.

This procedure yielded a distribution of Hi-C interaction strengths between each candidate scaffold and the sex chromosome (s_{sex}), as well as between the same scaffold and each autosome ($s_1, s_2, s_3, \ldots$). We then performed Wilcoxon rank-sum tests comparing s_{sex} against the distribution of autosomal interaction strengths ($s_1, s_2, s_3, \ldots$). Candidate scaffolds were retained as sex-linked only if their Hi-C interaction strength with the sex chromosome was significantly higher than that with autosomes (Wilcoxon rank-sum test, $p < 0.05$) and showed a fold change $\geq$ 2 of the interaction strength with sex chromosome compared to any of the autosomal interaction strength. Scaffoldings failing to meet either criterion were classified as false positives and excluded from further sex-linked analyses.

In *Gekko japonicus, Thecadactylus rapicauda,* and *Heteronotia binoei* we were not able to identify the sex-linked region with the sequencing depth method described above (**Figs. S4-S6**). For *Gekko japonicus* and *Thecadactylus rapicauda*, whole-genome sequencing (WGS) data of females (10 and 3 respectively) and males (10 and 3 respectively) were used for calculating the fixation index (*Fst*) between male and female to identify SDR. And for *Heteronotia binoei* we collected RAD-seq data from NCBI (SRR1752387-SRR1752398, including 4 males and 8 females) and performed similar analysis as above (i.e., call SNPs and calculate *Fst*) to identify the SDR. Firstly, WGS/RAD-seq data were mapped to the genome by BWA MEM. Variants were called by Freebayes (v1.1.0) (*107*) with default parameters after the alignment duplications were removed by MarkDuplicates of Picard (v2.23.8). The variant result was filtered by vcftools (v0.1.13) (*108*) with the parameter set "--recode-INFO-all --max-alleles 2 --min-alleles 2 --minDP 3 --minQ 30 --recode --remove-indels". *Fst* between males and females was calculated by vcftools with "--fst-window-size 500000", and was visualized with Manhattan plot from qqman R package (v0.1.8) (*109*) along each scaffold and manually checked for SDR with enriched high *Fst* signals.

The following steps were taken to curate the sex chromosomes in *Hemidactylus frenatus*, *Gehyra insulensis*, *Coleonyx brevis* and *Christinus marmoratus* due to X/Y and Z/W sequence collapse into a single scaffold in the initial assembly. Firstly, all sex-linked scaffolds (including those with and without chimeric errors) were split into contigs, then these contigs were scaffolded with Hi-C data by 3D-DNA and the same method used to check the chimeric error. The chimeric

errors of most species were curated, except for *Christinus marmoratus*. For *Christinus marmoratus*, the Z, W, and PAR contigs were separated, and scaffolded independently using 3D-DNA; we later scaffolded the Z and PAR scaffold with ALLHIC (v0.9.13) (*110*). We aligned the Hi-C data to the assembly with Juicer and identified an ~23 Mb region with similar male and female sequencing depth but with abnormal Hi-C interaction with Z-SDR, W-SDR and PAR. We mapped the sex-linked markers (collected from Gamble et al. (*18*)) to the genome and found that 251 out 587 markers were mapped to the region, suggesting it could be a young SDR instead of a PAR (**Fig. S3**). We failed to assemble both haplotypes of the region and were not able to curate the Hi-C map. Thus, the sequences associated with the region were combined into a single scaffold and named "chrSDR" in the genome. The completeness of the sex-linked sequences was assessed with the karyotype image using the same method as described in Zhou et al. (*111*).

After the autosome and sex chromosome curation the sequence was examined with purge_dups (v1.0.1) (*112*). Identified redundant sequences that were not sex-linked were removed. 'N's at the end of the scaffolds were also removed. BUSCO (v5.2.2) (*113*) was used to evaluate genome completeness with the sauropsida_odb10 database.

SDR in other geckos

We also analyzed the SDR in four additional gecko species. The RAD-seq data of *Cyrtodactylus pharbaungensis* was obtained from PRJNA692216 (*42*) and aligned to *Hemidactylus frenatus* genome using BWA with default parameters, and the SDR was identified with the *Fst* method described above. The male and female WGS data of *Saltuarius cornutus (19)* and *Coleonyx elegans (41)* were retrieved from NCBI PRJNA701686 and PRJNA682555, respectively. These sequences were aligned to *Nephrurus levis* and *Coleonyx brevis* genome, respectively and identified their SDR orthologous coordinates in the target species by the sequencing depth method described above. For *Sphaerodactylus townsendi*, both the genome (MPM_Stown_v2.3) and SDR data were obtained from Pinto et al. (*26*).

Sex-linked sequence confirmation with previous studies

Published sex-linked markers were collected from previous studies (*18, 28, 29*) and aligned to the assembly by BLASTN (v2.2.31+) (*114*) with "-outfmt 6 -evalue 1e-2". The best alignment of each marker was kept to confirm the sex-linked region. To obtain the homology between the gecko sex chromosome and chromosomes of chicken (GCF_016699485.2, served as reference), we performed whole-genome alignment using lastz (v1.04.00) (*115*), with the parameter set '--step=19 --hspthresh=2200 -inner=2000 --ydrop=3400 --gappedthresh=10000 --format=axt' and a score matrix for the comparison of distantly related species. Of note, we removed all the identified Y-SDR/W-SDR sequence between alignment to exclude their multiple mapping results with X-SDR/Z-SDR. Syntenic alignments were obtained with netSyntenic in kentUtils (v351). Alignments larger than 10 kb were kept. Results were compared with Augstenová et al. (*19*) and Keating et al. (*28*).

Contamination removal

We screened out contaminated sequences in each genome with the pipeline below. First, VecScreen (v2.2.31) was used to map against the UniVec database. Results were then classified to determine whether there was contamination from vector, adapter, linker, and primer in the sequence. We also BLASTNed the sequence against the NT database (release date 20220529), and classified the results using BASTA (v1.3.2.3) (*116*). Sequences would be considered as contamination if its most recent common ancestor is not eukaryote and were removed from the assembly.

Genome annotation

Repetitive elements were annotated with RepeatMasker (v4.1.2-p1) with Dfam library and parameter '-species Amniota'. The gene set was annotated by three methods as described in Zhou et al. (*117*). Firstly, the protein sequences of related species including *G. gallus* (GCF_016699485.2), *L. agilis* (GCF_009819535.1), *T. elegans* (GCF_009769535.1), and *S. townsendi* (GCF_021028975.2) obtained from NCBI were aligned to each gecko genome by Genblasta (v1.0.1) (*118*) with parameter set "-s -100 -p T -d 100000 -g T -e 1e-2 -a 0.5 -r 100 -c 0.5 -f F". Only alignments with alignment rate > 50% were kept and used in gene prediction by GeneWise (v2.4.1) (*119*) with default parameters. Each prediction result was merged based on the overlaps. We then randomly extract 1,000 genes for Augustus (v3.4.0) (*120*) to model training by autoAugTrain.pl with "--useexisting --verbose --verbose --verbose". The model was used for *de novo* prediction based on the N-masked genome by Augustus with default parameters. RNA-seq data of tissues from brain, kidney, eye, tail and gonad was independently aligned to the genome by HISAT2 (v2.2.1) (*121*), and the gene structure predicted by StringTie (v2.1.6) (*122*). The final gene set was merged from the above three annotations as described in Zhou et al.(*117*).

Whole genome alignment (WGA)

LAST (v1449) (*123*) was used to align each soft-masked genome (including 21 geckos and two outgroups, *L. agilis* and *T. elegans*) to *Correlophus sarasinorum* which served as the reference. Firstly, lastdb of LAST was used to build the database for reference with parameter set "-uNEAR -R01 -c". And each genome was aligned with reference by lastal with "-m50 -E0.05 -C2 -p" and we used the alignment matrix score generated by last-train with "--revsym --matsym --gapsym -E0.05 -C2". Finally, the MAF file was generated by last-split and last-postmask with the default parameter. The CHAIN file and NET files were generated by KENT tools (v351). Briefly, the MAF file generated by LAST was transformed into AXT file by mafToAxt and then transformed into CHAIN file by axtChain with parameter set "-minScore=5000 -linearGap". The CHAIN file was further processed by chainPreNet, chainNet, netSyntenic, to generate the final NET and MAF file. All pairwise WGAs were merged into a 24-way alignment by MULITZ (v11.2) with default parameters. The code for alignment and downstream processing is available at Github: https://github.com/Dived-Jin/Gecko_Sexchromosome.

Phylogeny analysis

The coalescence method was used to infer the phylogenetic relationship of the geckos. Initially, Trimal (v1.4.rev22) (*124*) was employed to remove gaps in the 24-way alignment with the '-

nogaps' parameter, resulting in 89.84 Mb alignments. These alignments were then divided into 1-Kb windows. Windows with alignment ratio < 80% in any species were excluded as described in Chen et al. (*125*), leaving a total of 68,040 windows. IQtree2 (v2.2.2.6) (*126*) was used to construct the phylogenetic tree of each window, with parameter set "-m MFP -b 100 -nt AUTO -safe -redo". The consensus tree was obtained from all 68,040 trees by Astral-hybrid (v1.15.2.3) (*127*) based on the weight of the branch length with default parameters. The branch lengths of the consensus tree were evaluated based on 89.84M 24-way alignments using RAxML-NG (v1.2.0) (*128*) with the '-evaluate' parameter.

Divergence time

We applied a similar method as Li et al. (*129*) to estimate the divergence time of geckos. The 89.84 Mb 24-way whole genome alignment was used as the input. We first used baseml from the PAML package (v4.5) (*130*) to estimate alpha and the substitution rate for generating the out.BV file which contains the Hessian matrix by gHmatrix before the MCMCTree estimated the divergence times. Posterior distributions of divergence times were independently estimated twice using Markov chain Monte Carlo sampling. Samples were drawn every 1,000 steps over a total of 5000 million steps, with a burn-in of 500 million steps being discarded. Time calibration points were obtained from previously published studies, including the divergence times of geckos (99.6-125 MYA) (*37*) and the split between geckos and other Squamata (176-213.2 MYA). Convergence was checked in two output files using Tracer(*131*).

Ancestral karyotype construction

A similar method as in Zhou et al. (*117*) was used to construct the gecko ancestral karyotype. Briefly, we utilized *Correlophus sarasinorum* as the reference to reconstruct the ancestral nodal karyotype. Firstly, the NET and CHAIN files generated by LAST, include 22 geckos (19 in this work and 3 published) and two outgroups (*L.agilis* (GCF_009819535.1) and *T. elegans* (GCF_009769535.1)), was used to identify conserved blocks across 22 species by DESCHRAMBLER (git commit 28686dda39144f9d8223dce663aadf0621002643) (*132*). Conserved blocks ≥ 300 Kb were kept, and ANGES (v1.01) (*133*) was used to construct the karyotype of every gecko ancestral node. The conserved blocks were also visualized with NGenomeSyn (v1.41) (*134*), color-coded based on the karyotype of gecko MRCA.

The ANGES reconstruction provided the ancestral order of the conserved blocks, which we used as a reference framework to interpret genome organization in extant species. For each inferred ancestral chromosome, we identified corresponding conserved blocks in extant genomes and compared pairs of closely related species, where one species retained the ancestral order while the other exhibited a different arrangement. Large structure variants (> 500 Kb) were checked using Hi-C data at 100 Kb resolution to distinguish true structural variants from potential assembly errors with the following step:

For each putative translocation, the translocated region (B) and its upstream (A) and downstream (C) syntenic regions were identified from whole-genome alignments between two closely related species (Species A and Species B). For each species, interaction strengths between region B and

its flanking regions (A1, C1 in Species A; A2, C2 in Species B) were calculated from normalized Hi-C contact matrices using HiCExplorer at 100-kb resolution.

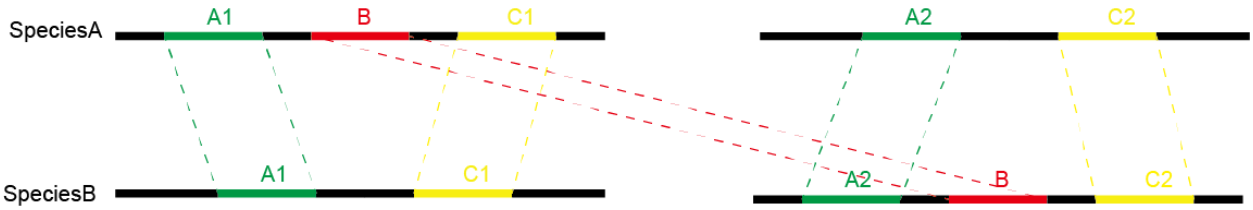

if the translocation is true:

- for SpeciesA: A1.vs.B and C1.vs.B > A2.vs.B and C2.vs.B

and

- for SpeciesB A2.vs.B and C2.vs.b > A1.vs.B and C1.vs.B

if the translocation is false:

- for SpeciesA: A1.vs.B and C1.vs.B < A2.vs.B and C2.vs.B

or

- for SpeciesB A2.vs.B and C2.vs.b < A1.vs.B and C1.vs.B

For each candidate inversion, the inverted region was divided into two halves (a: 5′; b: 3′), and its interactions with the upstream (c) and downstream (d) syntenic regions were examined. Hi-C interaction strengths between a–c, b–d, a–d, and b–c were compared between species.

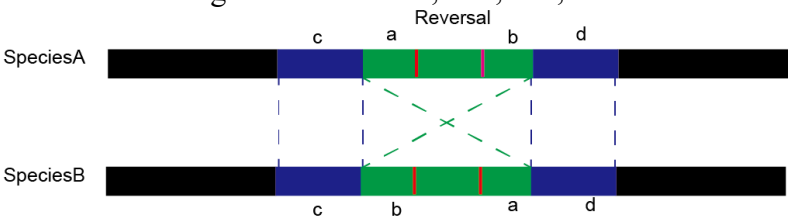

If the inversion is true

- for speciesA, a.vs.c and b.vs.d > a.vs.d and b.vs.c

and

- for speciesB: a.vs.d and b.vs.c > a.vs.c and b.vs.d

If the inversion is false:

- for speciesA: a.vs.c and b.vs.d < a.vs.d and b.vs.c

or

- for speciesB: a.vs.d and b.vs.c < a.vs.c and b.vs.d

For fusion or fission check, we plotted and manually examined the breakpoint regions with the Hi-C heatmap under 100 Kb resolution.

Putative rearrangements that were inconsistent with Hi-C interaction patterns were interpreted as likely assembly errors and were excluded from downstream analyses. After this filtering, chromosomal rearrangement including chromosome inversion, fusion, fission, and translocation was inferred with GRIMM (v2.01), comparing the block order and orientation (*135*). Rearrangements between X/Z and Y/W were inferred manually.

<u>Ortholog identification</u>

We identified one-to-one orthologs among the 19 geckos using the method as described in Zhou et al. (*117*). Briefly, for each species, genes were encoded into protein sequences and were BLASTPed (v2.2.26) (*136*) against the protein sequences of *Correlophus sarasinorum* (as the reference), with an e-value cutoff 1e-5. Reciprocal best hits (RBH) of each gene were kept as candidate orthologs. To ensure true orthology, we required conservation of local gene collinearity, which we defined as the preservation of gene order within the same chromosomal region between species. RBH pairs were retained only if they maintained the same flanking genes in both species. Finally, we merged pairwise orthologue lists according to the genomic coordinates of *Correlophus sarasinorum*. Of note, to exclude the effect of Y/W genes, we only used autosomal and X/Z-linked genes in the RBH ortholog identification. We also performed OrthoFinder (v2.5.5) (*137*) to identify orthologous groups for the 19 geckos and two outgroups based on their protein sequences with default parameters, except specifying the rooted species tree with "-s".

Sex chromosome analysis

Confirmation of the absence of sex chromosome turnover

Sex chromosome turnover involves the replacement of an ancestral sex chromosome with a new one. A key prediction of this process is that if recombination between sex chromosomes ceased prior to the divergence of two species, orthologous genes should cluster by chromosome type rather than by species in phylogenetic trees, Specifically, we expect the topology ((Z_A, Z_B), (W_A, W_B)) rather than ((Z_A, W_A), (Z_B, W_B))), where subscripts indicate species. Conversely, clustering by species suggests independent origins of sex chromosome.

We tested for possible sex chromosome turnover by examining orthologous genes located on sex chromosomes in at least two species. Our hypothesis was that if turnover occurred, ancestral sex-determining gene or closely linked genes should (i) reside in the oldest stratum (S0), (ii) participate in sex-determination pathways, and (iii) show evidence of chromosomal translocation or duplication events.

For X/Z-SDR genes, conserved collinearity across species allowed us to systematically identify candidate translocated genes. We first identified one-to-one orthologs using RBH (see above). Gene families were then reconstructed using OrthoFinder and phylogenetic trees were built using RAxML-NG. Trees were manually inspected for clustering patterns, if putative sex-linked genes clustered with autosomal rather than sex-linked orthologs, we concluded that the gene was unlikely to be involved in sex chromosome turnover.

For Y/W-SDR genes, the extensive degeneration and fragmentation characteristic of Y/W chromosomes precluded reliable collinearity-based comparisons. Therefore, we employed a direct phylogenetic approach without requiring conserved collinearity. Gene families containing Y/W-linked sequences were identified and phylogenetic trees were reconstructed using the same methods. We applied identical topological criteria, species-based clustering was interpreted as evidence against shared ancestral sex chromosomes, while chromosome-based clustering would support sex chromosome turnover. Importantly, no instances of chromosome-based clustering was observed across our dataset.

Non-randomness test of conserved block recruitment

Conserved blocks represent syntenic chromosomal segments inferred from ancestral karyotype reconstruction that maintain homologous genomic regions across gecko species. To test whether certain conserved blocks were recruited as SDR more frequently than expected by random chance, we developed a length-controlled randomization test that accounts for the heterogeneous size of conserved blocks across the gecko phylogeny.

Specifically, we first quantified *N* as the total number of independent SDR recruitment events observed across species. For each simulation, we randomly sampled *N* conserved blocks from the full set of available genomic conserved blocks, with sampling probability for each block weighted proportionally to its length to account for difference in size. This length-weighting approach controls for potential size-based biases in recruitment probability, as larger blocks might be more likely to be recruited simply due to their greater genomic footprint. We repeated this randomization process 10,000 times to generate a null distribution of recruitment counts for each individual conserved block. For each conserved block, we compared its empirically observed recruitment frequency, *n*, representing the number of times that block was recruited as an SDR across species against the corresponding null distribution generated through our randomization procedure. P-value was calculated as the proportion of simulation iteration where the focal block was randomly sampled at least n times, providing a quantitative measure of recruitment significance. A statistically significant p-value below 0.05 indicates the conserved block has been recruited as an SDR more frequently than expected under random recruitment model.

Strata analysis

Sex chromosome evolution can follow two distinct patterns following the cessation of recombination. Recombination suppression can proceed stepwise, producing discrete regions of distinct ages and degrees of degeneration known as evolutionary strata (*53*). Alternatively, recombination suppression may spread progressively, resulting in a continuous gradient of divergence between X–Y (or Z–W) along the chromosome (*2*). To distinguish between these two evolutionary scenarios in geckos sex chromosomes, we employed a statistical approach based on two datasets: X–Y (or Z–W) sequence alignments and gametolog pairwise *dS*.

To obtain X-Y (or Z-W) alignments, N-masked X- or Z-linked sequences (as reference) were aligned to N-masked Y- or W-linked sequences with LAST alignment tool. Firstly, lastdb of LAST was used to build the database for reference with parameter set "-R11 -P10 -c -uMAM8 HetGam". And N-masked X- or Z-linked genome was aligned to the reference by lastal with "-R11 -P10 -D1e9 -m100" and we used the alignment matrix score generated by last-train with "-R11 --revsym -D1e9 --sample-number=5000 -P10 HetGam". Finally, the MAF file was generated by last-split and last-postmask with the default parameter. MAF file generated by LAST was then transformed into AXT file by mafToAxt and then transformed into CHAIN file by axtChain with parameter set "-minScore=5000 -linearGap". The CHAIN file was further processed by chainPreNet, chainNet, netSyntenic, to generate the final NET and MAF file. The repeat regions of each species were removed in the MAF file based on the RepeatMask,

RepeatModel, and Tandem Repeats Finder (v4.09) (*138*) annotation by Maffilter (*139*). The X/Y or Z/W identity was calculated based on the reciprocal best MAF alignment obtained following the codes at: https://github.com/Dived-Jin/Gecko_Sexchromosome. The weighted-average identity of each alignment block was calculated in 10 Kb non-overlapped windows along the X/Z chromosome, requiring >500 bp alignment within the window.

To obtain gametolog pairs, Y/W protein sequences were BLASTPed against all X/Z + autosomal protein sequences. Only Y/W genes whose best hit were X/Z genes were kept, and we further examined the gene name to confirm their homology. Gametolog CDS alignment was built using PRANK (*140*) and *dS* was calculated using PAML codeml.

Evolutionary strata were then defined as contiguous chromosomal regions with internally homogeneous sequence identity that were separated by statistically significant shifts. Specifically, we performed a Wilcoxon rank-sum test to compare X-Y (or Z-W) identity values (or gametolog pairwise dS) between different regions. If $p < 0.05$, regions were classified as distinct strata. When no significant difference was detected, we referred that the region was undergoing gradual, continuous divergence without forming discrete evolutionary strata.

When visualizing the alignment, we manually examined the Hi-C map to determine whether it is the 5' or 3' end of the X/Y-SDR (or Z/W-SDR) that is close to PAR. For each species, all the MAF alignment was used to generate dotplot with a custom script, orienting the regions close to PAR to the top left. The identities were oriented along the X or Z chromosome, color-coded for visualization. For *Gekko japonicus, Thecadactylus rapicauda,* and *Heteronotia binoei*, the identity was calculated based on the called variants from the same heterogametic individual used in genome assembly in the 10 Kb non-overlapped windows.

We utilized both the alignment of X and Y (or Z and W) and the whole-genome alignment across different species to determine which chromosome (X/Z or Y/W) the genomic rearrangement happened, following the idea similar as in Zhou et al. (*55*). Briefly, take the X/Y species as an example, if rearrangement was found between X and Y, the rough breakpoint regions were manually identified and the alignment across different species were examined. If the synteny was well kept in the closely related species of the same family, the associated rearrangement was considered to have happened on Y; otherwise, the rearrangement was considered to have happened on X. Rearrangements between X and Y, as well as rearrangements across species were manually examined with Hi-C to exclude assembly artifacts.

Male mutation bias and strata age estimate

The alignment between X-Y | Z-W with homology chromosomes was generated by using the same method mentioned in the whole genome alignment. Briefly, for a species, we identified the homology chromosome by common ancestral karyotype. Then the homology chromosomes and Y (or W) sequence were mapped to the X (or Z) chromosome of this species by LAST with default parameters. Finally, the multiple MAFs were merged by MultiZ (*141*). To minimize the effects of mapping error and selection constraints, we limited this analysis in non-coding and non-repeat regions. The repeat regions of each species were removed in the MAF file based on the RepeatMasker, RepeatModeler and Tandem Repeats Finder annotation by Maffilter. We

further excluded the exon region as well as its 2 Kb flanking regions. The alignment length of X/Z-linked sequences is shown in **Table S18**.

The alignment segments of X-Y (or Z-W) and orthologous autosomes were extracted and concatenated. For each species, the substitution rates of X and Y (or Z and W) were estimated by baseml in PAML package under TN93 model. Finally, the male mutation bias (α) was calculated using the formula: $\alpha = 2/[(3X/Y)-1]$ or $\alpha = [(3Z/W)-1]/2$, following the approach originally developed by Miyata et al. (*57, 142, 143*). For species where recombination suppression occurred after speciation, α was calculated from terminal-branch divergence between X(Z) and Y(W). For lineages where recombination suppression predated species divergence (i.e., *Correlophus* in this study), α was estimated using the substitute rate accumulated along the shared ancestral branches where sex chromosome differentiation occurred. The 95% confidence interval (CI) for α was estimated by baseml bootstrap for 1000 times (**Table S18**). We did not apply formulations that incorporate autosomal substitution rates because few of the studied species share a common sex chromosome origin. Under this scenario, autosomal substitution rates primarily reflect mutations accumulated after speciation, therefore include substitutions occurring both before and after the emergence of sex chromosomes. Consequently, using autosomal rates would confound estimates of male mutation bias by combining effects from evolutionary periods before and after sex chromosome differentiation.

Our stratum age estimation follows the theoretical framework established by Cortez et al. (*144*), but with species-specific adaptations for male mutation bias correction. The fundamental challenge in estimating stratum ages lies in accounting for the different mutational processes operating before and after recombination cessation. Before recombination cessation (pre-stratification period), both sex chromosomes accumulate mutations at autosomal rates. After recombination cessation (post-stratification period), the heterogametic sex chromosome (Y or W) experiences accelerated mutation accumulation due to male mutation bias and reduced selection efficiency, while the homogametic sex chromosome (X or Z) continues to recombine in the heterogametic sex and thus maintains more autosome-like evolutionary dynamics.

To calculate the age of each stratum, the alignment segments of X, Y (or Z, W) and the orthologous chromosomes were concatenated, and then the substitution rates of each branch were calculated by baseml. Because the mutation rate between autosomes and sex chromosomes is different, post-stratification (m2) needs to be corrected to be the same as pre-stratification (m1). The post-stratification substitution rate of X or Z was corrected into the autosome rate based on the equation: $A(ZW) = (m2*(3\alpha+3))/(4+2\alpha)$, $A(XY) = (m2*(3\alpha+3))/(2+4\alpha)$. The post-stratification divergence rate (m2) was specifically calculated from the shared sex chromosome (X in XY systems, Z in ZW systems) because this chromosome provides the most reliable estimate of mutation accumulation following recombination cessation while avoiding the confounding effects of Y or W chromosome degeneration. Finally, the pre-stratification and corrected post-stratification substitution rate and the related divergence time were used to estimate the ages of the stratification (as shown in the following picture). The baseml bootstrap method was also used to obtain the 95% CI of the ages of the stratification. In Cortez et al. a correction factor *F* is used to account for male mutation bias. Here, because male mutation bias was estimated independently for each species, we directly used species-specific α values to convert XY substitution rates to autosomal rates.

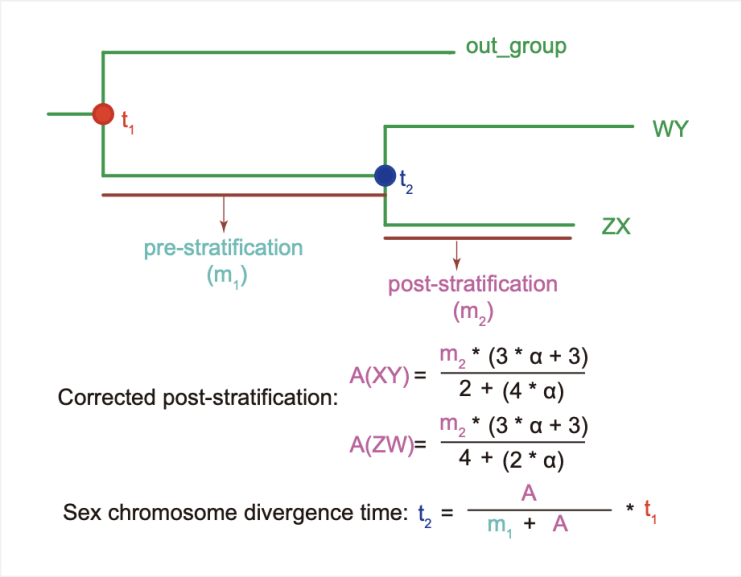

To validate the results, we first confirmed sequence neutrality of our concatenated non-coding alignment with GERP++ analysis (*145*) using a neutral phylogenetic tree estimated from genome-wide four-fold degenerate sites. The four-fold degenerate sites were first extracted with msa_view(v1.5) (*146*) from alignment and estimated the neutral phylogenetic tree with baseml. We then calculated the Rejected Substitutions (RS) score with GERP++ obtained from https://github.com/tvkent/GERPplusplus. In addition, we independently estimated divergence times using these four-fold degenerate sites.

We also calculated the time of sex chromosome divergence with the X/Y (or Z/W) divergence level and the inferred mutation rate in each lineage. Mutation rate of each lineage r_AA was inferred by dividing the substitution rate, inferred with whole genome alignment using RAxML-NG, by the species divergence time. We then corrected the mutation rate r_AA with male mutation bias α to obtain the mutation rate of the sex chromosome r_XY (or r_ZW) as:

$$r_{XY} = \frac{2 + 4\alpha}{3 + 3\alpha} r_{AA}$$

$$r_{ZW} = \frac{4 + 2\alpha}{3 + 3\alpha} r_{AA}$$

The time of sex chromosome divergence was then estimated by dividing the divergence level from the X-Y (or Z-W) alignment by the mutation rate of the sex chromosome (r_XY or r_ZW).

To test whether the observed temporal concentration of GSD origins around 10 Mya deviates from random expectation, we performed a phylogenetically constrained Monte Carlo simulation. For each of the 11 GSD species with sex chromosome age estimates, we defined a biological plausible interval bounded by two phylogenetic events, 1) an older bound, the divergence between the focal species and its nearest sister lineage with a different, independent sex chromosome origins. The GSD origin must postdate this split, otherwise the split-mate lineage

would carry the same SDR. 2) a younger bound, the divergence time between the focal species and its closest relative sharing the same SDR homology. The GSD origin must predate this split, otherwise the SDR could not be shared between the two species. For example, for *Nephrurus levis*, this interval is 20.36-37.71 MYA. 37.71 Mya is the *Nephrurus-Saltuarius* split (*Saltuarius* carries an independent SDR derived from GGA17, 22, 24, while *Nephrurus* uses GGA10 & 17), and 20.36 Mya is the divergence time between *Nephrurus* and *Underwoodisaurus* where both species share the GGA10 & 17 SDR (*19, 147*). Within each interval, a simulated origin age was drawn from a uniform distribution. We repeated this procedure for all 11 species to generate one null replicate and iterated 10,000 times to build the null distribution of the number of origins for every 5-million-year window. The observed number of origins within 7-12 Mya window was 5 of 11. Only two null replicate produces 5 or more origins in this window (empirical p-value < 0.01).

Classification of SDR genes

We combined the results of OrthoFinder and CAFE5 (v1.1) (*148*) to divide SDR genes of target species. First, OrthoFinder results ("Phylogenetic_Hierarchical_Orthogroups/N0.tsv" and "Gene_Duplication_Events/Duplications.tsv") were filtered to only include genes on the sex chromosome of the target species and the genes on the homologous chromosome in other geckos. We then run CAFE5 based on the filtered "N0.tsv" to estimate the gene family change in target species. We then categorized genes into: (A) genes reported as "support > 0.5" in target species in the filtered "Duplications.tsv"; (B) genes with gain signal detected by CAFE5 in target species; (C) genes solely found in target species; (D) genes that can find one-to-one in ≥ 10 geckos, either by OrthoFinder or by RBH method; (E) X/Y (or Z/W) gametolog pairs. Genes in categories (A), (B), (C) were considered later acquired on the SDR in target species, and genes in categories (D) and (E) were considered as genes that were ancestrally in the proto sex chromosome. Other genes (e.g., genes found in < 10 geckos and OrthoFinder did not have > 0.5 support for gene duplication at specific nodes) were considered unknown and excluded in downstream analysis. To test whether later acquired genes with specific functions were enriched, we performed GO enrichment analysis with an in-home pipeline with all SDR (X or Y or Z or W) genes as the background.

Transcriptome analysis

Expression level estimate

We quantified gene expression level with Kallisto (v0.46.1) (*149*). Notably, for species with XY sex determination system, we excluded the identified Y transcripts in the reference FASTA for females (XX); similarly for the ZW species we excluded the identified W transcripts in the reference for males (ZZ). Kallisto estimated counts of each gene were extracted and DESeq2 (v1.31.16) (*150*) was applied for count normalization. Normalized count was then transformed into units of Transcripts Per Million (TPM).

Cross species expression matrix normalization and ancestral state inference

Expression matrices of each species were taken and the log2(TPM+1)-transformed was taken. We used the same scaling method described in Brawand et al. (*72*) to normalize the log-transformed expression level across species. The derived scaling factors were also calculated and used to scale the expression values of all genes in the samples. We took the normalized expression matrix containing all one-to-one orthologs to perform PCA analysis with the "prcomp" function in R and the results were visualized with ggplot2.

For each sex-tissue combination, the ancestral expression level was estimated with the log10(TPM+1) across the phylogeny using `fastAnc` function in the R package "phytools"(v2.0) (*151*), assuming a Brownian motion model. We excluded left-head and right-head expression data in the analysis since the two tissues were only available for *Sphaerodactylus inigoi*. For each gene, the ancestral expression value at gecko MRCA before sex chromosome emerged (e.g. MRCA of *Nephrurus levis* and *Pygopus nigriceps* when inspecting the ancestral state of *Nephrurus levis*) was extracted. Within each tissue, the median of these ancestral expression values across samples was calculated. Tissue-preferential expression was determined based on these median ancestral values (see below) and subsequently compared with tissue preferential expression in extant species to assess whether tissue preference had changed during evolution.

Tissue preferential expression analysis

Tissue preferentially expressed genes are defined as genes showing the highest TPM (>1) in a specific tissue and having at least 2-fold higher expression compared to all other tissue. To examine whether specific genomic regions show higher proportion of testis preferentially expressed genes (TPEGs) than genomic background, we calculated the proportion of TPEGs in SDR-orthologous regions and subtracted the proportion of TPEGs in background-orthologous regions or each outgroup species with independent sex chromosome origins. Wilcoxon rank sum test was performed comparing these difference values against zero, representing no difference between SDR-ortholog and background regions. Current SDR expression patterns were included only for visualization purposes in boxplot. To test the generality of the model, we collected RNA-seq and SDR (or stratum S0 is possible) of other species from published studies (**Table S18**). If SDR is not available, we used the above sequencing depth method to identify the SDR.

Enrichment analysis of tissue preferentially expressed genes on the fused chromosome

To test whether the chromosome later fused into sex chromosome (hereafter referred to as the target chromosome) is enriched with testis preferentially expressed genes (TPEGs), we counted 1) the number of TPEGs in the target chromosome, 2) the number of non-TPEGs in the target chromosome, 3) the number of TPEGs in other genomic regions and 4) the number of non-TPEGs in other genomic regions. These four values were used to construct a 2×2 contingency table, and enrichment of TPEGs on the target chromosome was assessed using a chi-square test. The same procedure was applied to genes preferentially expressed in other tissues.

Dosage compensation analysis

For each species and each tissue, we retained genes with TPM ≥ 1 in both sexes. The ancestral gene expression was estimated with `fastAnc` from R package "phytools", assuming a Brownian

motion model, as described above. TPM values were log2-transformed and analysed using linear mixed-effects models implemented in the `lme4` R package (v1.1_38) (*152*):

m_expr <- lmer(Y ~ AZS+ (1 | indID)+(1 |geneID),

where Y is the log2-transformed TPM, AZS is a categorical factor with multiple levels representing gene class and sex context. We also included log(geneLength) as an offset term in modeling to account for its effect on expression estimates.

To assess dosage balance (DB) and dosage compensation (DC) with all the X/Z genes as a whole, AZS was set to include the following categorized factors:

- homogametic proto-sex genes (ancXZhom)
- heterogametic proto-sex genes (ancXZhet)
- homogametic X/Z genes (XZhom)
- heterogametic X/Z genes (XZhet)

DB can be assessed with the comparison between `XZhom` and `XZhet`, and DC was assessed by the comparison between `XZhet` and `ancXZhet`, where contrasts among proto-sex genes (ancXZhom vs. ancXZhet) was used as control.

To assess DB and DC when classifying X/Z genes into XZOPs and XZGPs, AZS was set to include the following categorized factors:

1. homogametic proto-sex genes without gametolog pair after X/Z evolution (ancXZOPhom)
1. homogametic proto-sex genes with gametolog pair after X/Z evolution (ancXZGPhom)
2. heterogametic proto-sex genes without gametolog pair after X/Z evolution (ancXZOPhet)
3. heterogametic proto-sex genes with gametolog pair after X/Z evolution (ancXZGPhet)
4. homogametic X/Z genes without gametolog pair (XZOPhom)
5. homogametic X/Z genes with gametolog pair (XZGPhom)
6. heterogametic X/Z genes without gametolog pair (XZOPhet)
7. heterogametic X/Z genes with gametolog pair (XZGPhet)

DB for the two different X/Z gene categories was assessed using the following comparisons:

1. XZOPhom vs. XZOPhet
2. XZGPhom vs. XZGPhet

DC for the same three X/Z gene categories was evaluated by comparing expression of X/Z genes to their proto sex chromosome counterparts in the heterogametic sex:

1. XZOPhet vs. ancXZOPhet
2. XZGPhet vs. ancXZGPhet

And to evaluate DB and DC level between XZOP and XZ+YW, similar analysis was performed with X/Z+Y/W gene expression level was used instead of X/ZGPs.

The above ratios were estimated from the fitted models using the `effects` R package (v4.2_4) (*153*). We obtained 95% confidence intervals by bootstrapping with `bootMer()` in `lme4` (100

replicates). We also computed per-gene log2-ratios and visualized their distributions using ggplot2.

We applied the same threshold as Catalán et al. (*83*) to categorize the degree of DB and DC:

1. fully DC or DB: |2FC|<0.25
2. partially DC or DB: 0.25 <|2FC|<0.75
3. fully unbalanced or uncompensated:|2FC|>0.75

Y/W gene survival analysis

Retention strategy analysis

We classified the ancestral X/Z-linked genes into two groups into X/ZGP and X/ZOP, based on whether its Y/W gametolog survived (**Table S10**). We performed GO enrichment analysis with an in-home pipeline (https://sourceforge.net/p/enrichmentpipeline/wiki/Home/) comparing X/ZGP with all the X/Z genes as the background. Briefly, protein sequences of all genes were first annotated using InterProScan, and GO terms were assigned based on the output. For each species, a GO annotation database was constructed using all genes with at least one assigned GO term. GO enrichment analysis was then performed by comparing X/ZGP genes against all X/Z-linked genes as the background set. For each GO term, enrichment was evaluated using a Chi-square test. The resulting p-values were corrected for multiple testing using the false discovery rate (FDR) method.

Retention feature analysis

Gene-level haploinsufficiency scores were obtained from DECIPHER database (https://www.deciphergenomics.org/files/downloads/HI_Predictions_Version3.bed.gz), These scores were originally computed by Huang et al.(*154*) using a supervised machine-learning framework trained on curated sets of experimentally validated haploinsufficient and haplosufficient human genes. HI scores quantify the probability (0-1 scale) that loss of a single functional copy of a gene results in detectable fitness or phenotypic consequence, incorporating genomic features including protein interaction network connectivity, evolutionary conservation, functional annotations, and tissue expression patterns.

Since DECIPHER HI predictions use hg19 coordinates while our human-gecko one-to-one orthologs were based on CHM13, we performed coordinate conversion using the UCSC liftOver tool with the hg19–CHM13 chain file provided by the T2T Consortium (https://github.com/marbl/CHM13). These CHM13-based coordinates were then intersected with our one-to-one ortholog sets to project human HI scores to the orthologs in *Correlophus sarasinorum* and the other gecko species. The cross-species application of human HI scores is supported by empirical evidence demonstrating evolutionary conservation of haploinsufficiency across diverse taxonomic groups (*155*), successful applications in comparative vertebrate genomics (*76, 156, 157*), and the conservation of underlying molecular mechanisms governing dosage sensitivity across vertebrates (*39, 158*).

Expression breadth of each gene is calculated according to Bellot et al. (*54*), by normalizing the expression of each X/Z-linked gene to the maximum TPM in any tissue, and taking the average expression across all tissues. dN/dS was calculated based on genes with one-to-one orthologs in all 19 geckos with the baseml free-ratio model. dN/dS of the tip branch was taken. These values were used to compare between X/ZGP and X/ZOP with Wilcoxon rank-sum test.

To examine whether survival rate was correlated with these features, the median values was taken for each species. For each index (i.e., HI score, expression breadth and dN/dS), these median values were then compared with the survival rate to test if they showed any correlation.

Supplementary Text

Confirmation of Y-linked sequence absence in *Pygopus nigriceps* genome

We only identify a total of 1.8 Mb regions (N50 = 108 Kb) showing different sequencing depth between male and female in our *Pygopus nigriceps* assembly. However, we were unable to further scaffold these small sequences with Hi-C or 10X data to improve the sequence continuity. And we were unable to detect any X/Y gametolog pairs based on the sequences. Therefore, these identified regions could be false positives. We therefore tried to identify and construct Y-linked sequences from the raw sequencing data.

Y-linked transcripts assembly from male RNA-seq data

RNA-seq reads from gonad, eye, tail, and brain of male and female were collected to detect the Y-linked genes by a similar method as Wang et al. (*159*) and Cortez et al. (*144*). First, male RNA-seq reads were aligned to the current assembly by TopHat (v2.1.2) (*160*). Then the unmapped reads were assembled into transcripts using SOAPdenovo-Trans (v1.03) (*161*) (seeds: k-mer 21bp, 23bp, 25bp, 27bp, 29bp) and Trinity (v2.15.1) (*162*). All transcripts were mapped back to the current assembly by BLAT (v319) (*163*). We discarded these transcripts with alignment ratio >0.5 and alignment identification>0.5. We also discarded these transcripts that could be aligned by female RNA-seq, with alignment ratio >0.5, using Bowtie2 (v2.4.1) (*164*). We used cdhit (V4.8.1) (*165*) to cluster transcripts to remove redundancy and Transdecoder (V5.7.1) (https://github.com/TransDecoder/TransDecoder) to identify protein-coding transcripts. Finally, a total of 6,823 transcripts were kept from the above filter steps (**Supplementary Text Table 1**). We cannot confirm which transcript belongs to the Y chromosome.

Y-linked sequence assembly

We also tried to extract Y-linked PacBio reads using the male-specific k-mer. For our data sets, the WGS data of one female and two males was used to generate 22-mer dataset by jellyfish (v2.3.1) (*166*), and the scripts in Behrens et al.(*167*) were used to obtain male specific 22-mers. We discarded 22-mer with depth < 7 (**Supplementary Text Fig. 1**) to reduce false positive results. Based on the male-specific 22-mer, HAST4TGS (https://github.com/BGI-Qingdao/HAST4TGS) was used to calculate the male-specific k-mer density for each PacBio read, and we only kept PacBio reads with male-specific 22-mer density ≥ 0.01. These PacBio reads were also mapped to our assembly by minimap2 (v2.14) (*168*) with "-cx map-pb", and those reads with alignment rate > 0.8 to the large (> 1 Mb) autosomal scaffolds were excluded. A total of 993Mb PacBio reads were kept. We used canu (v2.2) and NextDenovo (v2.4.0) to assemble the PacBio reads, and obtained 16.93 Mb and 3.62 Mb sequences, respectively (**Supplementary Text Table 2**). Unfortunately, we cannot annotate any gene that is homologous to the genes on chrX after used the depth method to filter the assembly (**Supplementary Text Table 2**).

Unfortunately, the above two methods did not help us find any high-confident Y-linked genes that were homologous to any of the X-linked genes in our assembly. It is possible that the Y chromosome of *Pygopus nigriceps* is largely degenerated and only PAR was kept. Since we were

not able to identify any reliable Y sequences for *Pygopus nigriceps*, we didn't perform any X/Y gametolog or sequence analysis of *Pygopus nigriceps* in this work.

Supplementary Text Table 1. Efforts to find *Pygopus nigriceps* Y-linked sequences from RNA-seq.

RNA assembly	genome alignment ratio < 0.5 & identify <0.5	aligned to female/male RNAseq, alignment < 0.5	cdhit cluster	Transdecoder
2,290,074	366,937	338,589	77,294	6,823

Supplementary Text Table 2. Efforts to find *Pygopus nigriceps* Y-linked sequences from whole genome sequencing data.

	raw data filter						assembly			alignment & depth filter		annotated X homologous (483)	
	male-specific 22-mer	Intersection (n)	filter depth < 7 (X)	extracted Pacbio (Gb)	Filter 22-mer density <0.01	alignment current genome < 80% (Gb)		canu (bp)	nextdenovo (bp)	canu	nn ext denovo	canu	next denovo
male1	683,649,258	87,090,731	81,759,743	176.02	5.35	0.99	total	16,931,595	3,626,801	6,680	00	0	0
male2	248,843,292						N50	21,838	108,317				

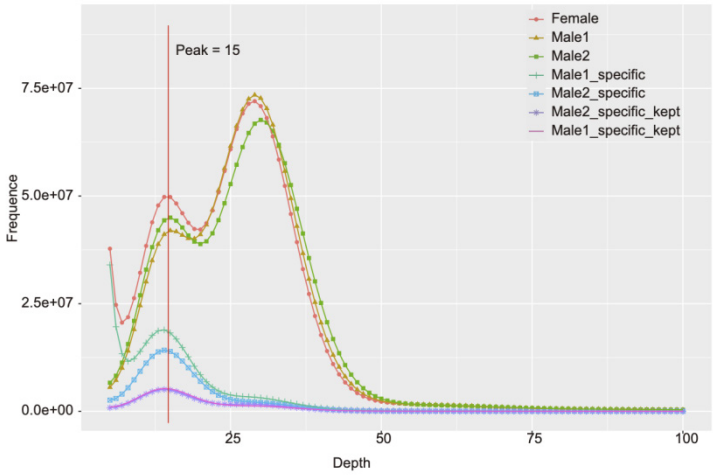

Supplementary Text Fig. 1. The sequence depth of *Pygopus nigriceps* reads.

Multiple sex chromosome systems arising from sex chromosome–autosome fusions

Our analysis uncovered remarkable complexity in gecko sex chromosome architecture, including two species with multiple sex chromosome systems: *Sphaerodactylus inigoi* (XX/XY1Y2) and *Coleonyx brevis* (X1X1X2X2/X1X2Y). Both systems arose through chromosome fusions between ancestral sex chromosomes and autosomes, creating neo-sex chromosome configurations (**Fig. 2A**). In the male *Sphaerodactylus inigoi*, the ancestral X derived from GAC2 is fused with the ancestral autosome GAC3, resulting into an XY1Y2 system where Y1 is the ancestral Y (itself a homolog of GAC2) and Y2 is the unfused GAC3 GAC3 that segregates as a neo-Y. Similarly, in the male *Coleonyx brevis* the ancestral Y, mainly derived from GAC13, is fused with the ancestral autosome GAC10, resulting into an X1YX2 system with the unfused GAC10 as the neo-X chromosome X2. Importantly, this fusion is distinct from the previously reported sex chromosome–autosome fusions in *Coleonyx mitratus* and *Coleonyx elegans*, involving different ancestral chromosomes (**Table S6**) (*169*), indicating multiple, independent origins of sex chromosome systems within the genus. The autosomal regions involved in these fusions showed no enrichment for gonad-biased genes (**Supplementary Text Fig. 2**), ruling out sexual antagonism as the driving force (*170*). Instead, alternative mechanisms such as meiotic drive or drift may underlie their evolutionary fixation (*171*), suggesting that multiple evolutionary pressures can shape sex chromosome architecture.

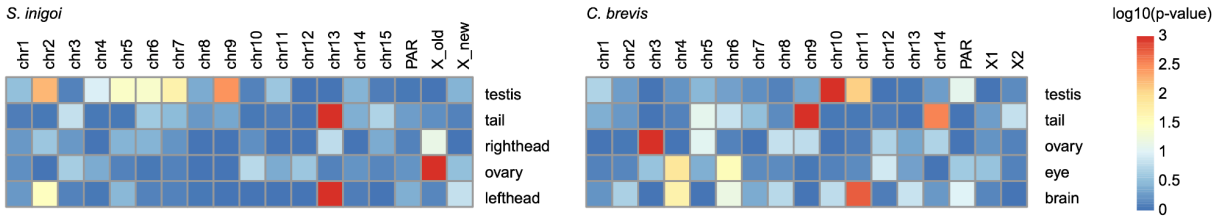

Supplementary Text Fig. 2. No enrichment of gonad preferentially expressed genes in the newly fused part of the sex chromosome (*Sphaerodactylus inigoi* X_new and *Coleonyx brevis* X2). For each chromosome-tissue combination, p.value is calculated based on the Chi-square test.

Candidate upstream sex determining genes in geckos

The identification of upstream sex-determining genes (USDGs) represents one of the most challenging yet crucial goals in sex chromosome biology (*12, 172*). While decades of research have elucidated sex determination cascades in model organisms, the molecular triggers that initiate sexual differentiation remain largely unknown across the vast majority of vertebrate species (*12, 173*). This knowledge gap is especially pronounced in non-model taxa, where the diversity of sex determination mechanisms suggests equally diverse molecular pathways that have yet to be characterized. To systematically identify candidate USDGs, we leveraged the principle that these critical regulators should reside within the oldest differentiated regions of sex chromosomes, where the initial sex-determining mutations first accumulated (*174*). We mapped orthologs of all known vertebrate sex-differentiation genes onto our gecko genome assemblies and examined their locations on SDRs (*175*) (**Supplementary Text Fig. 3A**). We classified species into three categories: I) species with known SDG(s) within their oldest differentiated region (including S0 and the whole SDR if the species has no clear strata pattern), II) species containing such genes in younger strata but not in the oldest SDR and III) species lacking any known SDGs within SDR (**Supplementary Text Fig. 3A & Table S25**).

Our analysis revealed a heterogeneous pattern in the distribution of known sex-differentiation genes across gecko sex chromosomes. Eleven geckos emerged as particularly promising for candidate gene identification, each harboring known SDGs within their oldest SDRs (**Supplementary Text Fig. 3A**). However, the specific genes involved varied dramatically across species, even among those that independently recruited the same ancestral genomic region as their sex chromosome. This pattern reveals a fascinating paradox: while certain genomic regions show non-random recruitment as sex chromosomes, the specific molecular triggers within these regions appear to evolve independently. For example, *Nephrurus levis*, *Correlophus* and *Gehyra insulensis* all recruited GAC16 as their sex chromosomes. *Nephrurus levis* exhibits the highest sequence divergence (Z-W pairwise $dS = 0.4262$) in *MEF2A*, a transcription factor important for testis development through NR4A1 regulation in mammals (*176*). In contrast, this same gene locates resides on a younger evolutionary stratum S1 in *Correlophus* with a lower *dS* value (~0.02) (**Table. S10**), and resides within the PAR in *Gehyra insulensis*, suggesting it plays no primary role in these two lineages. Other species in category I also showcase similar diverse candidate mechanisms. *Thecadactylus rapicauda* features *HMGB1* as a potential upstream regulator, *Paroedura stumpffi* harbors *SOX3* in its SDR, and *Gekko japonicus* contains *SNRNP40*, each supported by sex-biased expression patterns that suggest functional relevance to sexual differentiation (**Supplementary Text Fig. 3B & Table S25**). The diversity of these candidates underscores the remarkable evolutionary diversity in sex determination mechanisms, with each lineage apparently discovering independent molecular solutions to the fundamental challenge of sexual determination. We should emphasize that these inferences are based on a set of criteria rather than direct functional evidence. These candidates meet our selection criteria: they are located within the SDR (or S0 when evolutionary strata are present), have functional annotations consistent with roles in sex determination or early gonadal development, and show gonad preferential expression. Nevertheless, they should be considered preliminary candidates. Definitive identification of primary sex-determining genes will require functional validation, including expression analyses during early gonadal development and experimental perturbation.

Several gecko species completely lack any known SDG within their SDRs as in Category II/III geckos like *Christinus marmoratus, Coleonyx brevis, Hemidactylus frenatus* and *Heteronotia*

binoei, all of which seemingly represent evolutionary enigmas. The absence of recognizable SDGs in their SDR mirrors the findings in anole lizards (*54, 174*) and suggests that our current catalog of sex-determining mechanisms represents only a fraction of the molecular diversity that exists in nature (*177*). These "orphan" sex determination systems may include yet-to-be-discovered elements of the sex determining cascade, harbor entirely novel regulatory networks, or may represent cases where familiar pathways have diverged beyond current recognition through rapid molecular evolution.

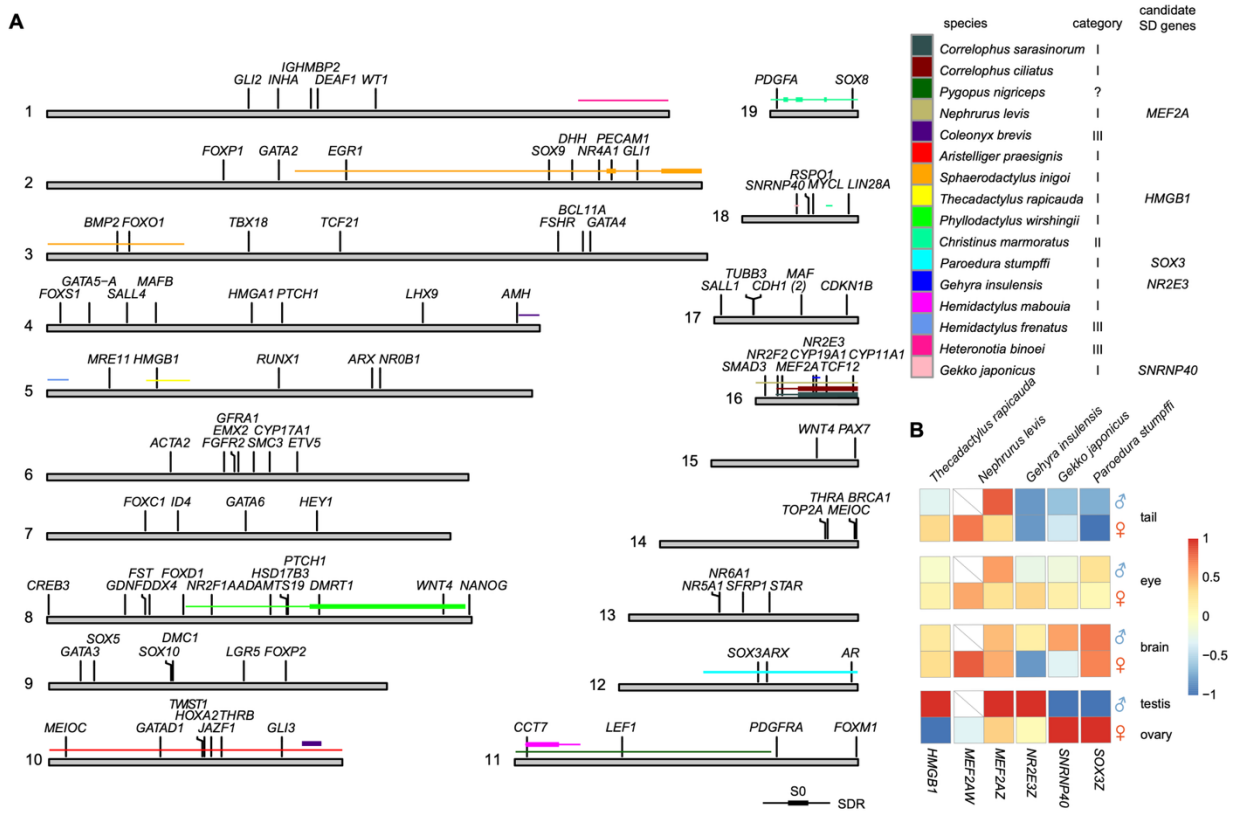

Supplementary Text Fig. 3. Candidate upstream sex determining genes (USDGs) in geckos.

(A) The orthologs of known vertebrate SDGs on the constructed gecko ancestral genome. The color bar indicates the orthologous SDR coordinate of each species, with the thick bar indicating the orthologous coordinates of the oldest stratum S0. Based on whether there are known SDGs in SDR (or S0), the geckos are classified into three categories. Candidate USDGs are also proposed for five geckos.

(B) Gene expression patterns in gonad and somatic tissues of candidate USDGs of five geckos. Z-score normalized log10(TPM) value is used in the heatmap.

Supplementary Figures

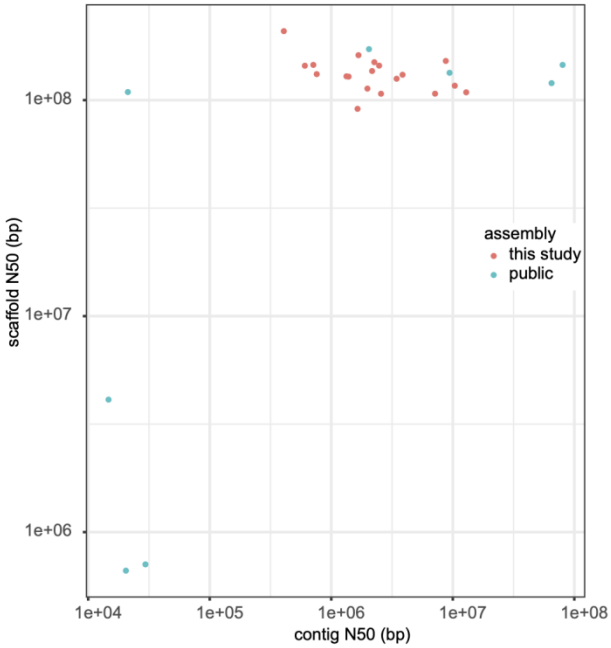

Fig. S1. Contig N50 and scaffold N50 of 27 gecko genome assemblies.

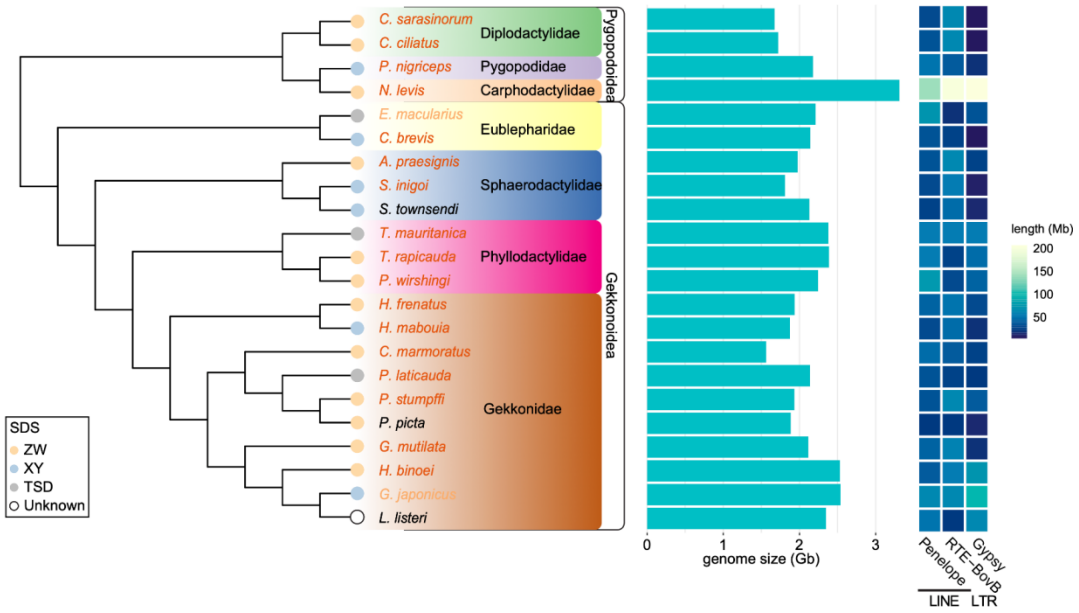

Fig. S2. Genome size and the repetitive DNA content within the studied geckos.

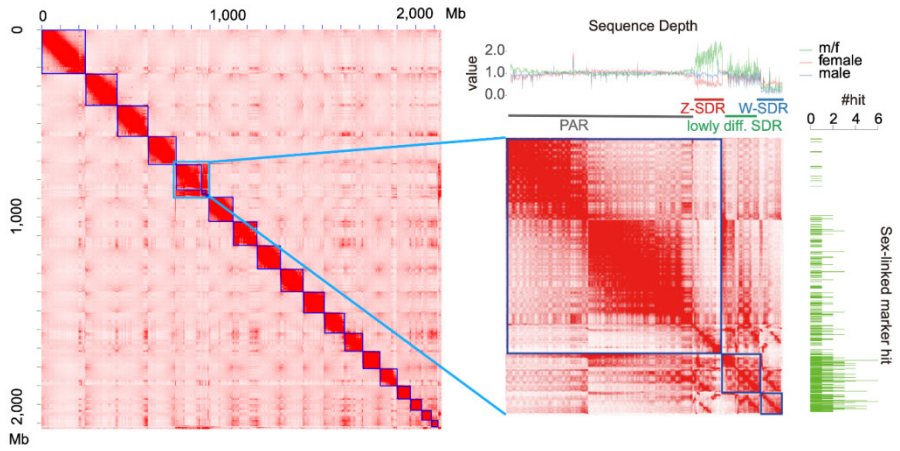

Fig. S3. Identification of sex chromosomes and SDR in *Christinus marmoratus*. Left: whole-genome Hi-C interaction map showing three scaffolds with strong intra-scaffold interaction. Right: sex-biased sequencing depth analysis revealing differential male/female coverage patterns. The middle scaffold in the right plot shows approximately equal male and female sequencing depth but contains 251 sex-linked markers, indicating a weakly differentiated SDR (lowly diff. SDR) that likely represents collapsed Z/W haplotypes in the assembly.

Fig. S4. Identification of sex-linked sequences and its SDR in *Heteronotia binoei.*
a, No difference in male and female normalized sequence depth under 500 Kb non-overlapping window, indicating that the sex-linked region may be too young thus sequences are too similar and collapsed in the assembly.
b, Whole genome screen for sex-linked sequence and its SDR using *Fst* between males and females in 500 Kb windows. Most outline dots are enriched in the 5' end of scaffold "chrZW" (marked by the green dash lines), indicating this scaffold is likely to be the sex-linked sequence and the 3' end is the SDR. The red line shows the top 5% value of *Fst*.

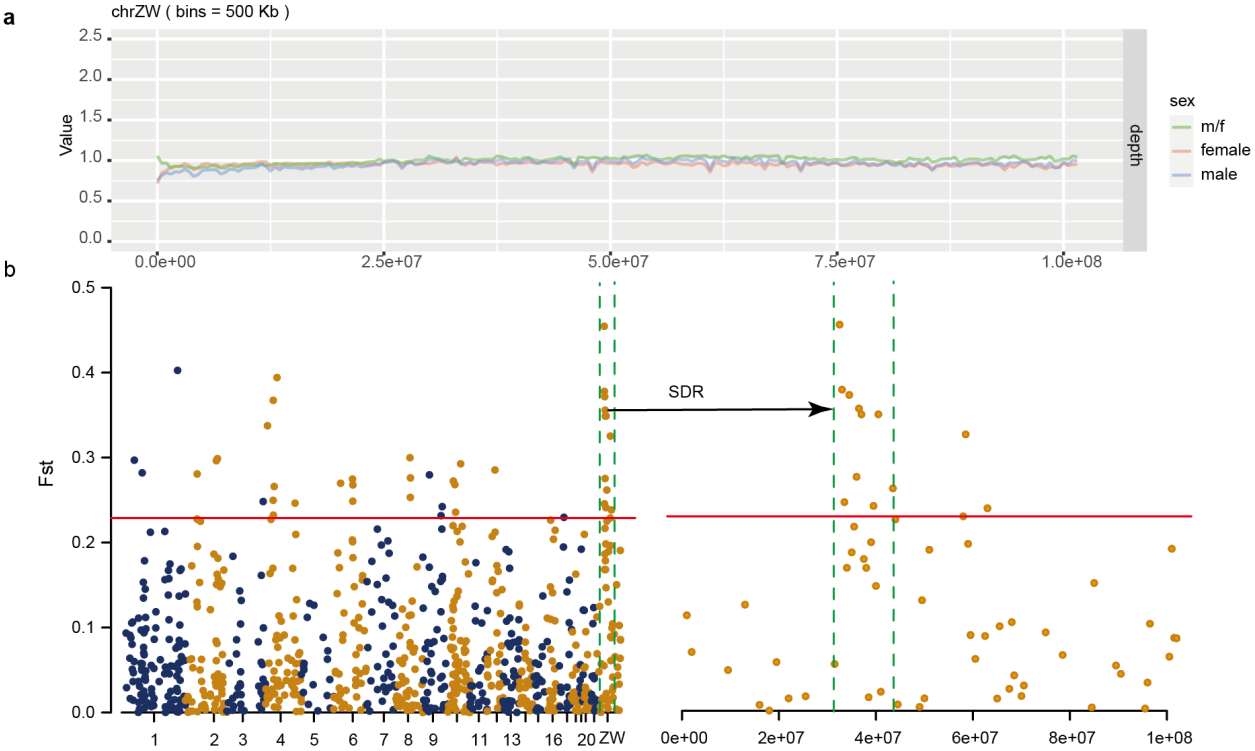

Fig. S5. Identification of sex-linked sequences and its SDR in *Thecadactylus rapicauda.*
a, No difference in male and female normalized sequence depth under 500 Kb non-overlapping window, indicating that the region may be too young thus sequences are too similar and collapsed in the assembly.
b, Whole genome screen for sex-linked sequence and its SDR using *Fst* between males and females in 500 Kb windows. Most outline dots are enriched in the middle part of scaffold "chrZW" (marked by the green dash lines), indicating this scaffold is likely to be the sex-linked sequence and the middle part is the SDR. The red line shows the top 5% value of *Fst*.

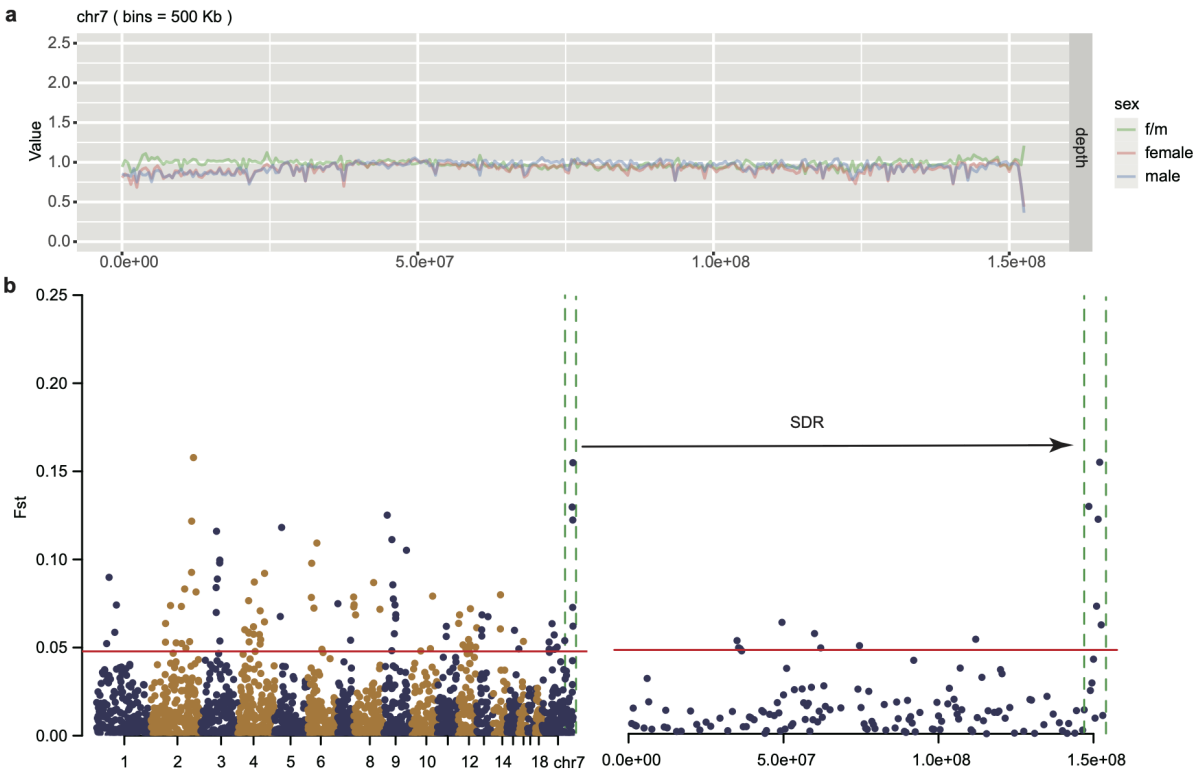

Fig. S6. Identification of sex-linked sequences and its SDR in *Gekko japonicus*.
a, No difference in male and female normalized sequence depth under 500 Kb non-overlapping window, indicating that the region may be too young thus sequences are too similar and collapsed in the assembly.
b, Whole genome screen for sex-linked sequence and its SDR using *Fst* between males and females in 500 Kb windows. Most outline dots are enriched in the 3' end of "chrXY" (marked by the green dash lines), indicating this scaffold is likely to be the sex-linked sequence and its 3' end is the SDR. The red line shows the top 5% value of *Fst*.

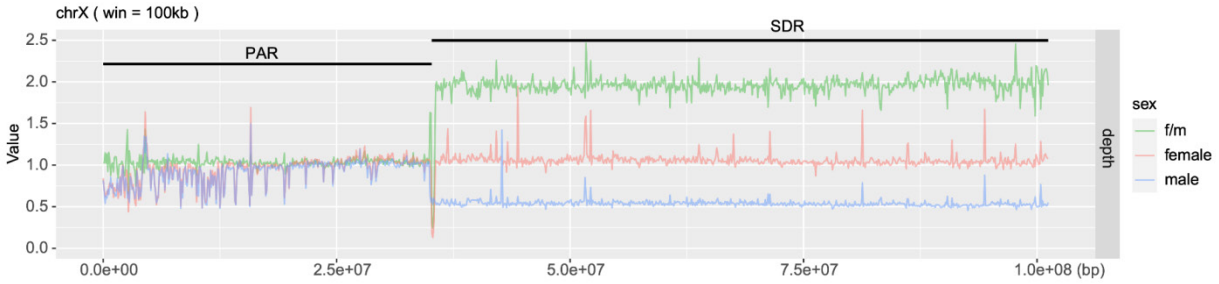

Fig. S7. Normalized male and female sequencing depth of *Pygopus nigriceps* X chromosome.

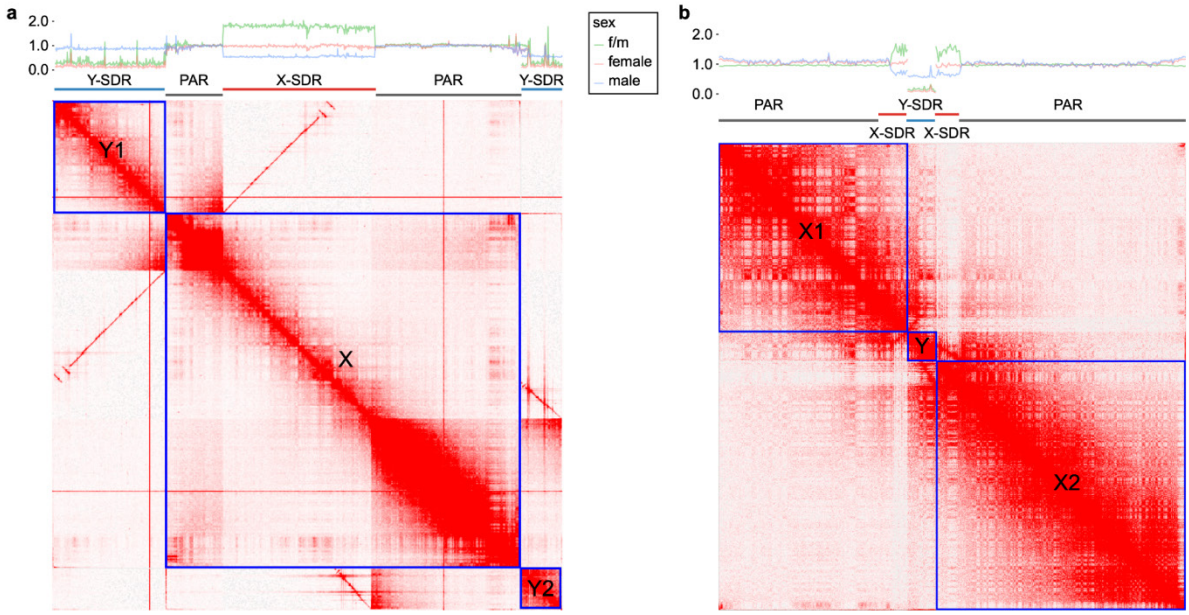

Fig. S8. The evidence of multiple sex chromosomes.
a, Evidence of multiple sex chromosomes Y1XY2 in *Sphaerodactylus inigoi.* Hi-C map shows the interaction between Y1 (upper-left) and Y2 (lower-right) is low (lower-left), suggesting that they are two separate chromosomes. Normalized male and female sequencing depth and the depth ratio are also plotted on the top. Based on sequencing depth and Hi-C contact, the assembled X contains two PARs, one pairs with Y1 and the other pairs with Y2.
b, Evidence of multiple sex chromosomes X1YX2 in *Coleonyx brevis.* Hi-C map shows the interaction between X1 (upper-left) and X2 (lower-right) is low (lower-left), suggesting that they are two separate chromosomes. Normalized male and female sequencing depth and the depth ratio are also plotted on the top. Based on sequencing depth and Hi-C contact, both assembled X1 and X2 contain PARs that pair with Y's 5' and 3' end, respectively.

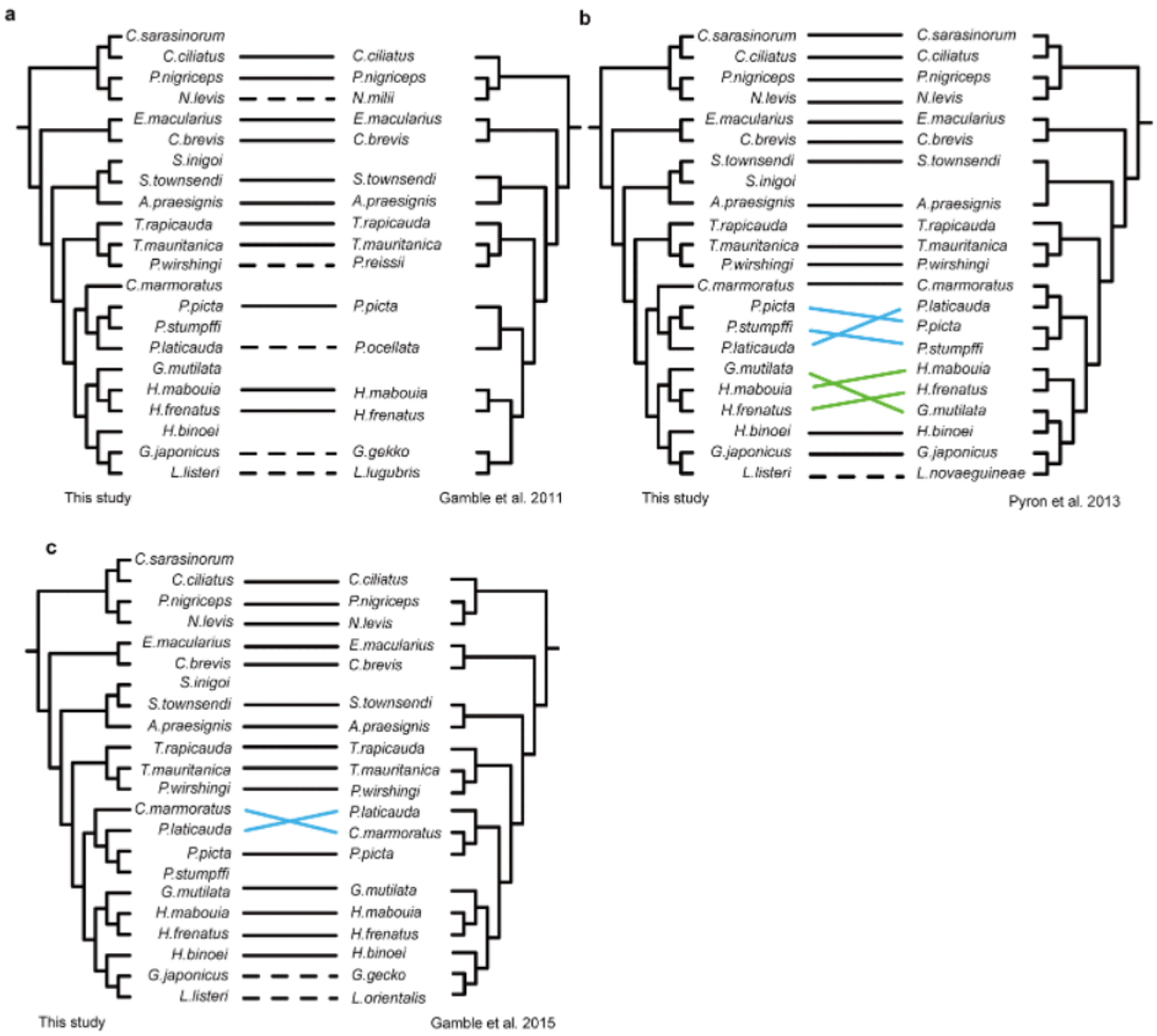

Fig. S9. Comparison of phylogenies among different studies. Blue and green solid lines represent nodes where topological conflicts occur. Dashed black lines represent the phylogenetic position agreement at the genus level.

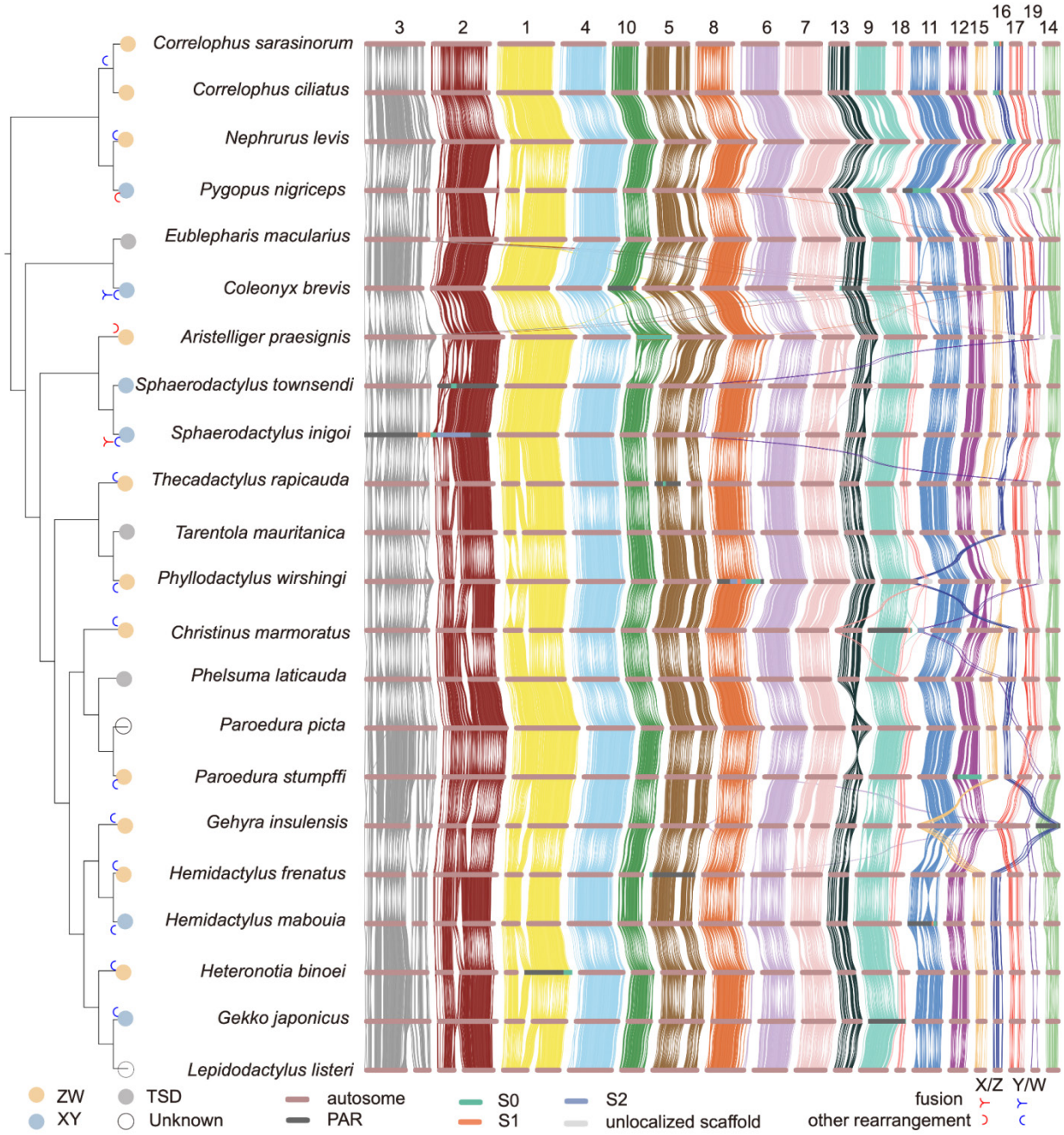

Fig. S10. Whole genome alignment across the 22 geckos covered in this study. Alignments are color-coded based on gecko ancestral chromosomes (GACs; noted at top) as in Fig. 2. For each sex chromosome, the PARs and stratum are highlighted with different colors. The inferred fusion and other rearrangement events associated with the sex chromosomes are shown on the tree. Dusty rose bar, autosome; grey bar, PAR; light grey, unlocalized scaffold.

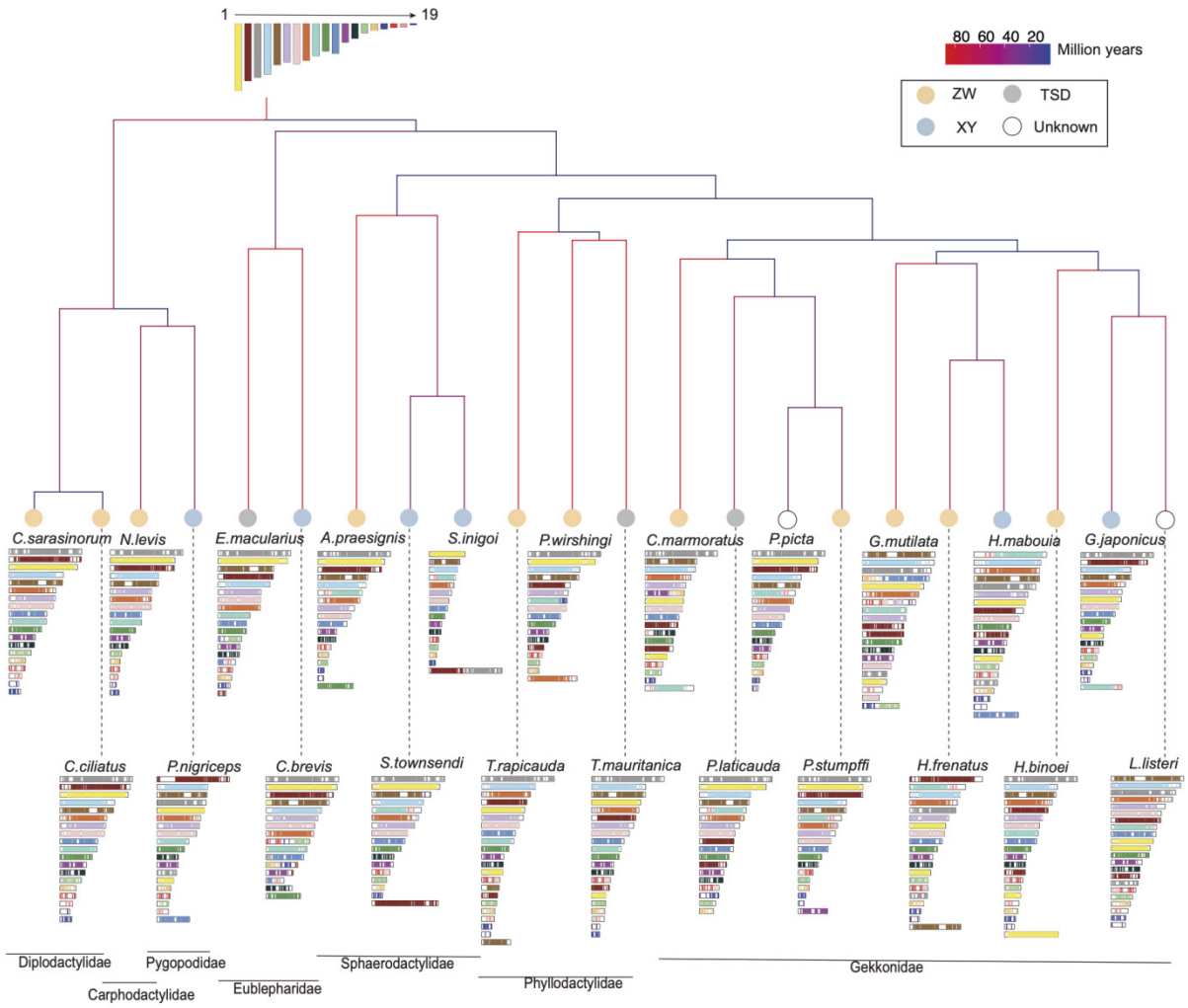

Fig. S11. The ancestral karyotype is obtained by using *Correlophus sarasinorum* as the reference under 300 Kb resolution. Block colors are consistent with Fig. 2. Coloring of the branches indicates divergence time.

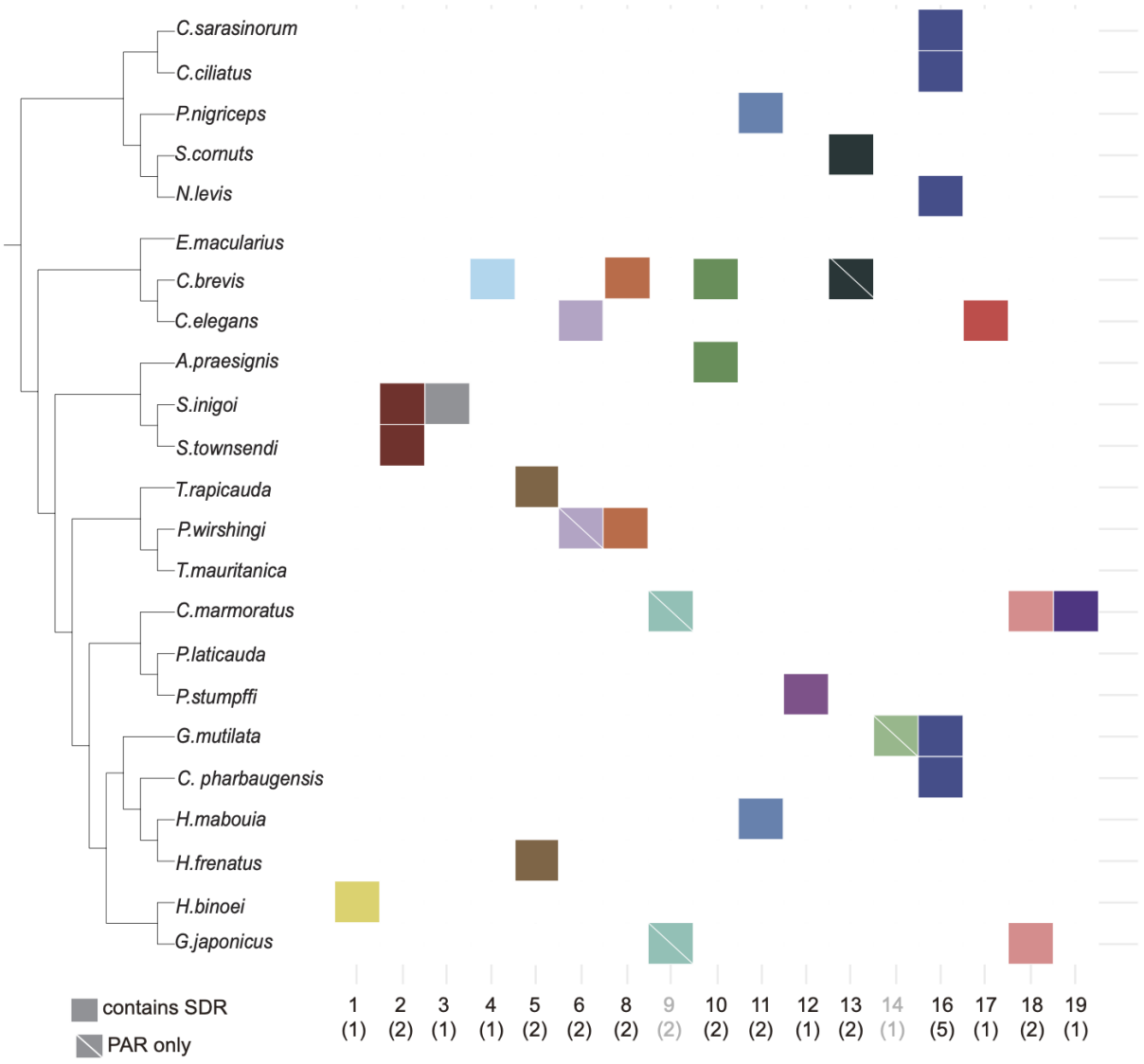

Fig. S12. Homologous gecko ancestral chromosomes detected in the sex chromosomes of all studied geckos. Boxes and arrows are color-coded by GAC. A diagonal line is drawn in the box when the GAC is homologous only to PAR. The parentheses under the GAC at the top indicate the number of times each GAC became sex chromosome, where the color indicates whether the GAC evolved into SDR in geckos (black: evolved into SDR, gray: evolved into PAR only).

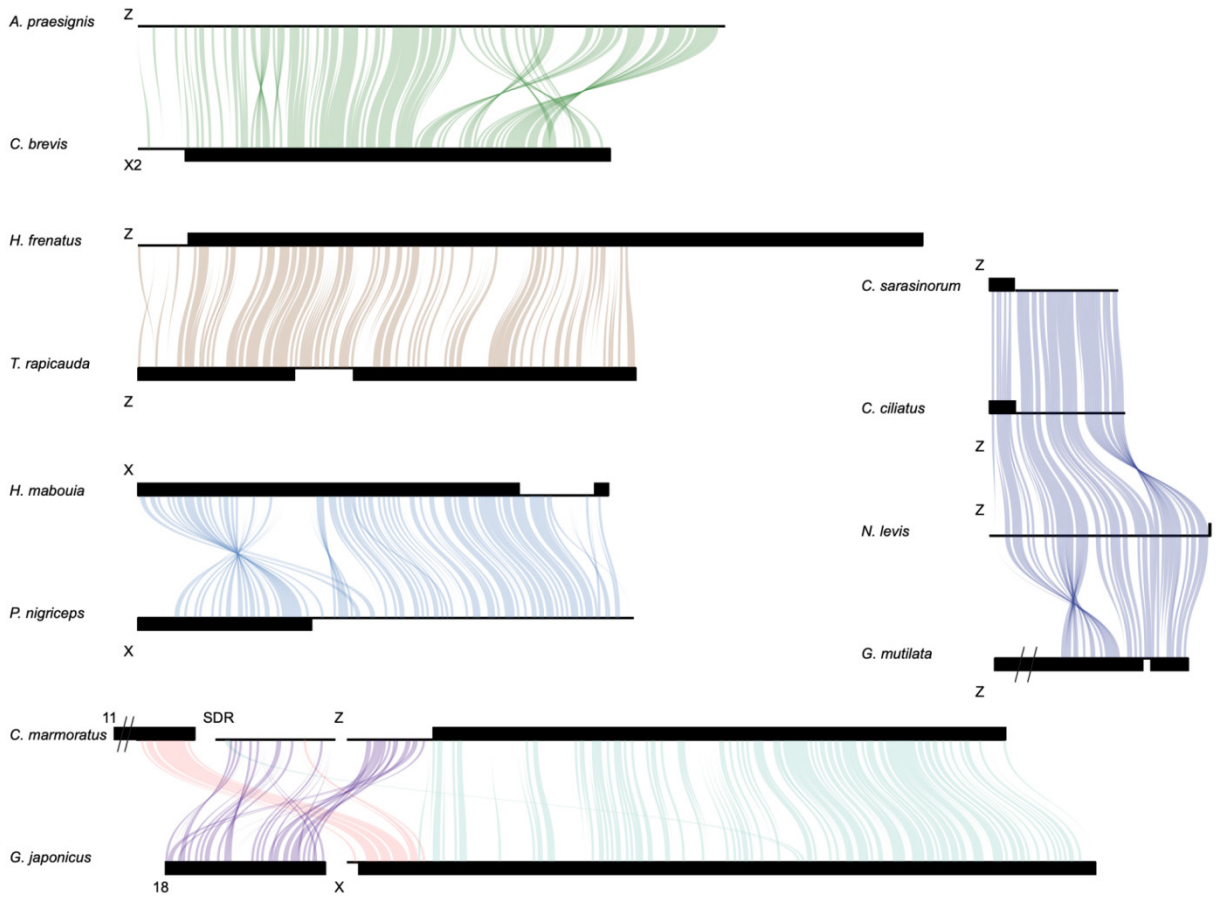

Fig. S13. Alignment of sex chromosomes that evolved from the same GAC shows that the SDR and PAR are not totally shared. Alignments are color-coded as in Fig. 2. Bold bar, PAR or autosome; thin bar, SDR.

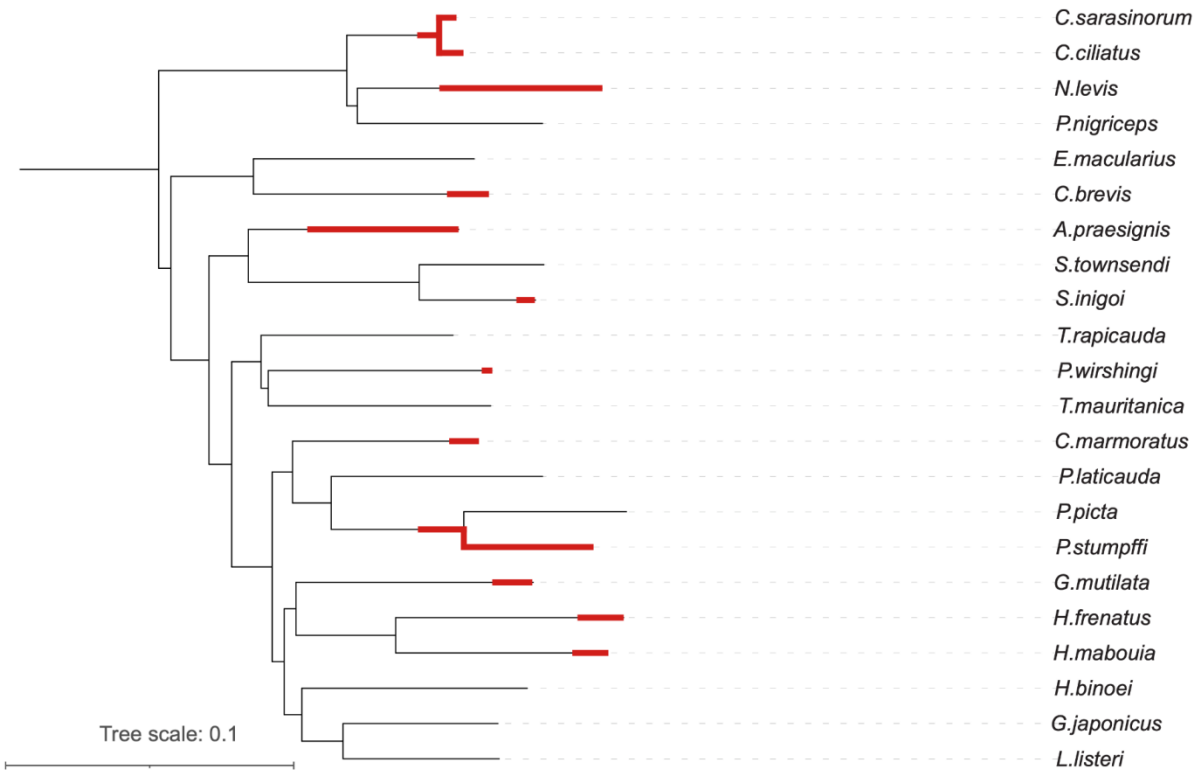

Fig. S14. Comparison of divergence between sex chromosomes and divergence between species. Red bars indicate the divergence between sex chromosomes. For species in which the sex chromosome predates species divergence (e.g. *Correlophus sarasinorum* and *Correlophus ciliatus*), red bars extend beyond the node of their most recent common ancestor (MRCA).

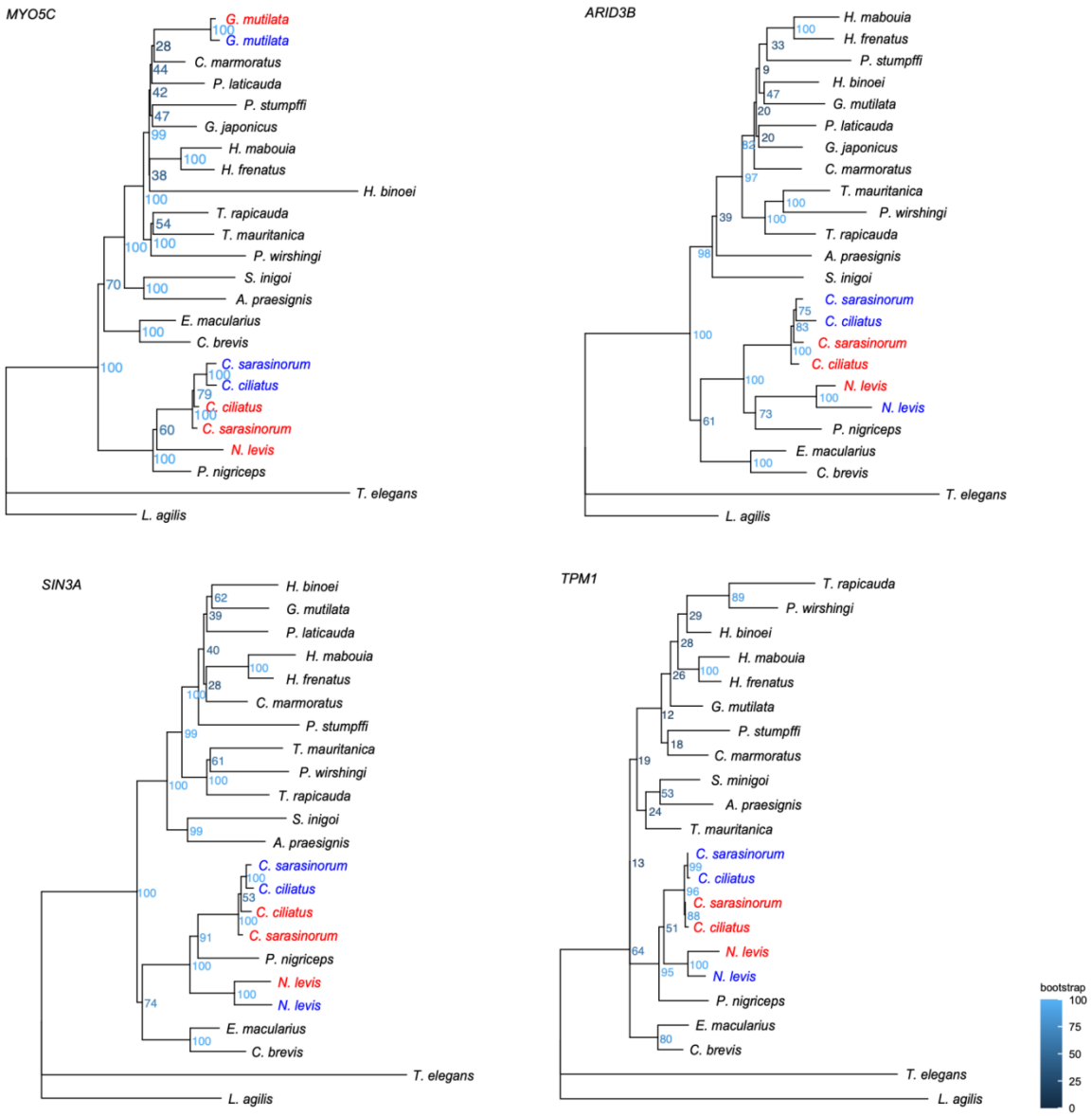

Fig. S15. Phylogenetic trees of example Z/W gametologs in *Correlophus sarasinorum*, *Correlophus ciliatus* and *Nephrurus levis*, all of which use GAC14 as their sex chromosome. Gene names are color-coded according to chromosomes (red, Z; blue, W; black, autosome/PAR). The Z-linked *Correlophus sarasinorum* - *Correlophus ciliatus* cluster and the W-linked *Correlophus sarasinorum* - *Correlophus ciliatus* cluster suggest the Z/W divergence happened before their speciation. The separated clustering of Z- and W-linked *Nephrurus levis* genes and *G.* suggests independent Z/W evolution in *Nephrurus levis* and *Gehyra insulensis.*

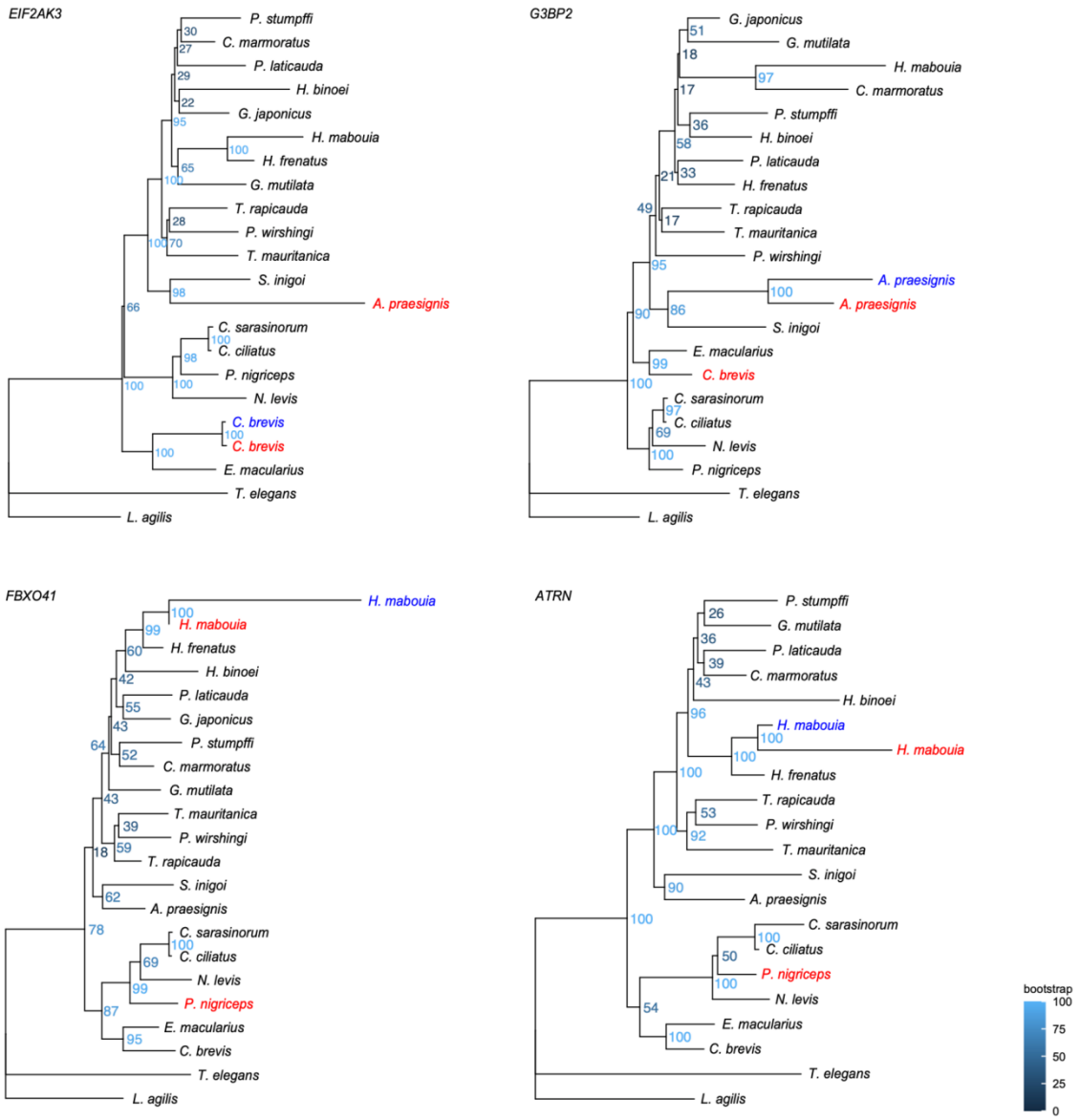

Fig. S16. Phylogenetic trees of exampled X/Y and Z/W gametologs in *Aristelliger praesignis* and *Coleonyx brevis* both of which use GAC10 as the sex chromosome, and in *Hemidactylus mabouia* and *Pygopus nigriceps* both of which use GAC11 as the sex chromosome. Gene names are color-coded according to chromosomes (red, X/Z; blue, Y/W; black, autosome/PAR).

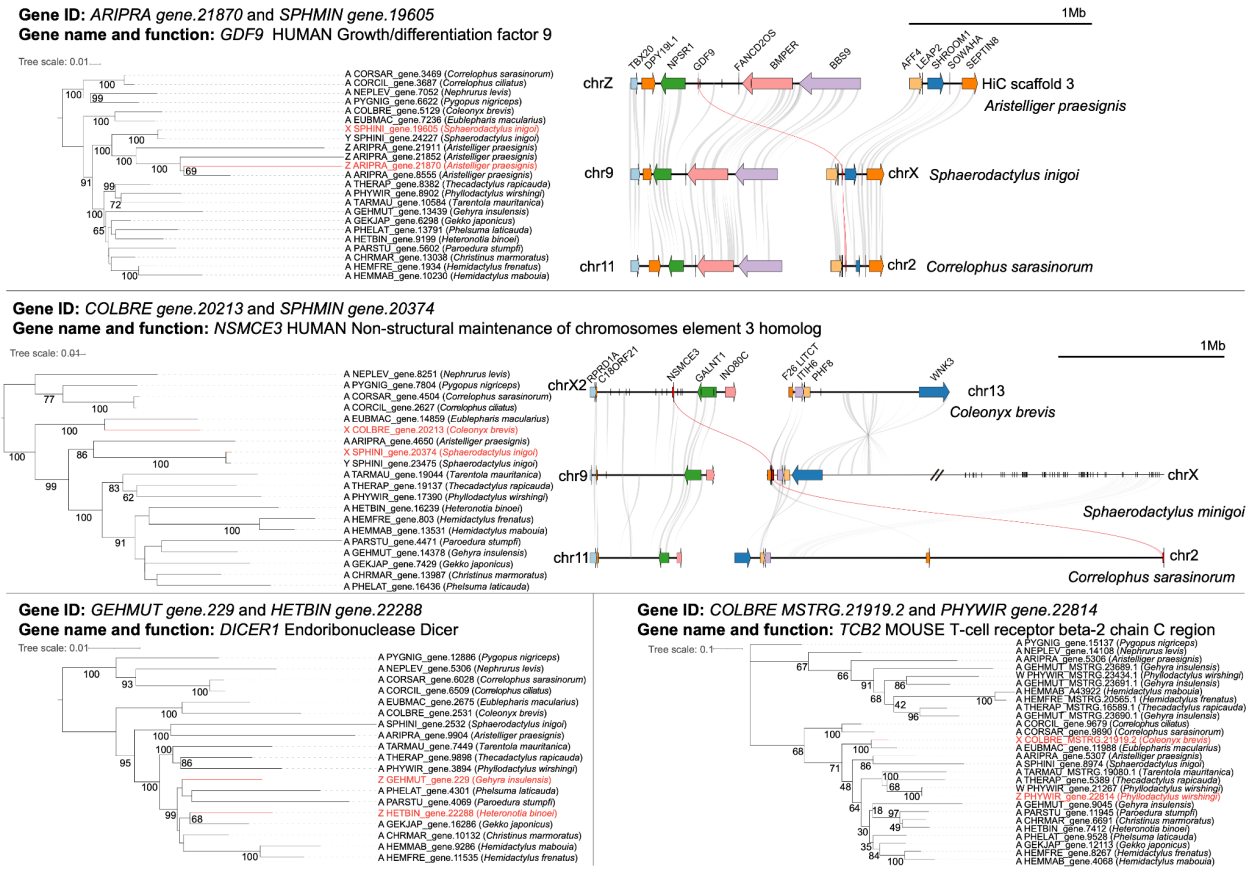

Fig. S17. Phylogenetic tree and collinearity map of the translocated gene and its flanking genes.

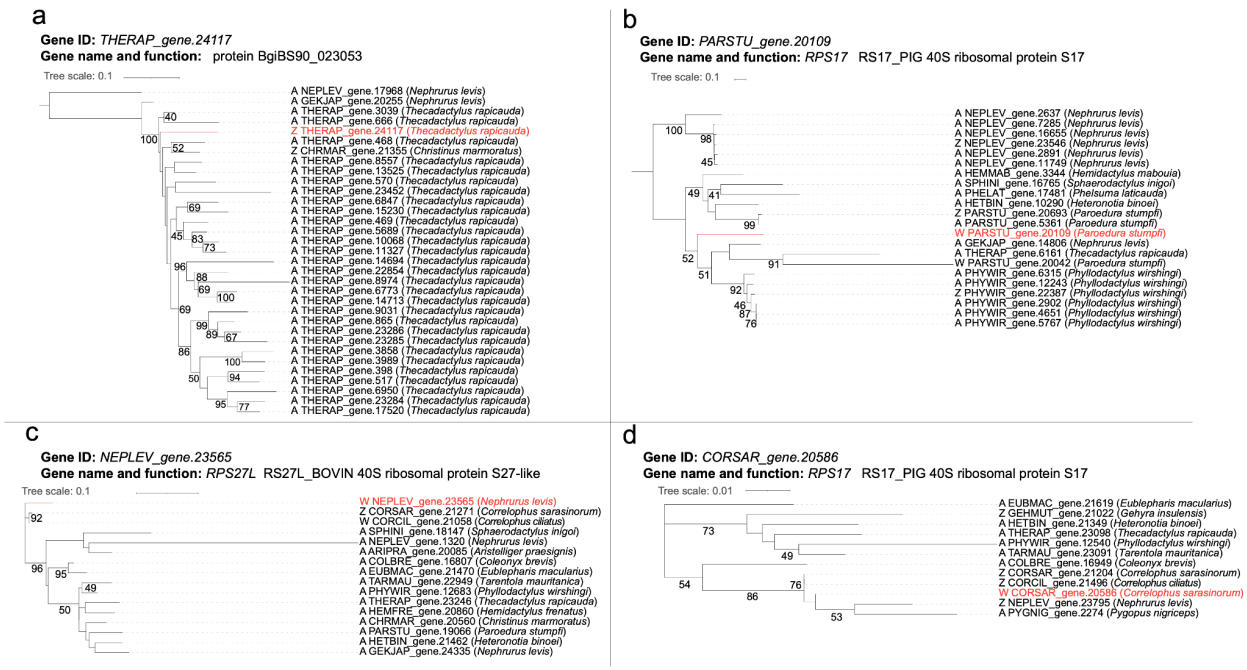

Fig. S18. Phylogeny of one Z-SDR gene (a) and three W-SDR genes (b, c, d) that cluster by species.

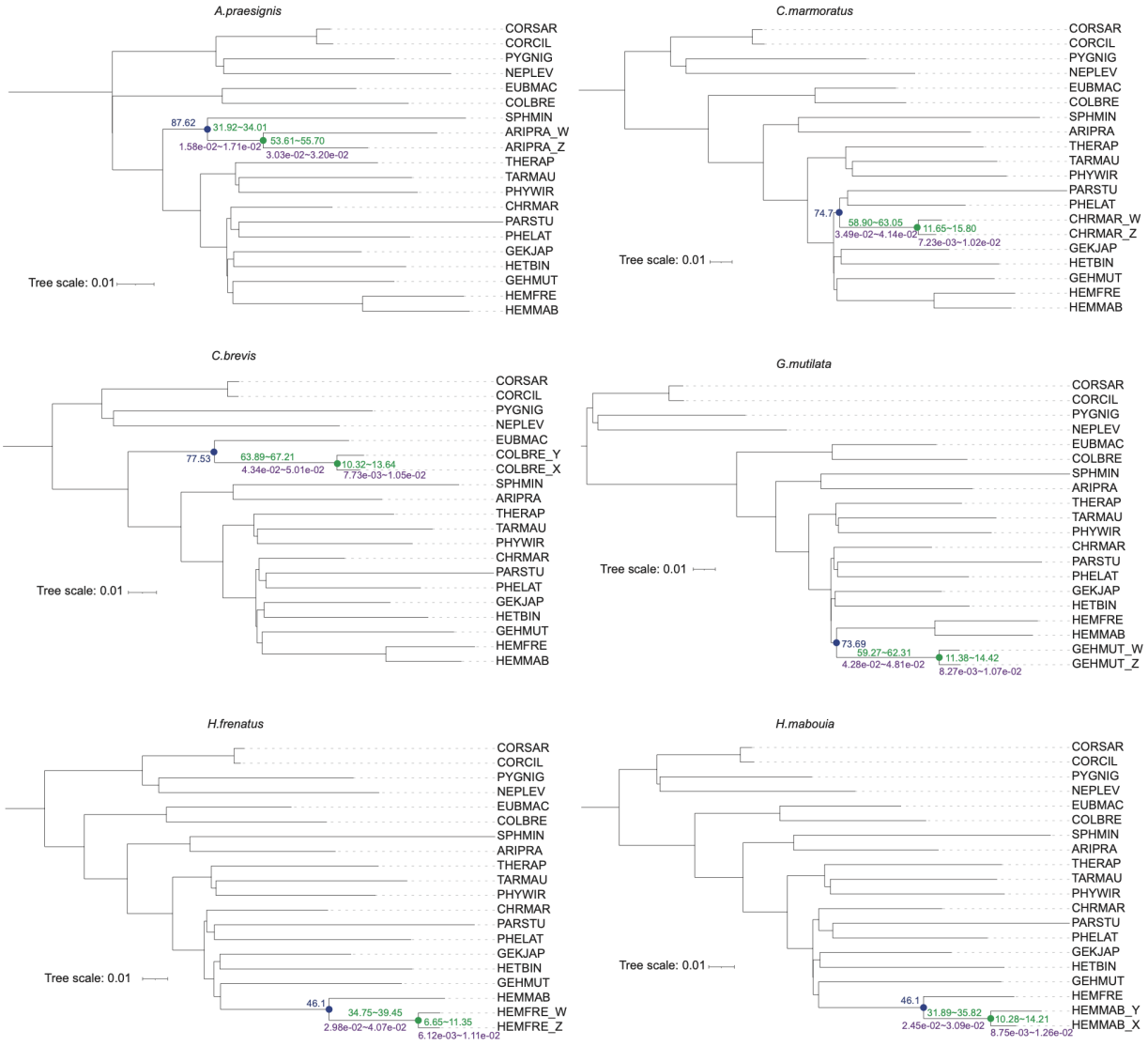

Fig. S19. Sex chromosome age estimate of each gecko. Phylogenetic trees were constructed based on the genome alignment and branch length indicates the substitution rate estimated by PAML baseml. The blue is species divergence time. The 95% confidence intervals of substitution rate and inferred corresponding millions of years (mutation-rate corrected) are shown in purple and green, respectively.

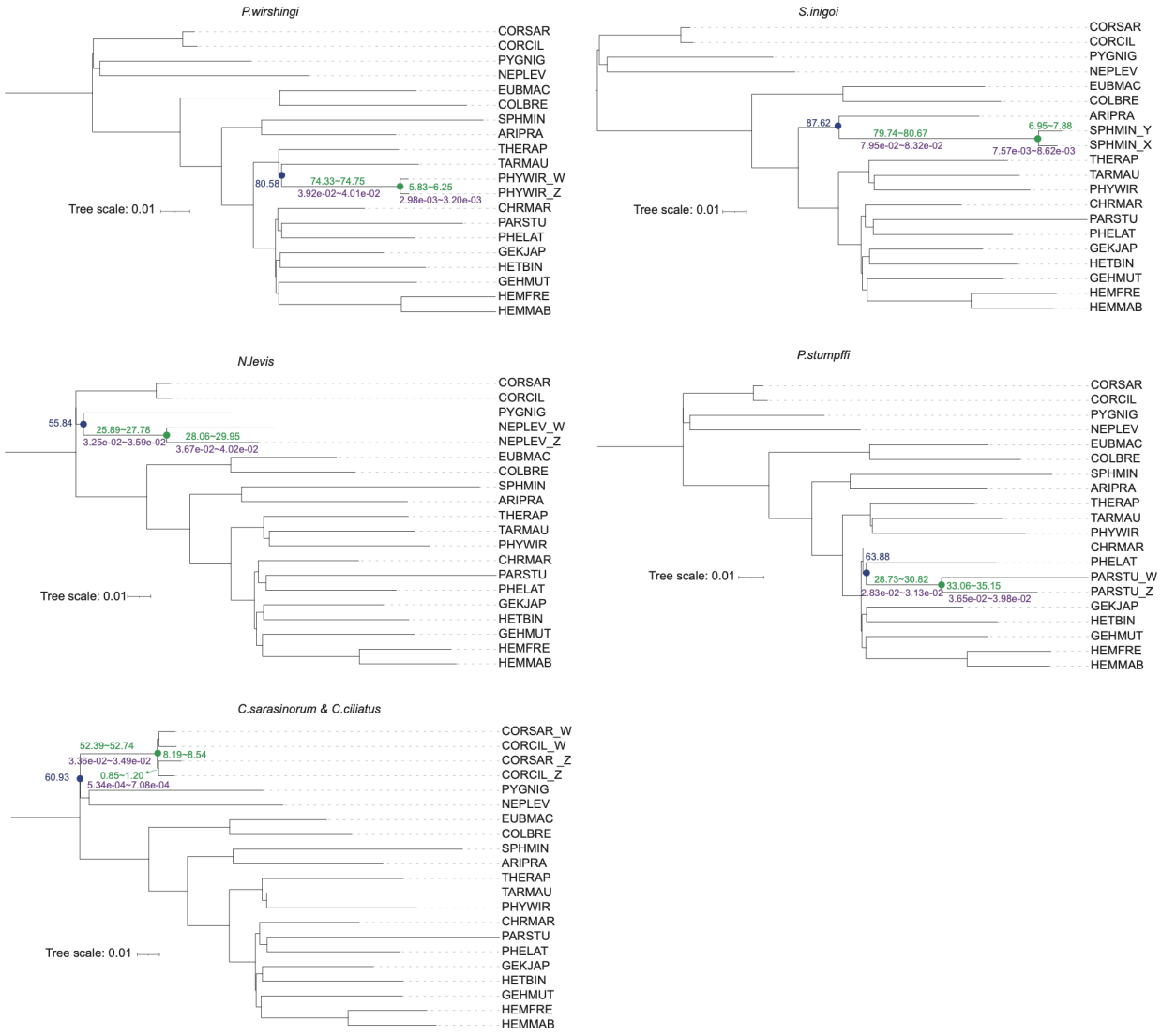

Fig. S20. Sex chromosome age estimate of each gecko. Phylogenetic trees were constructed based on the genome alignment and branch length indicates the substitution rate estimated by PAML baseml. The blue is species divergence time. The 95% confidence intervals of substitution rate and inferred corresponding millions of years (mutation-rate corrected) are shown in purple and green, respectively.

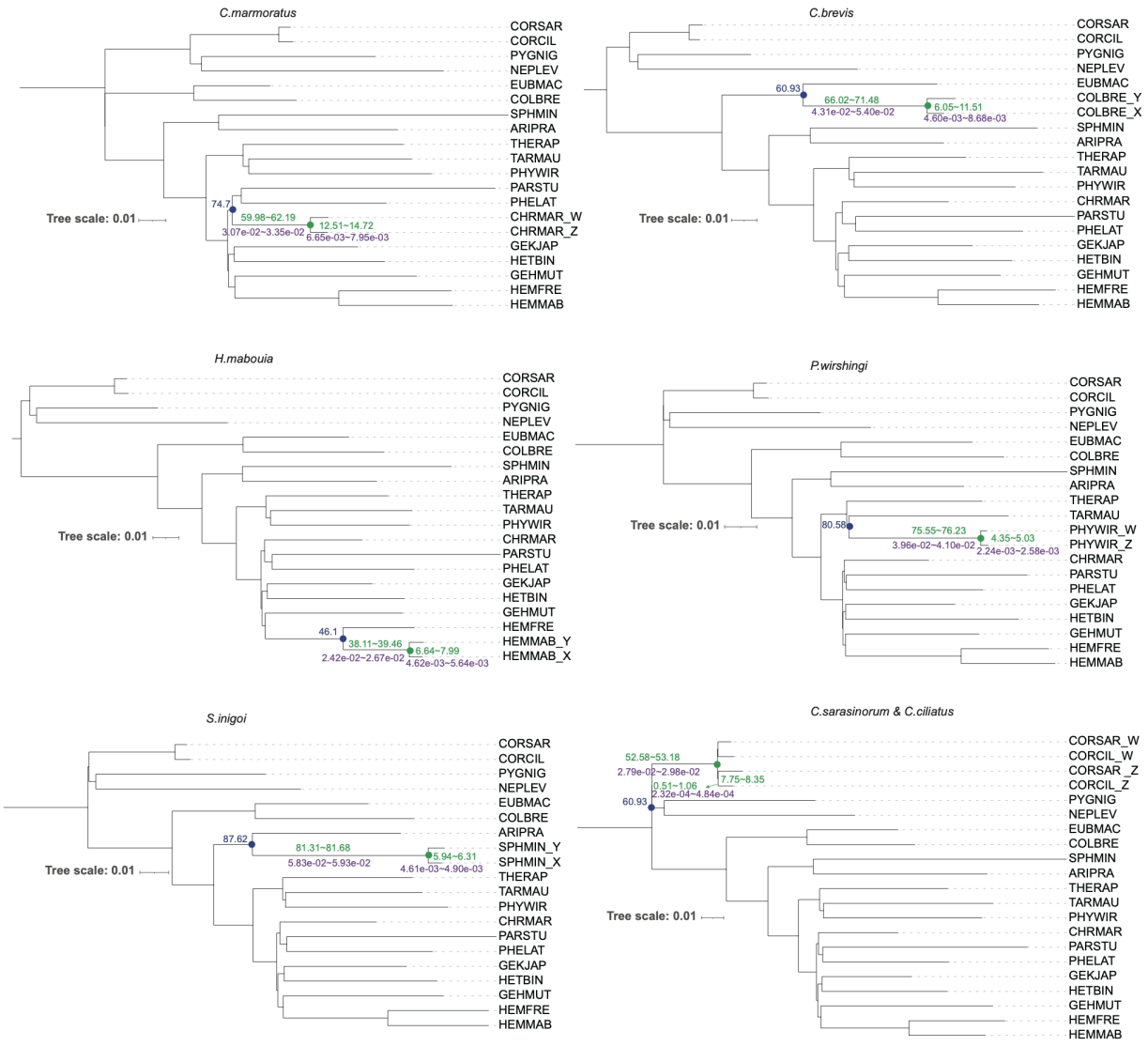

Fig. S21. The S1 age of each gecko. Phylogenetic trees were constructed based on the genome alignment and branch length indicates the substitution rate estimated by PAML baseml. The blue is species divergence time. The 95% confidence intervals of substitution rate and inferred corresponding millions of years (mutation-rate corrected) are shown in purple and green, respectively.

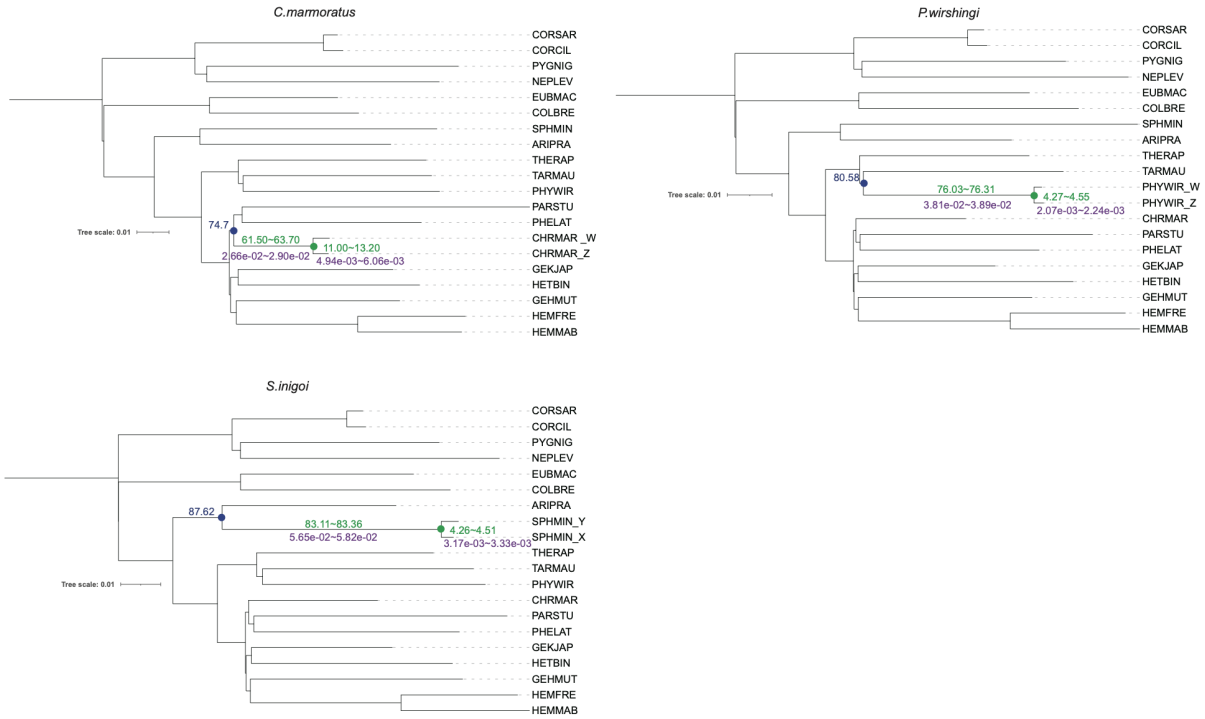

Fig. S22. The S2 age of each gecko. Phylogenetic trees were constructed based on the genome alignment and branch length indicates the substitution rate estimated by PAML baseml. The blue is species divergence time. The 95% confidence intervals of substitution rate and inferred corresponding millions of years (mutation-rate corrected) are shown in purple and green, respectively.

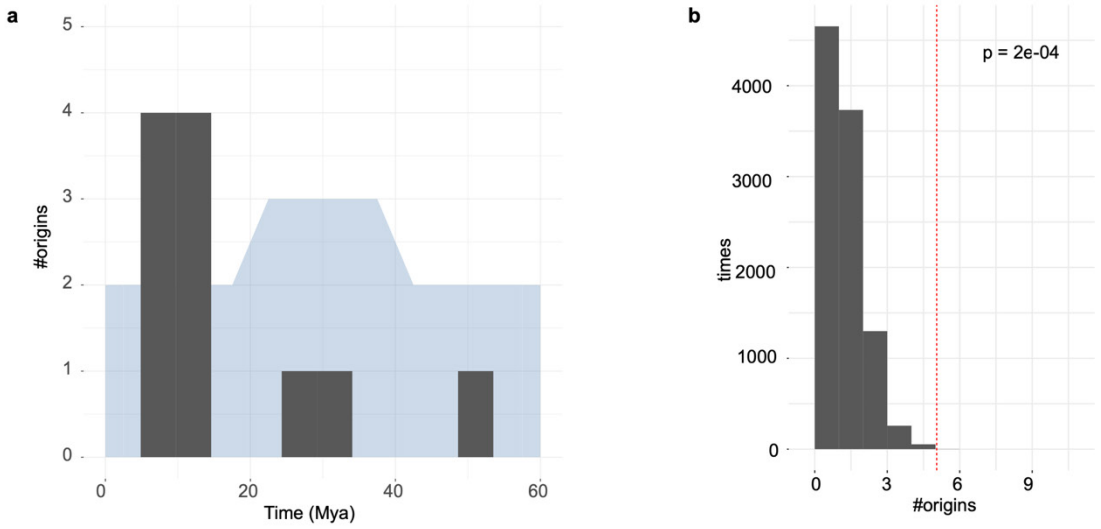

Fig. S23. Simulation and statistical test of temporal convergence around 10 MYA.
a, Comparison of the observed number of sex chromosome origins (black bars) and the null model assuming random sex chromosome origins. The blue area represents the 95% confident interval for every 5-million-year window across 10,000 simulations. Windows around 10 MYA surpass the 95% confident interval.
b, Comparison of the observed number of sex chromosome origins in 7-12 MYA window with null model generated from 10,000 simulations. The empirical p-value is calculated as the proportion of simulations that have ≥ 5, i.e., the observed sex chromosome origins, over the total 10,000 simulations.

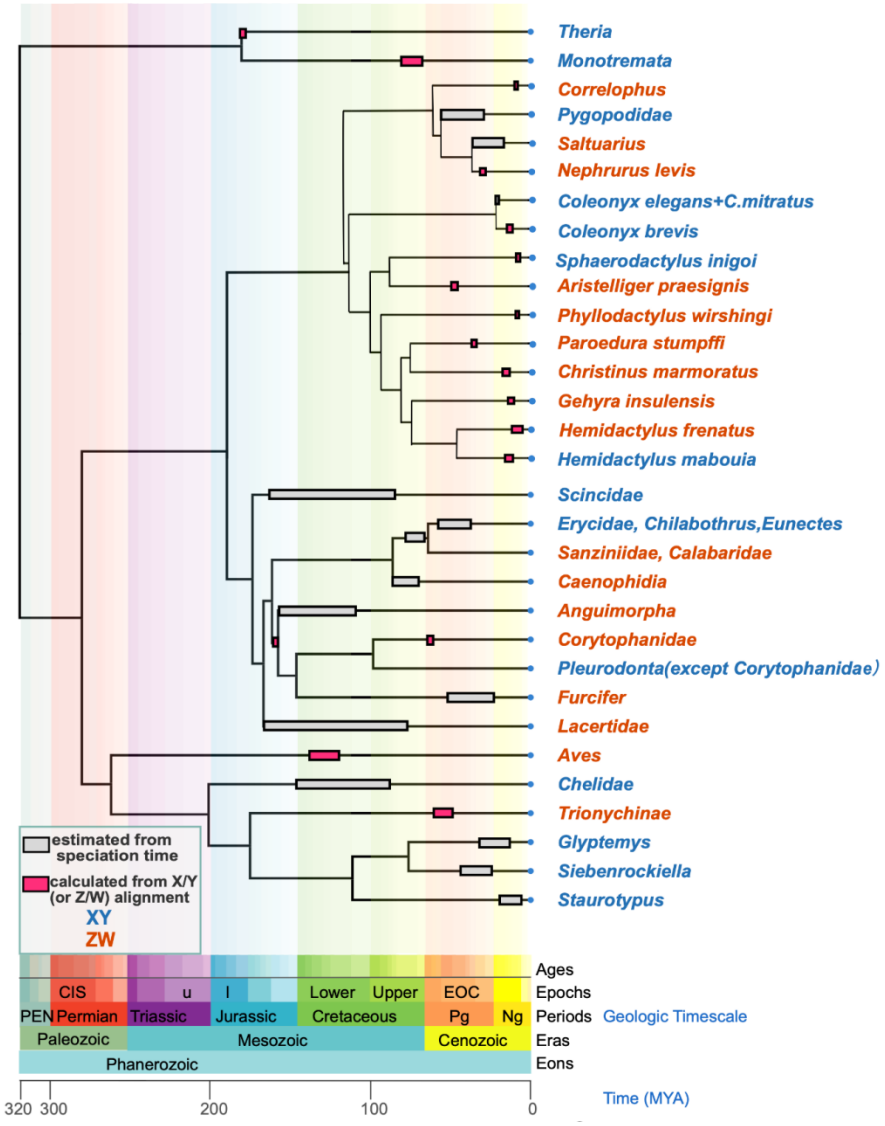

Fig. S24. Sex chromosome origin ages in amniotes. Red bars indicate robust estimates of sex chromosome ages estimated from X/Y (or Z/W) sequence divergence, while grey bars indicate rough estimates from speciation events. Data used for the plot are in Table S19.

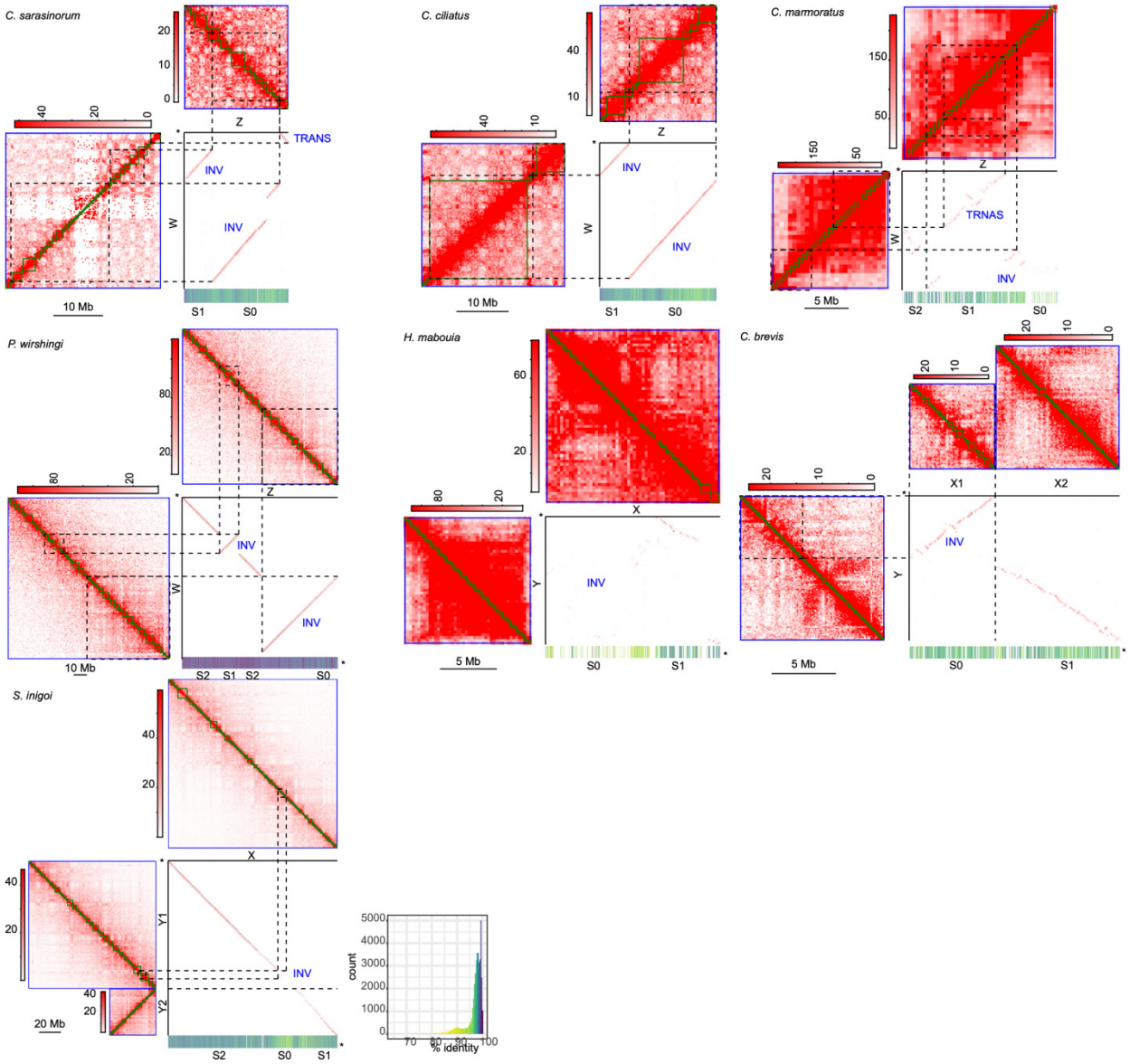

Fig. S25. Hi-C examination of the SVs between X and Y (and Z and W). SVs are highlighted with dashlines, and the color indicates whether it happens on X/Z (red) or Y/W (blue). TRANS, translocation; INV, inversion. The X/Z and Y/W are oriented so that the top left are regions closed to PAR. Regions close to PAR are indicated by asterisks. Sequence identities are also plotted along the X and Z chromosomes at the bottom. Demarcated strata are shown at the bottom. Only GSD species with >70% of Y-/W-linked sequences assembled onto one scaffold are shown.

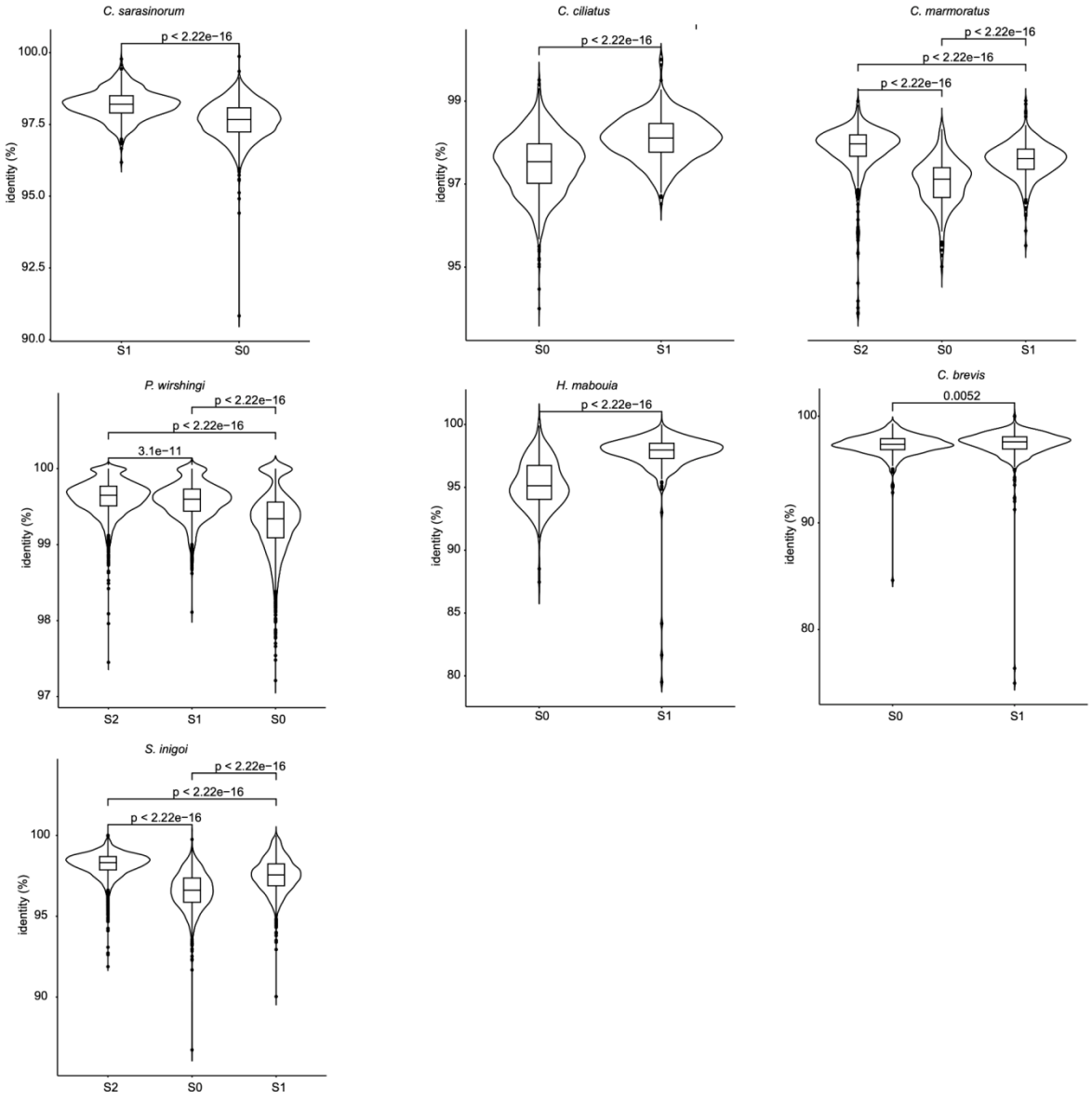

Fig. S26. Significant difference of sequence identity across examined regions (Wilcoxon rank sum test p.value < 0.05), suggesting that these species exhibit stepwise strata pattern in sex chromosome evolution.

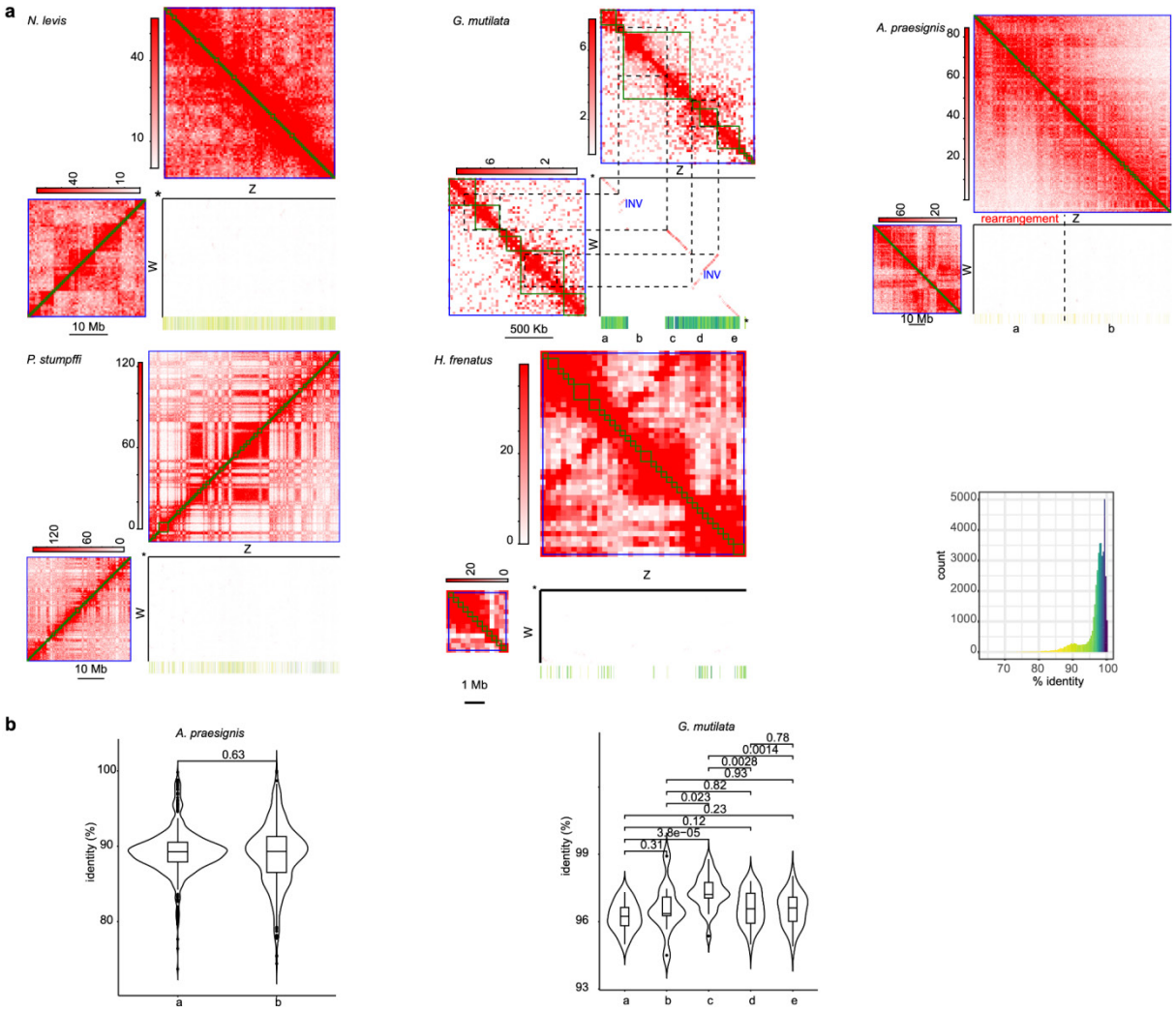

Fig. S27. Hi-C examination of the SVs between X and Y (and Z and W).

a, SVs are highlighted with dashlines, and the color indicates whether it happens on X/Z (red) or Y/W (blue). TRANS, translocation; INV, inversion. The X/Z and Y/W are oriented so that the top left are regions closed to PAR. Regions close to PAR are indicated by asterisks. Sequence identities are also plotted along the X and Z chromosomes at the bottom. Regions used in identity comparison are shown at the bottom. Only GSD species with >70% of Y-/W-linked sequences assembled onto one scaffold are shown.

b, No significant difference of sequence identity across examined regions (Wilcoxon rank sum test p.value > 0.01), suggesting that they do not exhibit stepwise strata pattern in sex chromosome evolution.

Fig. S28. Significant difference of gametolog pairwise dS across examined regions (Wilcoxon rank sum test p.value < 0.05) in *Correlophus sarasinorum, Correlophus ciliatus, Phyllodactylus wirshingi, Christinus marmoratus, Sphaerodactylus inigoi, Coleonyx brevis, Hemidactylus mabouia*, suggesting that these species exhibit stepwise strata pattern in sex chromosome evolution of these species. In contrast, no strata pattern is observed in *Paroedura stumpffi, Aristelliger praesignis, Gehyra insulensis, Nephrurus levis, Hemidactylus frenatus*.

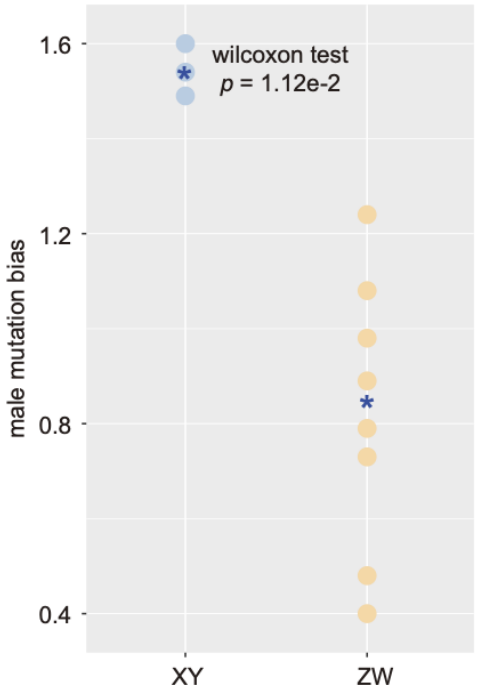

Fig. S29. Comparison male mutation bias between XY and ZW gecko species. Circles present the estimated male mutation bias and asterisks present the median value.

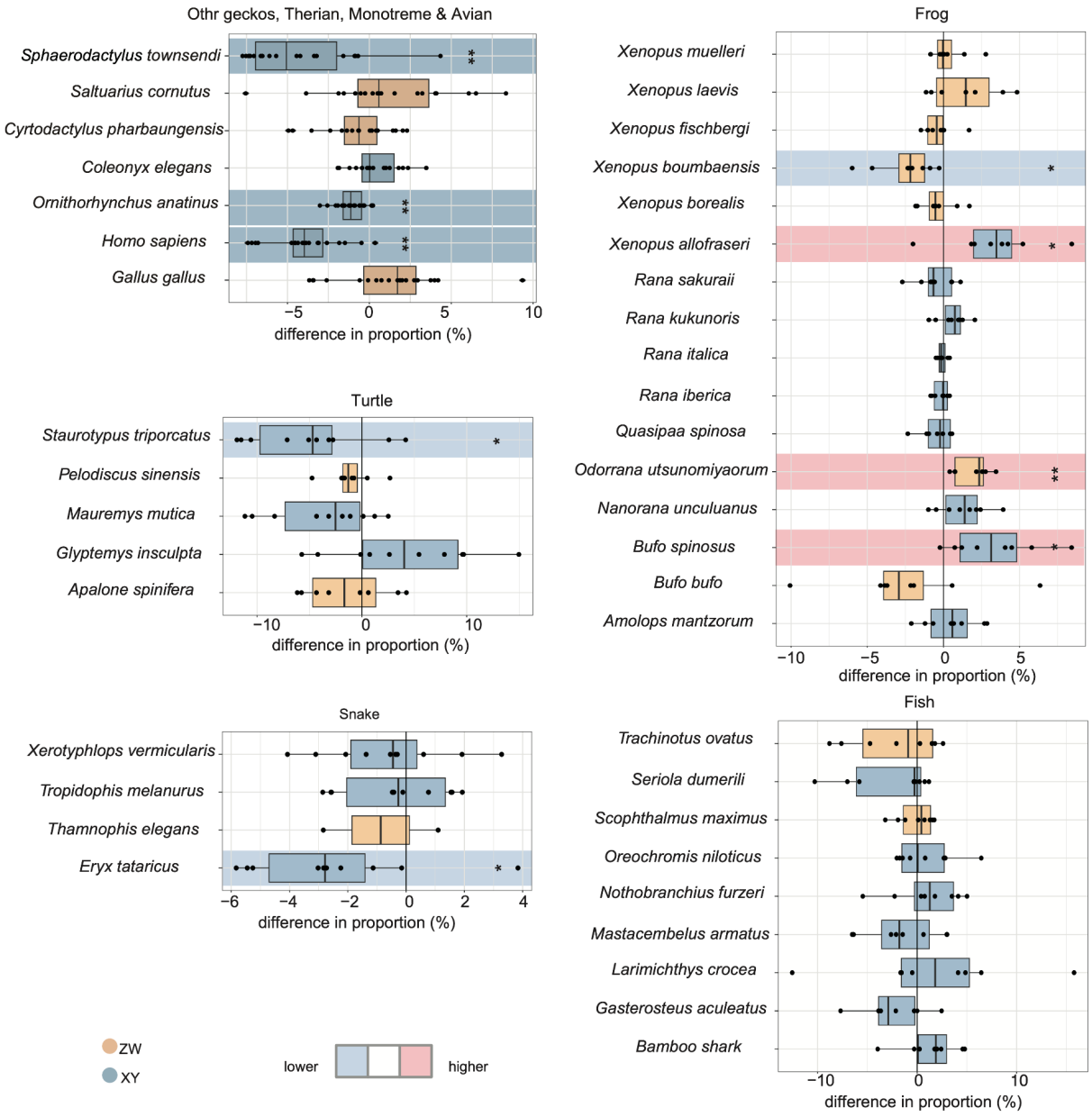

Fig. S30. Boxplot shows the ancestral proportion of testis preferentially expressed genes on the X/Z-SDR of each species compared to the proportion of gonad-bias genes from genomic background. Black dots indicate the ancestral states indicative by the difference in outgroup species. '**' indicates p-value < 0.01 and '*' indicates p-value < 0.05. Deviation direction is shown as the background in each boxplot: red, significantly higher than genomic background in outgroups; blue, significantly lower than genomic background in outgroups; white, no significant difference.

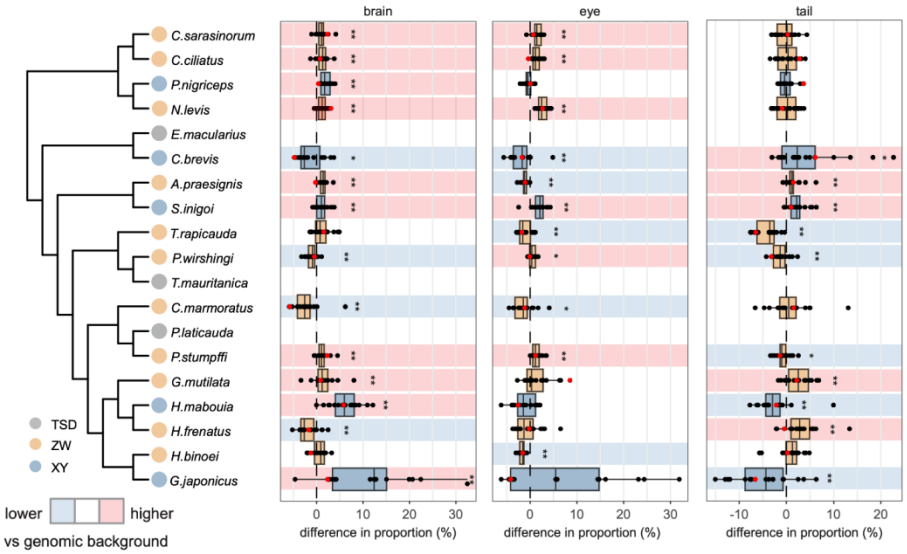

Fig. S31. Difference in the proportion of brain, eye, tail preferentially expressed genes on S0 of the X/Z-SDR and genomic background in each gecko (red) and the difference of orthologous genes in other geckos (black). Deviation direction is shown as the background in each boxplot: red, significantly higher than genomic background in geckos; blue, significantly lower than genomic background in geckos; white, no significant difference. '**' indicates p-value < 0.01 and '*' indicates p-value < 0.05.

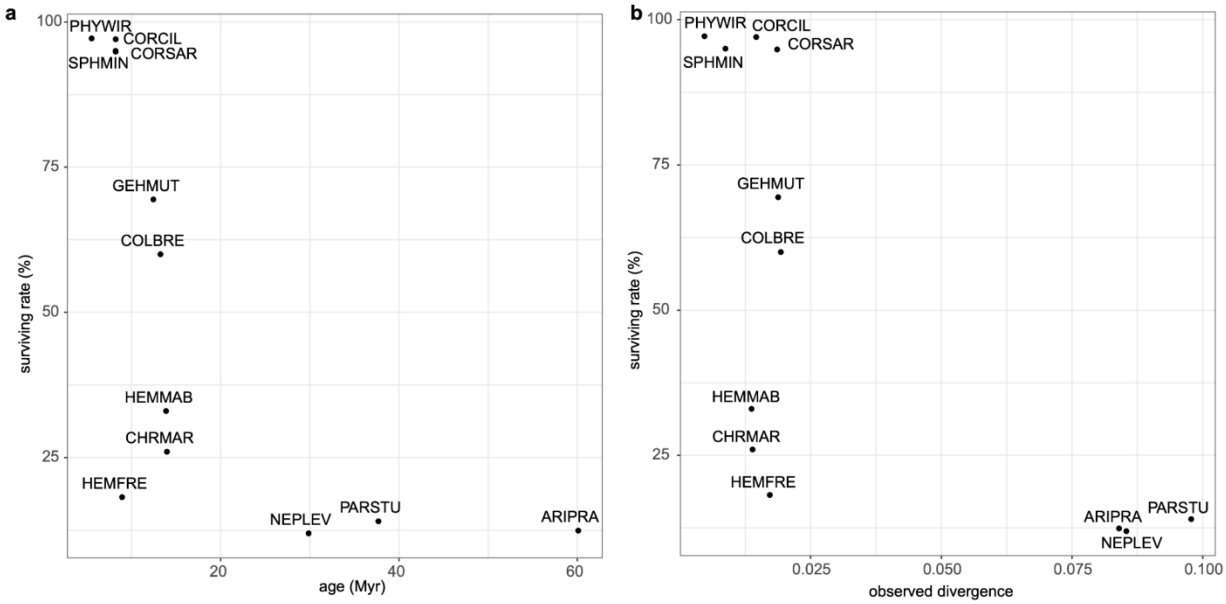

Fig. S32. Correlation between different degeneration metrics.
a, Correlation between Y/W gene surviving rate and age.
b, Correlation between Y/W gene surviving rate and observed sex chromosome divergence.

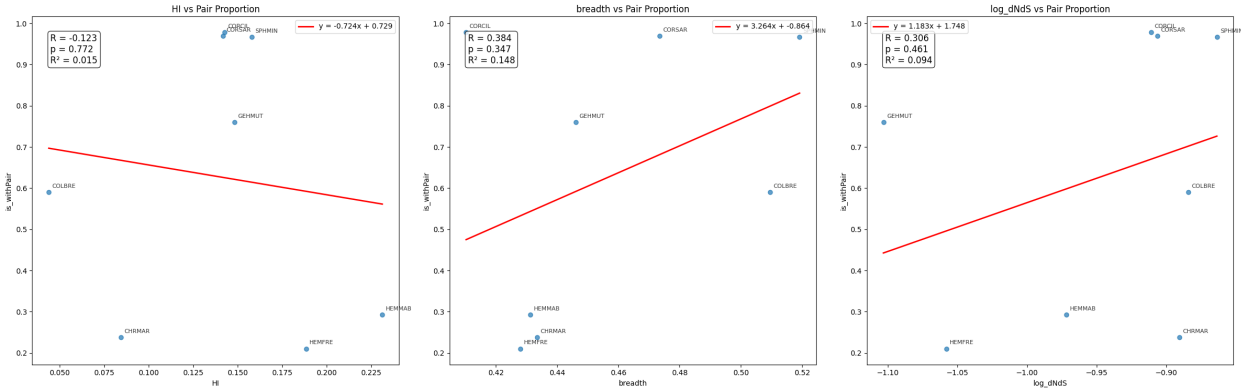

Fig. S33. Correlation between survival rate and HI score (left), expression breadth (middle) and log(dN/dS) (right).

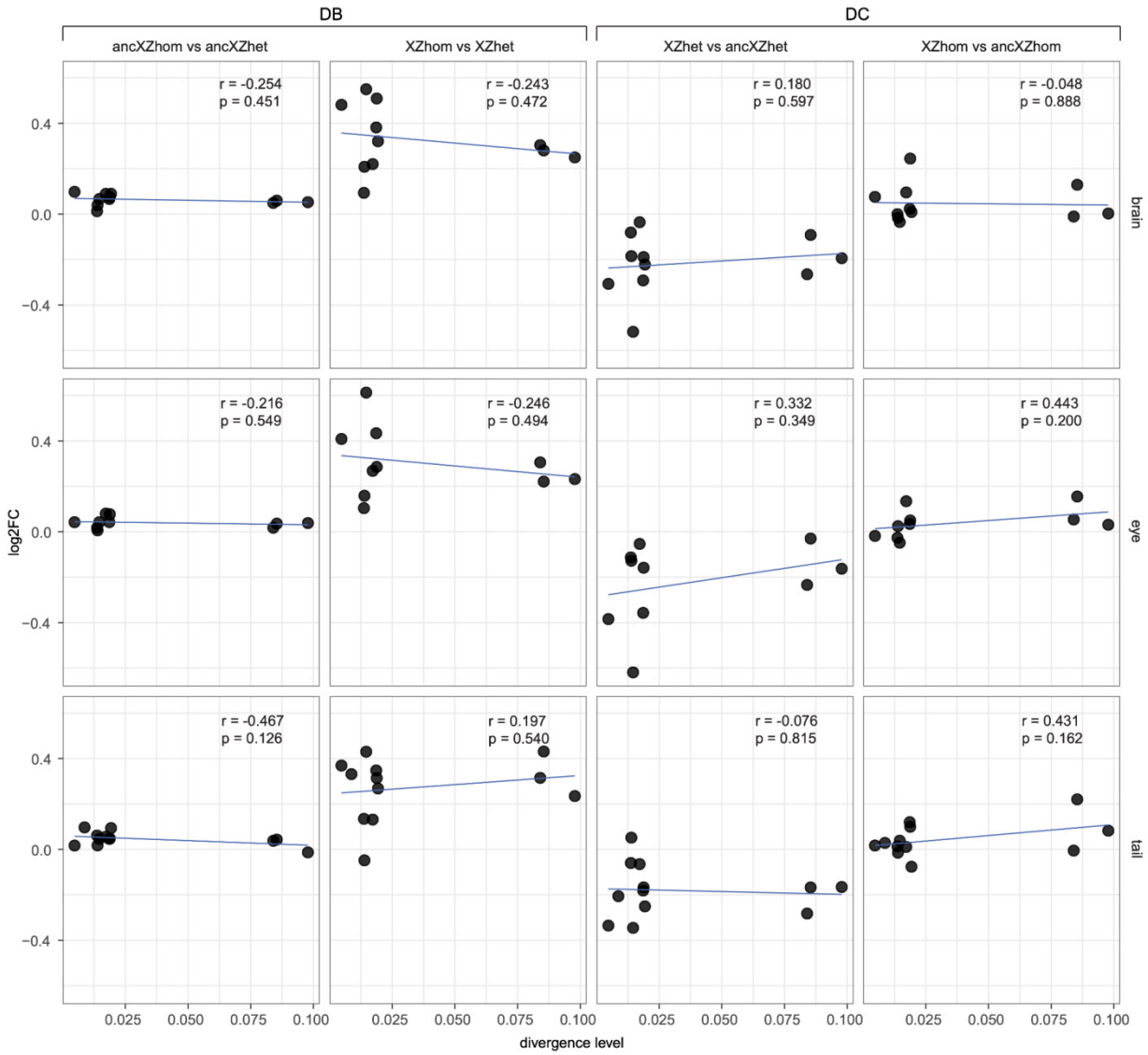

Fig. S34. Correlation between the extent of dosage balance (DB) and dosage compensation (DC) and sex chromosome divergence. For each tissue, we used the log2(homogametic/heterogametic) value estimated from the fitted model. ancXZhom, proto sex chromosome genes in homogametic sex; ancXZhet, proto sex chromosome genes in heterogametic sex; XZhom, X/Z genes in homogametic sex; XZhet, X/Z genes in heterogametic sex.

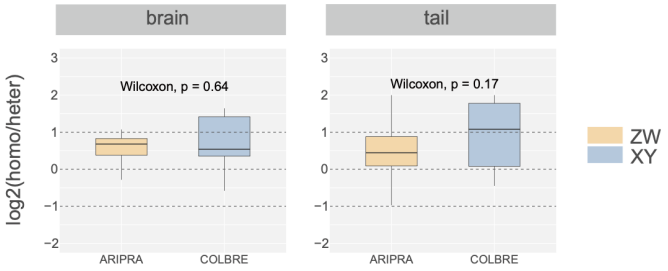

Fig. S35. Comparison of the log2(homogametic/heterogametic expression ratio) in somatic tissue of the shared 27 SDR genes between *Aristelliger praesignis* and *Coleonyx brevis*.

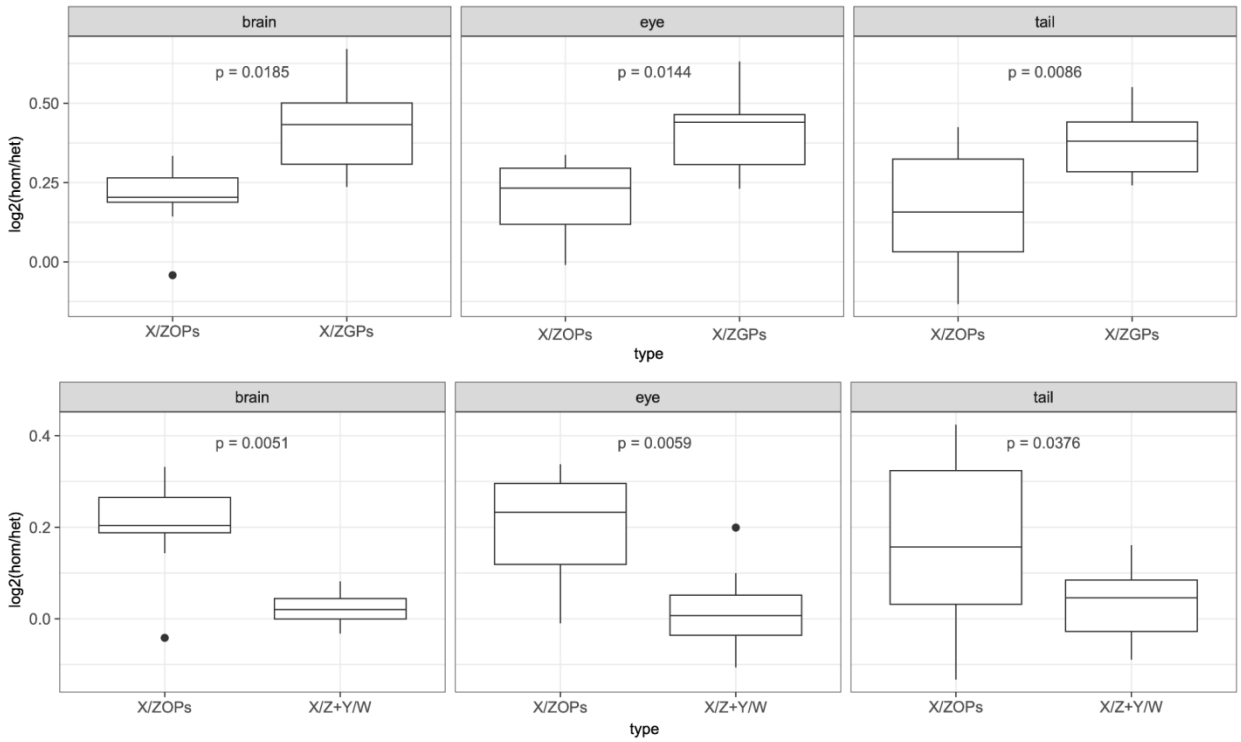

Fig. S36. Comparison of homogametic-vs-heterogametic estimated ratio between X/ZOPs and X/ZGPs (upper) and between X/ZOPs and X/Z+Y/W (lower). P-values are calculated by paired Wilcoxon ranksum test.

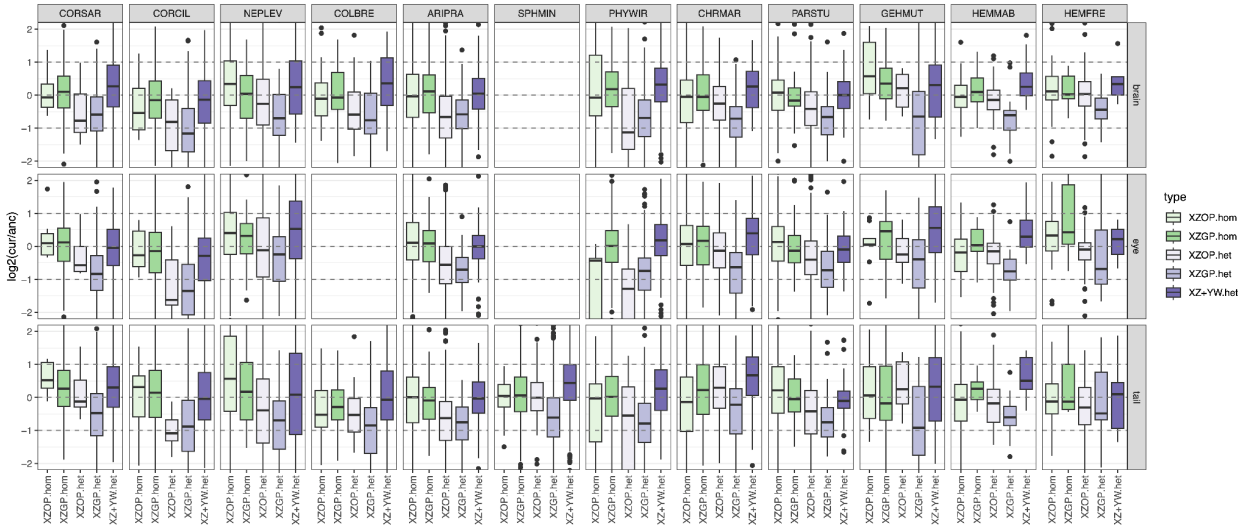

Fig. S37. Boxplots showing the degree of dosage compensation (i.e., current-vs-ancestral expression ratio) of X/Z-linked genes in homogametic sex and heterogametic sex. Hom, homogametic sex; het, heterogametic sex. XZOP, X/Z genes without gametolog pair, XZGP, X/Z genes with gametolog pair; XZ+YW: combining the expression of X/Z gene with its Y/W gametolog pair.

References and Notes

1. J. J. Bull, Sex determining mechanisms: An evolutionary perspective. *Experientia* **41**, 1285–1296 (1985). doi:10.1007/BF01952071 Medline

2. B. L. S. Furman, D. C. H. Metzger, I. Darolti, A. E. Wright, B. A. Sandkam, P. Almeida, J. J. Shu, J. E. Mank, Sex chromosome evolution: So many exceptions to the rules. *Genome Biol. Evol.* **12**, 750–763 (2020). doi:10.1093/gbe/evaa081 Medline

3. B. Vicoso, Molecular and evolutionary dynamics of animal sex-chromosome turnover. *Nat. Ecol. Evol.* **3**, 1632–1641 (2019). doi:10.1038/s41559-019-1050-8 Medline

4. L. Kratochvíl, M. Stöck, M. Rovatsos, M. Bullejos, A. Herpin, D. L. Jeffries, C. L. Peichel, N. Perrin, N. Valenzuela, M. J. Pokorná, Expanding the classical paradigm: What we have learnt from vertebrates about sex chromosome evolution. *Philos. Trans. R. Soc. London Ser. B* **376**, 20200097 (2021). doi:10.1098/rstb.2020.0097 Medline

5. S. D. Sarre, T. Ezaz, A. Georges, Transitions between sex-determining systems in reptiles and amphibians. *Annu. Rev. Genomics Hum. Genet.* **12**, 391–406 (2011). doi:10.1146/annurev-genom-082410-101518 Medline

6. T. Ezaz, K. Srikulnath, J. A. Graves, Origin of amniote sex chromosomes: An ancestral super-sex chromosome, or common requirements? *J. Hered.* **108**, 94–105 (2017). doi:10.1093/jhered/esw053 Medline

7. D. Bachtrog, M. Kirkpatrick, J. E. Mank, S. F. McDaniel, J. C. Pires, W. Rice, N. Valenzuela, Are all sex chromosomes created equal? *Trends Genet.* **27**, 350–357 (2011). doi:10.1016/j.tig.2011.05.005 Medline

8. L. Kratochvíl, T. Gamble, M. Rovatsos, Sex chromosome evolution among amniotes: Is the origin of sex chromosomes non-random? *Philos. Trans. R. Soc. London Ser. B* **376**, 20200108 (2021). doi:10.1098/rstb.2020.0108 Medline

9. E. Adkins-Regan, H. K. Reeve, Sexual dimorphism in body size and the origin of sex-determination systems. *Am. Nat.* **183**, 519–536 (2014). doi:10.1086/675303 Medline

10. T. Lesaffre, J. R. Pannell, C. Mullon, An explanation for the prevalence of XY over ZW sex determination in species derived from hermaphroditism. *Proc. Natl. Acad. Sci. U.S.A.* **121**, e2406305121 (2024). doi:10.1073/pnas.2406305121 Medline

11. A. E. Wright, R. Dean, F. Zimmer, J. E. Mank, How to make a sex chromosome. *Nat. Commun.* **7**, 12087 (2016). doi:10.1038/ncomms12087 Medline

12. Z. Zhu, L. Younas, Q. Zhou, Evolution and regulation of animal sex chromosomes. *Nat. Rev. Genet.* **26**, 59–74 (2025). doi:10.1038/s41576-024-00757-3 Medline

13. J. A. M. Graves, Evolution of vertebrate sex chromosomes and dosage compensation. *Nat. Rev. Genet.* **17**, 33–46 (2016). doi:10.1038/nrg.2015.2 Medline

14. P. A. Saunders, A. Muyle, Sex chromosome evolution: Hallmarks and question marks. *Mol. Biol. Evol.* **41**, msae218 (2024). doi:10.1093/molbev/msae218 Medline

15. D. Bachtrog, J. E. Mank, C. L. Peichel, M. Kirkpatrick, S. P. Otto, T.-L. Ashman, M. W. Hahn, J. Kitano, I. Mayrose, R. Ming, N. Perrin, L. Ross, N. Valenzuela, J. C. Vamosi;

Tree of Sex Consortium, Sex determination: Why so many ways of doing it? *PLOS Biol.* **12**, e1001899 (2014). doi:10.1371/journal.pbio.1001899 Medline

16. D. Bachtrog, Y-chromosome evolution: Emerging insights into processes of Y-chromosome degeneration. *Nat. Rev. Genet.* **14**, 113–124 (2013). doi:10.1038/nrg3366 Medline

17. M. Pokorná, L. Kratochvíl, Phylogeny of sex-determining mechanisms in squamate reptiles: Are sex chromosomes an evolutionary trap? *Zool. J. Linn. Soc.* **156**, 168–183 (2009). doi:10.1111/j.1096-3642.2008.00481.x

18. T. Gamble, J. Coryell, T. Ezaz, J. Lynch, D. P. Scantlebury, D. Zarkower, Restriction site-associated DNA sequencing (RAD-seq) reveals an extraordinary number of transitions among gecko sex-determining systems. *Mol. Biol. Evol.* **32**, 1296–1309 (2015). doi:10.1093/molbev/msv023 Medline

19. B. Augstenová, E. Pensabene, M. Veselý, L. Kratochvíl, M. Rovatsos, Are geckos special in sex determination? Independently evolved differentiated ZZ/ZW sex chromosomes in carphodactylid geckos. *Genome Biol. Evol.* **13**, evab119 (2021). doi:10.1093/gbe/evab119 Medline

20. T. Gamble, A review of sex determining mechanisms in geckos (Gekkota: Squamata). *Sex Dev.* **4**, 88–103 (2010). doi:10.1159/000289578 Medline

21. O. Wang, R. Chin, X. Cheng, M. K. Y. Wu, Q. Mao, J. Tang, Y. Sun, E. Anderson, H. K. Lam, D. Chen, Y. Zhou, L. Wang, F. Fan, Y. Zou, Y. Xie, R. Y. Zhang, S. Drmanac, D. Nguyen, C. Xu, C. Villarosa, S. Gablenz, N. Barua, S. Nguyen, W. Tian, J. S. Liu, J. Wang, X. Liu, X. Qi, A. Chen, H. Wang, Y. Dong, W. Zhang, A. Alexeev, H. Yang, J. Wang, K. Kristiansen, X. Xu, R. Drmanac, B. A. Peters, Efficient and unique cobarcoding of second-generation sequencing reads from long DNA molecules enabling cost-effective and accurate sequencing, haplotyping, and de novo assembly. *Genome Res.* **29**, 798–808 (2019). doi:10.1101/gr.245126.118 Medline

22. M. Schmid, C. Steinlein, T. Haaf, A. Mijares-Urrutia, Nascent ZW sex chromosomes in *Thecadactylus rapicauda* (Reptilia, Squamata, Phyllodactylidae). *Cytogenet. Genome Res.* **143**, 259–267 (2014). doi:10.1159/000366212 Medline

23. C. Moritz, Parthenogenesis in the endemic Australian lizard *Heteronotia binoei* (Gekkonidae). *Science* **220**, 735–737 (1983). doi:10.1126/science.220.4598.735 Medline

24. Y. Shibaike, Y. Takahashi, I. Arikura, R. Iiizumi, S. Kitakawa, M. Sakai, C. Imaoka, H. Shiro, H. Tanaka, N. Akakubo, M. Nakano, M. Watanabe, K. Ohne, S. Kubota, S. Kohno, H. Ota, Chromosome evolution in the lizard genus *Gekko* (Gekkonidae, Squamata, Reptilia) in the East Asian islands. *Cytogenet. Genome Res.* **127**, 182–190 (2009). doi:10.1159/000303334 Medline

25. M. Rovatsos, T. Gamble, S. V. Nielsen, A. Georges, T. Ezaz, L. Kratochvíl, Do male and female heterogamety really differ in expression regulation? Lack of global dosage balance in pygopodid geckos. *Philos. Trans. R. Soc. London Ser. B* **376**, 20200102 (2021). doi:10.1098/rstb.2020.0102 Medline

26. B. J. Pinto, S. E. Keating, S. V. Nielsen, D. P. Scantlebury, J. D. Daza, T. Gamble, Chromosome-level genome assembly reveals dynamic sex chromosomes in neotropical

leaf-litter geckos (Sphaerodactylidae: *Sphaerodactylus*). *J. Hered.* **113**, 272–287 (2022). doi:10.1093/jhered/esac016 Medline

27. M. Pokorná, M. Rábová, P. Ráb, M. A. Ferguson-Smith, W. Rens, L. Kratochvíl, Differentiation of sex chromosomes and karyotypic evolution in the eye-lid geckos (Squamata: Gekkota: Eublepharidae), a group with different modes of sex determination. *Chromosome Res.* **18**, 809–820 (2010). doi:10.1007/s10577-010-9154-7 Medline

28. S. E. Keating, E. Greenbaum, J. D. Johnson, T. Gamble, Identification of a cis-sex chromosome transition in banded geckos (Coleonyx, Eublepharidae, Gekkota). *J. Evol. Biol.* **35**, 1675–1682 (2022). doi:10.1111/jeb.14022 Medline

29. S. E. Keating, A. H. Griffing, S. V. Nielsen, D. P. Scantlebury, T. Gamble, Conserved ZZ/ZW sex chromosomes in Caribbean croaking geckos (*Aristelliger*: Sphaerodactylidae). *J. Evol. Biol.* **33**, 1316–1326 (2020). doi:10.1111/jeb.13682 Medline

30. S. V. Nielsen, J. D. Daza, B. J. Pinto, T. Gamble, ZZ/ZW sex chromosomes in the endemic Puerto Rican leaf-toed gecko (*Phyllodactylus wirshingi*). *Cytogenet. Genome Res.* **157**, 89–97 (2019). doi:10.1159/000496379 Medline

31. V. A. Trifonov, M. Giovannotti, P. C. M. O'Brien, M. Wallduck, F. Lovell, W. Rens, P. P. Parise-Maltempi, V. Caputo, M. A. Ferguson-Smith, Chromosomal evolution in Gekkonidae. I. Chromosome painting between *Gekko* and *Hemidactylus* species reveals phylogenetic relationships within the group. *Chromosome Res.* **19**, 843–855 (2011). doi:10.1007/s10577-011-9241-4 Medline

32. K. McBee, J. Bickham, J. Dixon, Male heterogamety and chromosomal variation in Caribbean geckos. *J. Herpetol.* **21**, 68–71 (1987). doi:10.2307/1564380

33. M. Koubová, M. Johnson Pokorná, M. Rovatsos, K. Farkačová, M. Altmanová, L. Kratochvíl, Sex determination in Madagascar geckos of the genus *Paroedura* (Squamata: Gekkonidae): are differentiated sex chromosomes indeed so evolutionary stable? *Chromosome Res.* **22**, 441–452 (2014). doi:10.1007/s10577-014-9430-z Medline

34. K. Matsubara, T. Gamble, Y. Matsuda, D. Zarkower, S. D. Sarre, A. Georges, J. A. M. Graves, T. Ezaz, Non-homologous sex chromosomes in two geckos (Gekkonidae: Gekkota) with female heterogamety. *Cytogenet. Genome Res.* **143**, 251–258 (2014). doi:10.1159/000366172 Medline

35. E. Pensabene, B. Augstenová, L. Kratochvíl, M. Rovatsos, Differentiated sex chromosomes, karyotype evolution, and spontaneous triploidy in carphodactylid geckos. *J. Hered.* **115**, 262–276 (2024). doi:10.1093/jhered/esae010 Medline

36. M. Pokorná, M. Giovannotti, L. Kratochvíl, F. Kasai, V. A. Trifonov, P. C. M. O'Brien, V. Caputo, E. Olmo, M. A. Ferguson-Smith, W. Rens, Strong conservation of the bird Z chromosome in reptilian genomes is revealed by comparative painting despite 275 million years divergence. *Chromosoma* **120**, 455–468 (2011). doi:10.1007/s00412-011-0322-0 Medline

37. J. D. Daza, V. R. Alifanov, A. M. Bauer, A redescription and phylogenetic reinterpretation of the fossil lizard *Hoburogekko suchanovi* Alifanov, 1989 (Squamata, Gekkota), from the Early Cretaceous of Mongolia. *J. Vertebr. Paleontol.* **32**, 1303–1312 (2012). doi:10.1080/02724634.2012.702706

38. R. R. Reisz, J. Müller, Molecular timescales and the fossil record: A paleontological perspective. *Trends Genet.* **20**, 237–241 (2004). doi:10.1016/j.tig.2004.03.007 Medline

39. M. Stöck, L. Kratochvíl, H. Kuhl, M. Rovatsos, B. J. Evans, A. Suh, N. Valenzuela, F. Veyrunes, Q. Zhou, T. Gamble, B. Capel, M. Schartl, Y. Guiguen, A brief review of vertebrate sex evolution with a pledge for integrative research: Towards '*sexomics*'. *Philos. Trans. R. Soc. London Ser. B* **376**, 20200426 (2021). doi:10.1098/rstb.2020.0426 Medline

40. M. King, Unbuckling the cladistic straight jacket: An exercise in elementary cytogenetics and a reply to Kluge (1994). *Herpetologica* **50**, 222–237 (1994).

41. E. Pensabene, L. Kratochvíl, M. Rovatsos, Independent evolution of sex chromosomes in eublepharid geckos, a lineage with environmental and genotypic sex determination. *Life* **10**, 342 (2020). doi:10.3390/life10120342 Medline

42. S. E. Keating, M. Blumer, L. L. Grismer, A. Lin, S. V. Nielsen, M. K. Thura, P. L. Wood Jr., E. S. H. Quah, T. Gamble, Sex chromosome turnover in bent-toed geckos (*Cyrtodactylus*). *Genes* **12**, 116 (2021). doi:10.3390/genes12010116 Medline

43. A. Kawai, J. Ishijima, C. Nishida, A. Kosaka, H. Ota, S. Kohno, Y. Matsuda, The ZW sex chromosomes of *Gekko hokouensis* (Gekkonidae, Squamata) represent highly conserved homology with those of avian species. *Chromosoma* **118**, 43–51 (2009). doi:10.1007/s00412-008-0176-2 Medline

44. D. L. Jeffries, G. Lavanchy, R. Sermier, M. J. Sredl, I. Miura, A. Borzée, L. N. Barrow, D. Canestrelli, P.-A. Crochet, C. Dufresnes, J. Fu, W.-J. Ma, C. M. Garcia, K. Ghali, A. G. Nicieza, R. P. O'Donnell, N. Rodrigues, A. Romano, Í. Martínez-Solano, I. Stepanyan, S. Zumbach, A. Brelsford, N. Perrin, A rapid rate of sex-chromosome turnover and non-random transitions in true frogs. *Nat. Commun.* **9**, 4088 (2018). doi:10.1038/s41467-018-06517-2 Medline

45. A. El Taher, F. Ronco, M. Matschiner, W. Salzburger, A. Böhne, Dynamics of sex chromosome evolution in a rapid radiation of cichlid fishes. *Sci. Adv.* **7**, eabe8215 (2021). doi:10.1126/sciadv.abe8215 Medline

46. K. A. Behrens, S. Koblmueller, T. D. Kocher, Diversity of sex chromosomes in vertebrates: Six novel sex chromosomes in basal haplochromines (Teleostei: Cichlidae). *Genome Biol. Evol.* **16**, evae152 (2024). doi:10.1093/gbe/evae152 Medline

47. S. P. Otto, J. R. Pannell, C. L. Peichel, T.-L. Ashman, D. Charlesworth, A. K. Chippindale, L. F. Delph, R. F. Guerrero, S. V. Scarpino, B. F. McAllister, About PAR: The distinct evolutionary dynamics of the pseudoautosomal region. *Trends Genet.* **27**, 358–367 (2011). doi:10.1016/j.tig.2011.05.001 Medline

48. T. Westerhold, N. Marwan, A. J. Drury, D. Liebrand, C. Agnini, E. Anagnostou, J. S. K. Barnet, S. M. Bohaty, D. De Vleeschouwer, F. Florindo, T. Frederichs, D. A. Hodell, A. E. Holbourn, D. Kroon, V. Lauretano, K. Littler, L. J. Lourens, M. Lyle, H. Pälike, U. Röhl, J. Tian, R. H. Wilkens, P. A. Wilson, J. C. Zachos, An astronomically dated record of Earth's climate and its predictability over the last 66 million years. *Science* **369**, 1383–1387 (2020). doi:10.1126/science.aba6853 Medline

49. J. L. Blois, E. A. Hadly, Mammalian response to Cenozoic climatic change. *Annu. Rev. Earth Planet. Sci.* **37**, 181–208 (2009). doi:10.1146/annurev.earth.031208.100055

50. J. Agustí, L. Cabrera, M. Garcés, M. Llenas, "Mammal turnover and global climate change in the late Miocene terrestrial record of the Vallès-Penedès Basin (NE Spain)" in *The Evolution of Neogene Terrestrial Ecosystems in Europe*, J. Agustí, L. Rook, P. Andrews, Eds., vol. 1 of *Hominoid Evolution and Climate Change in Europe* (Cambridge Univ. Press, 1999), pp. 397–412.

51. V. Hernández-Ballarín, P. Peláez-Campomanes, Impact of global climate in the diversity patterns of middle Miocene rodents from the Madrid Basin (Spain). *Palaeogeogr. Palaeoclimatol. Palaeoecol.* **472**, 108–118 (2017). doi:10.1016/j.palaeo.2017.01.029

52. R. Marin, D. Cortez, F. Lamanna, M. M. Pradeepa, E. Leushkin, P. Julien, A. Liechti, J. Halbert, T. Brüning, K. Mössinger, T. Trefzer, C. Conrad, H. N. Kerver, J. Wade, P. Tschopp, H. Kaessmann, Convergent origination of a *Drosophila*-like dosage compensation mechanism in a reptile lineage. *Genome Res.* **27**, 1974–1987 (2017). doi:10.1101/gr.223727.117 Medline

53. B. T. Lahn, D. C. Page, Four evolutionary strata on the human X chromosome. *Science* **286**, 964–967 (1999). doi:10.1126/science.286.5441.964 Medline

54. D. W. Bellott, J. F. Hughes, H. Skaletsky, L. G. Brown, T. Pyntikova, T.-J. Cho, N. Koutseva, S. Zaghlul, T. Graves, S. Rock, C. Kremitzki, R. S. Fulton, S. Dugan, Y. Ding, D. Morton, Z. Khan, L. Lewis, C. Buhay, Q. Wang, J. Watt, M. Holder, S. Lee, L. Nazareth, J. Alföldi, S. Rozen, D. M. Muzny, W. C. Warren, R. A. Gibbs, R. K. Wilson, D. C. Page, Mammalian Y chromosomes retain widely expressed dosage-sensitive regulators. *Nature* **508**, 494–499 (2014). doi:10.1038/nature13206 Medline

55. Q. Zhou, J. Zhang, D. Bachtrog, N. An, Q. Huang, E. D. Jarvis, M. T. P. Gilbert, G. Zhang, Complex evolutionary trajectories of sex chromosomes across bird taxa. *Science* **346**, 1246338 (2014). doi:10.1126/science.1246338 Medline

56. C.-I. Wu, A. W. Davis, Evolution of postmating reproductive isolation: The composite nature of Haldane's rule and its genetic bases. *Am. Nat.* **142**, 187–212 (1993). doi:10.1086/285534 Medline

57. T. Miyata, H. Hayashida, K. Kuma, K. Mitsuyasu, T. Yasunaga, Male-driven molecular evolution: A model and nucleotide sequence analysis. *Cold Spring Harb. Symp. Quant. Biol.* **52**, 863–867 (1987). doi:10.1101/SQB.1987.052.01.094 Medline

58. L. A. Bergeron, S. Besenbacher, J. Zheng, P. Li, M. F. Bertelsen, B. Quintard, J. I. Hoffman, Z. Li, J. St. Leger, C. Shao, J. Stiller, M. T. P. Gilbert, M. H. Schierup, G. Zhang, Evolution of the germline mutation rate across vertebrates. *Nature* **615**, 285–291 (2023). doi:10.1038/s41586-023-05752-y Medline

59. L. Kratochvíl, D. Frynta, Body size, male combat and the evolution of sexual dimorphism in eublepharid geckos (Squamata: Eublepharidae). *Biol. J. Linn. Soc. Lond.* **76**, 303–314 (2002). doi:10.1111/j.1095-8312.2002.tb02089.x

60. B. E. Dial, L. C. Fitzpatrick, The energetic costs of tail autotomy to reproduction in the lizard *Coleonyx brevis* (Sauria: Gekkonidae). *Oecologia* **51**, 310–317 (1981). doi:10.1007/BF00540899 Medline

61. A. Atzori, F. Berti, T. Cencetti, S. Fornasiero, M. Tamburini, M. A. L. Zuffi, Advances in methodologies of sexing and marking less dimorphic gekkonid lizards: The study case of the Moorish gecko, *Tarentola mauritanica*. *Amphib. Reptil.* **28**, 449–454 (2007). doi:10.1163/156853807781374719

62. J. G. Phillips, T. J. Hagey, M. Hagemann, E. Gering, Analysis of morphological change during a co-invading assemblage of lizards in the Hawaiian Islands. *Evol. Biol.* **51**, 257–268 (2024). doi:10.1007/s11692-024-09631-w

63. R. A. How, M. A. Cowan, R. J. Teale, L. H. Schmitt, Environmental correlates of reptile variation on the Houtman Abrolhos archipelago, eastern Indian Ocean. *J. Biogeogr.* **47**, 2017–2028 (2020). doi:10.1111/jbi.13881

64. J. F. Husak, Sex, size & gender roles: Evolutionary studies of sexual size dimorphism. *Ornithol. Appl.* **112**, 183–185 (2010). doi:10.1525/cond.2010.112.1.183

65. L. A. Anjos, C. F. D. Rocha, Reproductive ecology of the invader species gekkonid lizard *Hemidactylus mabouia* in an area of southeastern Brazil. *Iheringia Ser. Zool.* **98**, 205–209 (2008). doi:10.1590/S0073-47212008000200006

66. D.-I. Kim, I.-K. Park, H. Ota, J. J. Fong, J.-S. Kim, Y.-P. Zhang, S.-R. Li, W.-J. Choi, D. Park, Patterns of morphological variation in the Schlegel's Japanese gecko (*Gekko japonicus*) across populations in China, Japan, and Korea. *J. Ecol. Environ.* **43**, 34 (2019). doi:10.1186/s41610-019-0132-5

67. A. Y. Albert, S. P. Otto, Sexual selection can resolve sex-linked sexual antagonism. *Science* **310**, 119–121 (2005). doi:10.1126/science.1115328 Medline

68. H. K. Reeve, D. W. Pfennig, Genetic biases for showy males: Are some genetic systems especially conducive to sexual selection? *Proc. Natl. Acad. Sci. U.S.A.* **100**, 1089–1094 (2003). doi:10.1073/pnas.0337427100 Medline

69. I. M. Hastings, Population genetics: XYZW as nature's language of love? *Heredity* **96**, 278–279 (2006). doi:10.1038/sj.hdy.6800795 Medline

70. A. F. Kahrl, R. R. Snook, J. L. Fitzpatrick, Fertilization mode drives sperm length evolution across the animal tree of life. *Nat. Ecol. Evol.* **5**, 1153–1164 (2021). doi:10.1038/s41559-021-01488-y Medline

71. A. F. Kahrl, R. R. Snook, J. L. Fitzpatrick, Fertilization mode differentially impacts the evolution of vertebrate sperm components. *Nat. Commun.* **13**, 6809 (2022). doi:10.1038/s41467-022-34609-7 Medline

72. D. Brawand, M. Soumillon, A. Necsulea, P. Julien, G. Csárdi, P. Harrigan, M. Weier, A. Liechti, A. Aximu-Petri, M. Kircher, F. W. Albert, U. Zeller, P. Khaitovich, F. Grützner, S. Bergmann, R. Nielsen, S. Pääbo, H. Kaessmann, The evolution of gene expression levels in mammalian organs. *Nature* **478**, 343–348 (2011). doi:10.1038/nature10532 Medline

73. Z. Y. Wang, E. Leushkin, A. Liechti, S. Ovchinnikova, K. Mößinger, T. Brüning, C. Rummel, F. Grützner, M. Cardoso-Moreira, P. Janich, D. Gatfield, B. Diagouraga, B. de Massy, M. E. Gill, A. H. F. M. Peters, S. Anders, H. Kaessmann, Transcriptome and

translatome co-evolution in mammals. *Nature* **588**, 642–647 (2020). doi:10.1038/s41586-020-2899-z Medline

74. D. Bachtrog, The temporal dynamics of processes underlying Y chromosome degeneration. *Genetics* **179**, 1513–1525 (2008). doi:10.1534/genetics.107.084012 Medline

75. J. F. Hughes, H. Skaletsky, L. G. Brown, T. Pyntikova, T. Graves, R. S. Fulton, S. Dugan, Y. Ding, C. J. Buhay, C. Kremitzki, Q. Wang, H. Shen, M. Holder, D. Villasana, L. V. Nazareth, A. Cree, L. Courtney, J. Veizer, H. Kotkiewicz, T.-J. Cho, N. Koutseva, S. Rozen, D. M. Muzny, W. C. Warren, R. A. Gibbs, R. K. Wilson, D. C. Page, Strict evolutionary conservation followed rapid gene loss on human and rhesus Y chromosomes. *Nature* **483**, 82–86 (2012). doi:10.1038/nature10843 Medline

76. D. W. Bellott, D. C. Page, Dosage-sensitive functions in embryonic development drove the survival of genes on sex-specific chromosomes in snakes, birds, and mammals. *Genome Res.* **31**, 198–210 (2021). doi:10.1101/gr.268516.120 Medline

77. D. Charlesworth, The timing of genetic degeneration of sex chromosomes. *Philos. Trans. R. Soc. London Ser. B* **376**, 20200093 (2021). doi:10.1098/rstb.2020.0093 Medline

78. D. Crowson, S. C. H. Barrett, S. I. Wright, Purifying and positive selection influence patterns of gene loss and gene expression in the evolution of a plant sex chromosome system. *Mol. Biol. Evol.* **34**, 1140–1154 (2017). doi:10.1093/molbev/msx064 Medline

79. J. A. Graves, Sex chromosome specialization and degeneration in mammals. *Cell* **124**, 901–914 (2006). doi:10.1016/j.cell.2006.02.024 Medline

80. L. Gu, J. R. Walters, Evolution of sex chromosome dosage compensation in animals: A beautiful theory, undermined by facts and bedeviled by details. *Genome Biol. Evol.* **9**, 2461–2476 (2017). doi:10.1093/gbe/evx154 Medline

81. S. Ohno, *Sex Chromosomes and Sex-Linked Genes*, vol. 1 of *Monographs on Endocrinology* (Springer, 2013).

82. J. A. Birchler, N. C. Riddle, D. L. Auger, R. A. Veitia, Dosage balance in gene regulation: Biological implications. *Trends Genet.* **21**, 219–226 (2005). doi:10.1016/j.tig.2005.02.010 Medline

83. A. Catalán, J. Merondun, U. Knief, J. B. W. Wolf, Chromatin accessibility, not 5mC methylation covaries with partial dosage compensation in crows. *PLOS Genet.* **19**, e1010901 (2023). doi:10.1371/journal.pgen.1010901 Medline

84. D. R. Schield, D. C. Card, N. R. Hales, B. W. Perry, G. M. Pasquesi, H. Blackmon, R. H. Adams, A. B. Corbin, C. F. Smith, B. Ramesh, J. P. Demuth, E. Betrán, M. Tollis, J. M. Meik, S. P. Mackessy, T. A. Castoe, The origins and evolution of chromosomes, dosage compensation, and mechanisms underlying venom regulation in snakes. *Genome Res.* **29**, 590–601 (2019). doi:10.1101/gr.240952.118 Medline

85. M. W. Pennell, J. E. Mank, C. L. Peichel, Transitions in sex determination and sex chromosomes across vertebrate species. *Mol. Ecol.* **27**, 3950–3963 (2018). doi:10.1111/mec.14540 Medline

86. N. Valenzuela, V. A. Lance, Eds., *Temperature-Dependent Sex Determination in Vertebrates* (Smithsonian Institution Scholarly Press, 2004).

87. J. Jin, Dived-Jin/Gecko_Sexchromosome: Gecko_sexchromsome, v1.0.0, Zenodo (2026); https://doi.org/10.5281/zenodo.18973980.

88. J. Hansen, M. Sato, G. Russell, P. Kharecha, Climate sensitivity, sea level and atmospheric carbon dioxide. *Philos. Trans. R. Soc. London Ser. A* **371**, 20120294 (2013). doi:10.1098/rsta.2012.0294 Medline

89. S. S. Rao, M. H. Huntley, N. C. Durand, E. K. Stamenova, I. D. Bochkov, J. T. Robinson, A. L. Sanborn, I. Machol, A. D. Omer, E. S. Lander, E. L. Aiden, A 3D map of the human genome at kilobase resolution reveals principles of chromatin looping. *Cell* **159**, 1665–1680 (2014). doi:10.1016/j.cell.2014.11.021 Medline

90. C. S. Chin, P. Peluso, F. J. Sedlazeck, M. Nattestad, G. T. Concepcion, A. Clum, C. Dunn, R. O'Malley, R. Figueroa-Balderas, A. Morales-Cruz, G. R. Cramer, M. Delledonne, C. Luo, J. R. Ecker, D. Cantu, D. R. Rank, M. C. Schatz, Phased diploid genome assembly with single-molecule real-time sequencing. *Nat. Methods* **13**, 1050–1054 (2016). doi:10.1038/nmeth.4035 Medline

91. J. Ruan, H. Li, Fast and accurate long-read assembly with wtdbg2. *Nat. Methods* **17**, 155–158 (2020). doi:10.1038/s41592-019-0669-3 Medline

92. J. Hu, Z. Wang, Z. Sun, B. Hu, A. O. Ayoola, F. Liang, J. Li, J. R. Sandoval, D. N. Cooper, K. Ye, J. Ruan, C.-L. Xiao, D. Wang, D.-D. Wu, S. Wang, NextDenovo: An efficient error correction and accurate assembly tool for noisy long reads. *Genome Biol.* **25**, 107 (2024). doi:10.1186/s13059-024-03252-4 Medline

93. S. Koren, B. P. Walenz, K. Berlin, J. R. Miller, N. H. Bergman, A. M. Phillippy, Canu: Scalable and accurate long-read assembly via adaptive *k*-mer weighting and repeat separation. *Genome Res.* **27**, 722–736 (2017). doi:10.1101/gr.215087.116 Medline

94. S. Nurk, B. P. Walenz, A. Rhie, M. R. Vollger, G. A. Logsdon, R. Grothe, K. H. Miga, E. E. Eichler, A. M. Phillippy, S. Koren, HiCanu: Accurate assembly of segmental duplications, satellites, and allelic variants from high-fidelity long reads. *Genome Res.* **30**, 1291–1305 (2020). doi:10.1101/gr.263566.120 Medline

95. A. Rhie, S. A. McCarthy, O. Fedrigo, J. Damas, G. Formenti, S. Koren, M. Uliano-Silva, W. Chow, A. Fungtammasan, J. Kim, C. Lee, B. J. Ko, M. Chaisson, G. L. Gedman, L. J. Cantin, F. Thibaud-Nissen, L. Haggerty, I. Bista, M. Smith, B. Haase, J. Mountcastle, S. Winkler, S. Paez, J. Howard, S. C. Vernes, T. M. Lama, F. Grutzner, W. C. Warren, C. N. Balakrishnan, D. Burt, J. M. George, M. T. Biegler, D. Iorns, A. Digby, D. Eason, B. Robertson, T. Edwards, M. Wilkinson, G. Turner, A. Meyer, A. F. Kautt, P. Franchini, H. W. Detrich 3rd, H. Svardal, M. Wagner, G. J. P. Naylor, M. Pippel, M. Malinsky, M. Mooney, M. Simbirsky, B. T. Hannigan, T. Pesout, M. Houck, A. Misuraca, S. B. Kingan, R. Hall, Z. Kronenberg, I. Sović, C. Dunn, Z. Ning, A. Hastie, J. Lee, S. Selvaraj, R. E. Green, N. H. Putnam, I. Gut, J. Ghurye, E. Garrison, Y. Sims, J. Collins, S. Pelan, J. Torrance, A. Tracey, J. Wood, R. E. Dagnew, D. Guan, S. E. London, D. F. Clayton, C. V. Mello, S. R. Friedrich, P. V. Lovell, E. Osipova, F. O. Al-Ajli, S. Secomandi, H. Kim, C. Theofanopoulou, M. Hiller, Y. Zhou, R. S. Harris, K. D. Makova, P. Medvedev, J. Hoffman, P. Masterson, K. Clark, F. Martin, K. Howe, P. Flicek, B. P. Walenz, W. Kwak, H. Clawson, M. Diekhans, L. Nassar, B. Paten, R. H. S. Kraus, A. J. Crawford, M. T. P. Gilbert, G. Zhang, B. Venkatesh, R. W. Murphy, K.-P. Koepfli, B.

Shapiro, W. E. Johnson, F. Di Palma, T. Marques-Bonet, E. C. Teeling, T. Warnow, J. M. Graves, O. A. Ryder, D. Haussler, S. J. O'Brien, J. Korlach, H. A. Lewin, K. Howe, E. W. Myers, R. Durbin, A. M. Phillippy, E. D. Jarvis, Towards complete and error-free genome assemblies of all vertebrate species. *Nature* **592**, 737–746 (2021). doi:10.1038/s41586-021-03451-0 Medline

96. N. C. Durand, M. S. Shamim, I. Machol, S. S. P. Rao, M. H. Huntley, E. S. Lander, E. L. Aiden, Juicer provides a one-click system for analyzing loop-resolution Hi-C experiments. *Cell Syst.* **3**, 95–98 (2016). doi:10.1016/j.cels.2016.07.002 Medline

97. O. Dudchenko, S. S. Batra, A. D. Omer, S. K. Nyquist, M. Hoeger, N. C. Durand, M. S. Shamim, I. Machol, E. S. Lander, A. P. Aiden, E. L. Aiden, De novo assembly of the *Aedes aegypti* genome using Hi-C yields chromosome-length scaffolds. *Science* **356**, 92–95 (2017). doi:10.1126/science.aal3327 Medline

98. N. C. Durand, J. T. Robinson, M. S. Shamim, I. Machol, J. P. Mesirov, E. S. Lander, E. L. Aiden, Juicebox provides a visualization system for Hi-C contact maps with unlimited zoom. *Cell Syst.* **3**, 99–101 (2016). doi:10.1016/j.cels.2015.07.012 Medline

99. O. Dudchenko, M. S. Shamim, S. S. Batra, N. C. Durand, N. T. Musial, R. Mostofa, M. Pham, B. G. St Hilaire, W. Yao, E. Stamenova, M. Hoeger, S. K. Nyquist, V. Korchina, K. Pletch, J. P. Flanagan, A. Tomaszewicz, D. McAloose, C. Pérez Estrada, B. J. Novak, A. D. Omer, E. L. Aiden, The Juicebox Assembly Tools module facilitates *de novo* assembly of mammalian genomes with chromosome-length scaffolds for under $1000. bioRxiv 254797 [Preprint] (2018); https://doi.org/10.1101/254797.

100. C. Yang, Y. Zhou, S. Marcus, G. Formenti, L. A. Bergeron, Z. Song, X. Bi, J. Bergman, M. M. C. Rousselle, C. Zhou, L. Zhou, Y. Deng, M. Fang, D. Xie, Y. Zhu, S. Tan, J. Mountcastle, B. Haase, J. Balacco, J. Wood, W. Chow, A. Rhie, M. Pippel, M. M. Fabiszak, S. Koren, O. Fedrigo, W. A. Freiwald, K. Howe, H. Yang, A. M. Phillippy, M. H. Schierup, E. D. Jarvis, G. Zhang, Evolutionary and biomedical insights from a marmoset diploid genome assembly. *Nature* **594**, 227–233 (2021). doi:10.1038/s41586-021-03535-x Medline

101. H. Li, Aligning sequence reads, clone sequences and assembly contigs with BWA-MEM. arXiv:1303.3997 [q-bio.GN] (2013).

102. P. Danecek, J. K. Bonfield, J. Liddle, J. Marshall, V. Ohan, M. O. Pollard, A. Whitwham, T. Keane, S. A. McCarthy, R. M. Davies, H. Li, Twelve years of SAMtools and BCFtools. *Gigascience* **10**, giab008 (2021). doi:10.1093/gigascience/giab008 Medline

103. A. R. Quinlan, I. M. Hall, BEDTools: A flexible suite of utilities for comparing genomic features. *Bioinformatics* **26**, 841–842 (2010). doi:10.1093/bioinformatics/btq033 Medline

104. H. Wickham, ggplot2. *Wiley Interdiscip. Rev. Comput. Stat.* **3**, 180–185 (2011). doi:10.1002/wics.147

105. F. Ramírez, V. Bhardwaj, L. Arrigoni, K. C. Lam, B. A. Grüning, J. Villaveces, B. Habermann, A. Akhtar, T. Manke, High-resolution TADs reveal DNA sequences underlying genome organization in flies. *Nat. Commun.* **9**, 189 (2018). doi:10.1038/s41467-017-02525-w Medline

106. Y. Zhang, R. P. McCord, Y.-J. Ho, B. R. Lajoie, D. G. Hildebrand, A. C. Simon, M. S. Becker, F. W. Alt, J. Dekker, Spatial organization of the mouse genome and its role in recurrent chromosomal translocations. *Cell* **148**, 908–921 (2012). doi:10.1016/j.cell.2012.02.002 Medline

107. E. Garrison, G. Marth, Haplotype-based variant detection from short-read sequencing. arXiv:1207.3907 [q-bio.GN] (2012).

108. P. Danecek, A. Auton, G. Abecasis, C. A. Albers, E. Banks, M. A. DePristo, R. E. Handsaker, G. Lunter, G. T. Marth, S. T. Sherry, G. McVean, R. Durbin; 1000 Genomes Project Analysis Group, The variant call format and VCFtools. *Bioinformatics* **27**, 2156–2158 (2011). doi:10.1093/bioinformatics/btr330 Medline

109. S. D. Turner, qqman: An R package for visualizing GWAS results using Q-Q and manhattan plots. *J. Open Source Softw.* **3**, 731 (2018). doi:10.21105/joss.00731

110. X. Zhang, S. Zhang, Q. Zhao, R. Ming, H. Tang, Assembly of allele-aware, chromosomal-scale autopolyploid genomes based on Hi-C data. *Nat. Plants* **5**, 833–845 (2019). doi:10.1038/s41477-019-0487-8 Medline

111. Y. Zhou, X. Zhan, J. Jin, L. Zhou, J. Bergman, X. Li, M. M. C. Rousselle, M. R. Belles, L. Zhao, M. Fang, J. Chen, Q. Fang, L. Kuderna, T. Marques-Bonet, H. Kitayama, T. Hayakawa, Y.-G. Yao, H. Yang, D. N. Cooper, X. Qi, D.-D. Wu, M. H. Schierup, G. Zhang, Eighty million years of rapid evolution of the primate Y chromosome. *Nat. Ecol. Evol.* **7**, 1114–1130 (2023). doi:10.1038/s41559-022-01974-x Medline

112. D. Guan, S. A. McCarthy, J. Wood, K. Howe, Y. Wang, R. Durbin, Identifying and removing haplotypic duplication in primary genome assemblies. *Bioinformatics* **36**, 2896–2898 (2020). doi:10.1093/bioinformatics/btaa025 Medline

113. M. Manni, M. R. Berkeley, M. Seppey, F. A. Simão, E. M. Zdobnov, BUSCO update: Novel and streamlined workflows along with broader and deeper phylogenetic coverage for scoring of eukaryotic, prokaryotic, and viral genomes. *Mol. Biol. Evol.* **38**, 4647–4654 (2021). doi:10.1093/molbev/msab199 Medline

114. Z. Zhang, S. Schwartz, L. Wagner, W. Miller, A greedy algorithm for aligning DNA sequences. *J. Comput. Biol.* **7**, 203–214 (2000). doi:10.1089/10665270050081478 Medline

115. R. S. Harris, "Improved pairwise alignment of genomic DNA," thesis, The Pennsylvania State University, 2007.

116. T. Kahlke, P. J. Ralph, BASTA – Taxonomic classification of sequences and sequence bins using last common ancestor estimations. *Methods Ecol. Evol.* **10**, 100–103 (2019). doi:10.1111/2041-210X.13095

117. Y. Zhou, L. Shearwin-Whyatt, J. Li, Z. Song, T. Hayakawa, D. Stevens, J. C. Fenelon, E. Peel, Y. Cheng, F. Pajpach, N. Bradley, H. Suzuki, M. Nikaido, J. Damas, T. Daish, T. Perry, Z. Zhu, Y. Geng, A. Rhie, Y. Sims, J. Wood, B. Haase, J. Mountcastle, O. Fedrigo, Q. Li, H. Yang, J. Wang, S. D. Johnston, A. M. Phillippy, K. Howe, E. D. Jarvis, O. A. Ryder, H. Kaessmann, P. Donnelly, J. Korlach, H. A. Lewin, J. Graves, K. Belov, M. B. Renfree, F. Grutzner, Q. Zhou, G. Zhang, Platypus and echidna genomes reveal

mammalian biology and evolution. *Nature* **592**, 756–762 (2021). doi:10.1038/s41586-020-03039-0 Medline

118. R. She, J. S. Chu, K. Wang, J. Pei, N. Chen, GenBlastA: Enabling BLAST to identify homologous gene sequences. *Genome Res.* **19**, 143–149 (2009). doi:10.1101/gr.082081.108 Medline

119. E. Birney, M. Clamp, R. Durbin, GeneWise and Genomewise. *Genome Res.* **14**, 988–995 (2004). doi:10.1101/gr.1865504 Medline

120. M. Stanke, O. Keller, I. Gunduz, A. Hayes, S. Waack, B. Morgenstern, AUGUSTUS: *ab initio* prediction of alternative transcripts. *Nucleic Acids Res.* **34**, W435–W439 (2006). doi:10.1093/nar/gkl200 Medline

121. D. Kim, J. M. Paggi, C. Park, C. Bennett, S. L. Salzberg, Graph-based genome alignment and genotyping with HISAT2 and HISAT-genotype. *Nat. Biotechnol.* **37**, 907–915 (2019). doi:10.1038/s41587-019-0201-4 Medline

122. M. Pertea, G. M. Pertea, C. M. Antonescu, T. C. Chang, J. T. Mendell, S. L. Salzberg, StringTie enables improved reconstruction of a transcriptome from RNA-seq reads. *Nat. Biotechnol.* **33**, 290–295 (2015). doi:10.1038/nbt.3122 Medline

123. S. M. Kiełbasa, R. Wan, K. Sato, P. Horton, M. C. Frith, Adaptive seeds tame genomic sequence comparison. *Genome Res.* **21**, 487–493 (2011). doi:10.1101/gr.113985.110 Medline

124. S. Capella-Gutiérrez, J. M. Silla-Martínez, T. Gabaldón, trimAl: A tool for automated alignment trimming in large-scale phylogenetic analyses. *Bioinformatics* **25**, 1972–1973 (2009). doi:10.1093/bioinformatics/btp348 Medline

125. L. Chen, Q. Qiu, Y. Jiang, K. Wang, Z. Lin, Z. Li, F. Bibi, Y. Yang, J. Wang, W. Nie, W. Su, G. Liu, Q. Li, W. Fu, X. Pan, C. Liu, J. Yang, C. Zhang, Y. Yin, Y. Wang, Y. Zhao, C. Zhang, Z. Wang, Y. Qin, W. Liu, B. Wang, Y. Ren, R. Zhang, Y. Zeng, R. R. da Fonseca, B. Wei, R. Li, W. Wan, R. Zhao, W. Zhu, Y. Wang, S. Duan, Y. Gao, Y. E. Zhang, C. Chen, C. Hvilsom, C. W. Epps, L. G. Chemnick, Y. Dong, S. Mirarab, H. R. Siegismund, O. A. Ryder, M. T. P. Gilbert, H. A. Lewin, G. Zhang, R. Heller, W. Wang, Large-scale ruminant genome sequencing provides insights into their evolution and distinct traits. *Science* **364**, eaav6202 (2019). doi:10.1126/science.aav6202 Medline

126. B. Q. Minh, H. A. Schmidt, O. Chernomor, D. Schrempf, M. D. Woodhams, A. von Haeseler, R. Lanfear, IQ-TREE 2: New models and efficient methods for phylogenetic inference in the genomic era. *Mol. Biol. Evol.* **37**, 1530–1534 (2020). doi:10.1093/molbev/msaa015 Medline

127. C. Zhang, M. Rabiee, E. Sayyari, S. Mirarab, ASTRAL-III: Polynomial time species tree reconstruction from partially resolved gene trees. *BMC Bioinformatics* **19** (suppl. 6), 153 (2018). doi:10.1186/s12859-018-2129-y Medline

128. A. M. Kozlov, D. Darriba, T. Flouri, B. Morel, A. Stamatakis, RAxML-NG: A fast, scalable and user-friendly tool for maximum likelihood phylogenetic inference. *Bioinformatics* **35**, 4453–4455 (2019). doi:10.1093/bioinformatics/btz305 Medline

129. F. Li, R. V. Rane, V. Luria, Z. Xiong, J. Chen, Z. Li, R. A. Catullo, P. C. Griffin, M. Schiffer, S. Pearce, S. F. Lee, K. McElroy, A. Stocker, J. Shirriffs, F. Cockerell, C. Coppin, C. M. Sgrò, A. Karger, J. W. Cain, J. A. Weber, G. Santpere, M. W. Kirschner, A. A. Hoffmann, J. G. Oakeshott, G. Zhang, Phylogenomic analyses of the genus *Drosophila* reveals genomic signals of climate adaptation. *Mol. Ecol. Resour.* **22**, 1559–1581 (2022). doi:10.1111/1755-0998.13561 Medline

130. Z. Yang, PAML 4: Phylogenetic analysis by maximum likelihood. *Mol. Biol. Evol.* **24**, 1586–1591 (2007). doi:10.1093/molbev/msm088 Medline

131. A. Rambaut, A. J. Drummond, D. Xie, G. Baele, M. A. Suchard, Posterior summarization in Bayesian phylogenetics using Tracer 1.7. *Syst. Biol.* **67**, 901–904 (2018). doi:10.1093/sysbio/syy032 Medline

132. J. Kim, M. Farré, L. Auvil, B. Capitanu, D. M. Larkin, J. Ma, H. A. Lewin, Reconstruction and evolutionary history of eutherian chromosomes. *Proc. Natl. Acad. Sci. U.S.A.* **114**, E5379–E5388 (2017). doi:10.1073/pnas.1702012114 Medline

133. B. R. Jones, A. Rajaraman, E. Tannier, C. Chauve, ANGES: Reconstructing ANcestral GEnomeS maps. *Bioinformatics* **28**, 2388–2390 (2012). doi:10.1093/bioinformatics/bts457 Medline

134. W. He, J. Yang, Y. Jing, L. Xu, K. Yu, X. Fang, NGenomeSyn: An easy-to-use and flexible tool for publication-ready visualization of syntenic relationships across multiple genomes. *Bioinformatics* **39**, btad121 (2023). doi:10.1093/bioinformatics/btad121 Medline

135. G. Tesler, GRIMM: Genome rearrangements web server. *Bioinformatics* **18**, 492–493 (2002). doi:10.1093/bioinformatics/18.3.492 Medline

136. S. F. Altschul, W. Gish, W. Miller, E. W. Myers, D. J. Lipman, Basic local alignment search tool. *J. Mol. Biol.* **215**, 403–410 (1990). doi:10.1016/S0022-2836(05)80360-2 Medline

137. D. M. Emms, S. Kelly, OrthoFinder: Phylogenetic orthology inference for comparative genomics. *Genome Biol.* **20**, 238 (2019). doi:10.1186/s13059-019-1832-y Medline

138. G. Benson, Tandem repeats finder: A program to analyze DNA sequences. *Nucleic Acids Res.* **27**, 573–580 (1999). doi:10.1093/nar/27.2.573 Medline

139. J. Y. Dutheil, S. Gaillard, E. H. Stukenbrock, MafFilter: A highly flexible and extensible multiple genome alignment files processor. *BMC Genomics* **15**, 53 (2014). doi:10.1186/1471-2164-15-53 Medline

140. A. Löytynoja, "Phylogeny-aware alignment with PRANK" in *Multiple Sequence Alignment Methods*, D. J. Russell, Ed., vol. 1079 of *Methods in Molecular Biology* (Springer, 2014), pp. 155–170.

141. M. Blanchette, W. J. Kent, C. Riemer, L. Elnitski, A. F. A. Smit, K. M. Roskin, R. Baertsch, K. Rosenbloom, H. Clawson, E. D. Green, D. Haussler, W. Miller, Aligning multiple genomic sequences with the threaded blockset aligner. *Genome Res.* **14**, 708–715 (2004). doi:10.1101/gr.1933104 Medline

142. V. Link, D. Aguilar-Gómez, C. Ramírez-Suástegui, L. D. Hurst, D. Cortez, Male mutation bias is the main force shaping chromosomal substitution rates in monotreme mammals. *Genome Biol. Evol.* **9**, 2198–2210 (2017). doi:10.1093/gbe/evx155 Medline

143. E. Axelsson, N. G. Smith, H. Sundström, S. Berlin, H. Ellegren, Male-biased mutation rate and divergence in autosomal, Z-linked and W-linked introns of chicken and turkey. *Mol. Biol. Evol.* **21**, 1538–1547 (2004). doi:10.1093/molbev/msh157 Medline

144. D. Cortez, R. Marin, D. Toledo-Flores, L. Froidevaux, A. Liechti, P. D. Waters, F. Grützner, H. Kaessmann, Origins and functional evolution of Y chromosomes across mammals. *Nature* **508**, 488–493 (2014). doi:10.1038/nature13151 Medline

145. E. V. Davydov, D. L. Goode, M. Sirota, G. M. Cooper, A. Sidow, S. Batzoglou, Identifying a high fraction of the human genome to be under selective constraint using GERP++. *PLOS Comput. Biol.* **6**, e1001025 (2010). doi:10.1371/journal.pcbi.1001025 Medline

146. Y. Zhou, Y. Liang, K. H. Lynch, J. J. Dennis, D. S. Wishart, PHAST: A fast phage search tool. *Nucleic Acids Res.* **39** (suppl. 2), W347–W352 (2011). doi:10.1093/nar/gkr485 Medline

147. T. Gamble, E. Greenbaum, T. R. Jackman, A. M. Bauer, Into the light: Diurnality has evolved multiple times in geckos. *Biol. J. Linn. Soc. Lond.* **115**, 896–910 (2015). doi:10.1111/bij.12536

148. F. K. Mendes, D. Vanderpool, B. Fulton, M. W. Hahn, CAFE 5 models variation in evolutionary rates among gene families. *Bioinformatics* **36**, 5516–5518 (2021). doi:10.1093/bioinformatics/btaa1022 Medline

149. N. L. Bray, H. Pimentel, P. Melsted, L. Pachter, Near-optimal probabilistic RNA-seq quantification. *Nat. Biotechnol.* **34**, 525–527 (2016). doi:10.1038/nbt.3519 Medline

150. M. I. Love, W. Huber, S. Anders, Moderated estimation of fold change and dispersion for RNA-seq data with DESeq2. *Genome Biol.* **15**, 550 (2014). doi:10.1186/s13059-014-0550-8 Medline

151. L. J. Revell, phytools 2.0: An updated R ecosystem for phylogenetic comparative methods (and other things). *PeerJ* **12**, e16505 (2024). doi:10.7717/peerj.16505 Medline

152. D. Bates, M. Mächler, B. Bolker, S. Walker, Fitting linear mixed-effects models using lme4. *J. Stat. Softw.* **67**, 1–48 (2015). doi:10.18637/jss.v067.i01

153. J. Fox, S. Weisberg, *An R Companion to Applied Regression* (Sage Publications, ed. 3, 2018).

154. N. Huang, I. Lee, E. M. Marcotte, M. E. Hurles, Characterising and predicting haploinsufficiency in the human genome. *PLOS Genet.* **6**, e1001154 (2010). doi:10.1371/journal.pgen.1001154 Medline

155. M. de Clare, P. Pir, S. G. Oliver, Haploinsufficiency and the sex chromosomes from yeasts to humans. *BMC Biol.* **9**, 15 (2011). doi:10.1186/1741-7007-9-15 Medline

156. L. Xu, Q. Zhou, The female-specific W chromosomes of birds have conserved gene contents but are not feminized. *Genes* **11**, 1126 (2020). doi:10.3390/genes11101126 Medline

157. C. L. Peichel, S. R. McCann, J. A. Ross, A. F. S. Naftaly, J. R. Urton, J. N. Cech, J. Grimwood, J. Schmutz, R. M. Myers, D. M. Kingsley, M. A. White, Assembly of the threespine stickleback Y chromosome reveals convergent signatures of sex chromosome evolution. *Genome Biol.* **21**, 177 (2020). doi:10.1186/s13059-020-02097-x Medline

158. N. C. Lister, A. M. Milton, H. R. Patel, S. A. Waters, B. J. Hanrahan, K. L. McIntyre, A. M. Livernois, W. B. Horspool, L. K. Wee, A. R. Ringel, S. Mundlos, M. I. Robson, L. Shearwin-Whyatt, F. Grützner, J. A. M. Graves, A. Ruiz-Herrera, P. D. Waters, Incomplete transcriptional dosage compensation of chicken and platypus sex chromosomes is balanced by post-transcriptional compensation. *Proc. Natl. Acad. Sci. U.S.A.* **121**, e2322360121 (2024). doi:10.1073/pnas.2322360121 Medline

159. Y. Wang, R. B. Gasser, D. Charlesworth, Q. Zhou, Evolution of sexual systems, sex chromosomes and sex-linked gene transcription in flatworms and roundworms. *Nat. Commun.* **13**, 3239 (2022). doi:10.1038/s41467-022-30578-z Medline

160. C. Trapnell, L. Pachter, S. L. Salzberg, TopHat: Discovering splice junctions with RNA-Seq. *Bioinformatics* **25**, 1105–1111 (2009). doi:10.1093/bioinformatics/btp120 Medline

161. Y. Xie, G. Wu, J. Tang, R. Luo, J. Patterson, S. Liu, W. Huang, G. He, S. Gu, S. Li, X. Zhou, T.-W. Lam, Y. Li, X. Xu, G. K.-S. Wong, J. Wang, SOAPdenovo-Trans: *de novo* transcriptome assembly with short RNA-Seq reads. *Bioinformatics* **30**, 1660–1666 (2014). doi:10.1093/bioinformatics/btu077 Medline

162. M. G. Grabherr, B. J. Haas, M. Yassour, J. Z. Levin, D. A. Thompson, I. Amit, X. Adiconis, L. Fan, R. Raychowdhury, Q. Zeng, Z. Chen, E. Mauceli, N. Hacohen, A. Gnirke, N. Rhind, F. di Palma, B. W. Birren, C. Nusbaum, K. Lindblad-Toh, N. Friedman, A. Regev, Full-length transcriptome assembly from RNA-Seq data without a reference genome. *Nat. Biotechnol.* **29**, 644–652 (2011). doi:10.1038/nbt.1883 Medline

163. W. J. Kent, BLAT—The BLAST-like alignment tool. *Genome Res.* **12**, 656–664 (2002). doi:10.1101/gr.229202 Medline

164. B. Langmead, S. L. Salzberg, Fast gapped-read alignment with Bowtie 2. *Nat. Methods* **9**, 357–359 (2012). doi:10.1038/nmeth.1923 Medline

165. W. Li, A. Godzik, Cd-hit: A fast program for clustering and comparing large sets of protein or nucleotide sequences. *Bioinformatics* **22**, 1658–1659 (2006). doi:10.1093/bioinformatics/btl158 Medline

166. G. Marçais, C. Kingsford, A fast, lock-free approach for efficient parallel counting of occurrences of *k*-mers. *Bioinformatics* **27**, 764–770 (2011). doi:10.1093/bioinformatics/btr011 Medline

167. K. A. Behrens, S. Koblmüller, T. D. Kocher, Sex chromosomes in the tribe *Cyprichromini* (Teleostei: Cichlidae) of Lake Tanganyika. *Sci. Rep.* **12**, 17998 (2022). doi:10.1038/s41598-022-23017-y Medline

168. H. Li, Minimap2: Pairwise alignment for nucleotide sequences. *Bioinformatics* **34**, 3094–3100 (2018). doi:10.1093/bioinformatics/bty191 Medline

169. A. Lisachov, K. Tishakova, S. Romanenko, L. Lisachova, G. Davletshina, D. Prokopov, L. Kratochvíl, P. O Brien, M. Ferguson-Smith, P. Borodin, V. Trifonov, Robertsonian

fusion triggers recombination suppression on sex chromosomes in *Coleonyx* geckos. *Sci. Rep.* **13**, 15502 (2023). doi:10.1038/s41598-023-39937-2 Medline

170. D. Charlesworth, B. Charlesworth, Sex differences in fitness and selection for centric fusions between sex-chromosomes and autosomes. *Genet. Res.* **35**, 205–214 (1980). doi:10.1017/S0016672300014051 Medline

171. M. W. Pennell, M. Kirkpatrick, S. P. Otto, J. C. Vamosi, C. L. Peichel, N. Valenzuela, J. Kitano, Y fuse? Sex chromosome fusions in fishes and reptiles. *PLOS Genet.* **11**, e1005237 (2015). doi:10.1371/journal.pgen.1005237 Medline

172. B. Capel, Vertebrate sex determination: Evolutionary plasticity of a fundamental switch. *Nat. Rev. Genet.* **18**, 675–689 (2017). doi:10.1038/nrg.2017.60 Medline

173. B. J. Pinto, T. Gamble, C. H. Smith, M. A. Wilson, A lizard is never late: Squamate genomics as a recent catalyst for understanding sex chromosome and microchromosome evolution. *J. Hered.* **114**, 445–458 (2023). doi:10.1093/jhered/esad023 Medline

174. D. Thépot, Sex chromosomes and master sex-determining genes in turtles and other reptiles. *Genes* **12**, 1822 (2021). doi:10.3390/genes12111822 Medline

175. Z.-X. Zhu, K. Matsubara, F. Shams, J. Dobry, E. Wapstra, T. Gamble, S. D. Sarre, A. Georges, J. A. Marshall Graves, Q. Zhou, T. Ezaz, Diversity of reptile sex chromosome evolution revealed by cytogenetic and linked-read sequencing. *Zool. Res.* **43**, 719–733 (2022). doi:10.24272/j.issn.2095-8137.2022.127 Medline

176. C. Daems, L. J. Martin, C. Brousseau, J. J. Tremblay, MEF2 is restricted to the male gonad and regulates expression of the orphan nuclear receptor NR4A1. *Mol. Endocrinol.* **28**, 886–898 (2014). doi:10.1210/me.2013-1407 Medline

177. J. Hodgkin, Exploring the envelope. Systematic alteration in the sex-determination system of the nematode *Caenorhabditis elegans*. *Genetics* **162**, 767–780 (2002). doi:10.1093/genetics/162.2.767 Medline